Research Paper

THEMED ISSUE: Cenozoic Tectonics, Magmatism, and Stratigraphy of the Snake River Plain–Yellowstone Region and Adjacent Areas

GEOSPHERE

GEOSPHERE; v. 12, no. 1

doi:10.1130/GES01162.1

28 figures; 5 tables; 10 supplemental files

CORRESPONDENCE: coblem@stanford.edu

CITATION: Coble, M.A., and Mahood, G.A., 2016, Geology of the High Rock caldera complex, northwest Nevada, and implications for intense rhyolitic volcanism associated with flood basalt magmatism and the initiation of the Snake River Plain–Yellowstone trend: Geosphere, v. 12, no. 1, p. 58–113, doi:10.1130/GES01162.1.

Received 5 December 2014
Revision received 1 October 2015
Accepted 28 October 2015
Published online 23 December 2015

Geology of the High Rock caldera complex, northwest Nevada, and implications for intense rhyolitic volcanism associated with flood basalt magmatism and the initiation of the Snake River Plain–Yellowstone trend

Matthew A. Coble and Gail A. Mahood

Department of Geological Sciences, Stanford University, 450 Serra Mall, Stanford, California 94305-2115, USA

ABSTRACT

We present the geologic history of the High Rock caldera complex (HRCC; Nevada, USA), a major mid-Miocene silicic center associated with flood basalt volcanism. Based on 70 $^{40}Ar/^{39}Ar$ ages and new 1:24,000- and 1:100,000-scale geologic mapping, we document that between ca. 16.5 and 15.5 Ma a minimum of ~700 km^3 of rhyolitic magma erupted from the HRCC, covering an area of ~8300 km^2 in northwestern Nevada and southern Oregon (USA). The volcanism immediately followed eruption of the Steens flood basalt in the region, and was contemporaneous with eruption of compositionally similar rhyolites from the McDermitt volcanic field (MVF) to the east. The HRCC and MVF together mark the starting point for the eastward-younging trend of voluminous rhyolitic calderas of the Snake River Plain–Yellowstone trend.

The HRCC comprises 4 major calderas, 24–40 km in diameter, that young from north-northeast to south-southwest: the Virgin Valley caldera formed on eruption of the 16.38 Ma high-silica alkali rhyolite Idaho Canyon Tuff; the overlapping Badger Mountain caldera collapsed due to eruption of the 16.34 Ma crystal-rich, low-silica rhyolite Summit Lake Tuff; eruption of the moderately peralkaline high-silica alkali rhyolite Soldier Meadow Tuff at 16 Ma resulted in formation of the Hanging Rock caldera; and the Cottonwood Creek caldera formed on eruption of the newly recognized, 15.70 Ma tuff of Yellow Rock Canyon, which is zoned from high-silica alkali rhyolite to trachyte. The four calderas contain caldera fill deposits, including pumice and ash falls, lahars, phreatomagmatic deposits, and well-bedded lacustrine deposits, which preserve diverse mid-Miocene fossil fauna and flora. Au and U mineralization developed along ring fractures of the Virgin Valley and Cottonwood Creek calderas. After silicic volcanism largely ceased, trachyte, trachyandesite, and alkalic basaltic lavas erupted through the caldera lakes.

Intense silicic volcanism at the HRCC during the interval 16.4–15.5 Ma overlapped the eruption of the Steens and Columbia River Basalts, strongly suggesting a petrogenetic link. We propose that the HRCC and MVF caldera centers are localized where dikes of Steens flood basalt encountered transitional crust west of the craton with a composition and thickness that allowed significant partial melting, based on the O and Nd isotopic values of the rhyolites, which require involvement of crustal melts in their origin. Steens Basalt eruptions largely ceased in the area by the time the oldest caldera-forming ignimbrites erupted at both the HRCC and MVF, indicating that once large silicic magma bodies aggregated in the crust, they intercepted flood basalt dikes. We suggest that the roots of the HRCC and MVF are composed of large volumes of gabbroic intrusions and cumulates formed by fractional crystallization of HRCC magmas, which strengthened the middle crust beneath the calderas; major basin-bounding normal faults are diverted around them, but outflow ignimbrites are prominently offset by Basin and Range faults.

INTRODUCTION

Continental flood basalt provinces represent extraordinary magmatic events during which 10^5–10^6 km^3 of basaltic lava are erupted over timespans as short as 10^5–10^6 m.y. (e.g., Courtillot and Renne, 2003; Bryan and Ernst, 2008). It has been increasingly recognized that they are spatially and temporarily associated with significant volumes of rhyolite erupted as ignimbrites and lavas (e.g., Garland et al., 1995; Bryan et al., 2002, 2010; Courtillot and Renne, 2003; Gibson et al., 2006; Pankhurst et al., 2011; Coble and Mahood, 2012). The youngest and best-exposed continental flood basalt province on Earth is located in the northwestern United States (Fig. 1), represented by the Steens and Columbia River Basalts (e.g., Camp et al., 2013); consequently, it is the locale in which the relationship of flood basalt to rhyolite can be best studied. Although ~98% of the volume of magma that erupted in Washington, Oregon, and Nevada from 16.9 to 15.0 Ma was mafic (Reidel et al., 2013), locally rhyolitic volcanism far exceeded the volume of basalt erupted (Rytuba and McKee, 1984; Cummings et al., 2000; Brueseke et al., 2007; Shervais and Hanan, 2008; Coble and Mahood, 2012). Here the footprint of flood basalt magmatism and its thermal effects on the continental crust can be determined, and the age, location, and volume of silicic magmatism relative to the more voluminous mafic eruptions can be used to differentiate between various models for the origin of flood basalt magmatism.

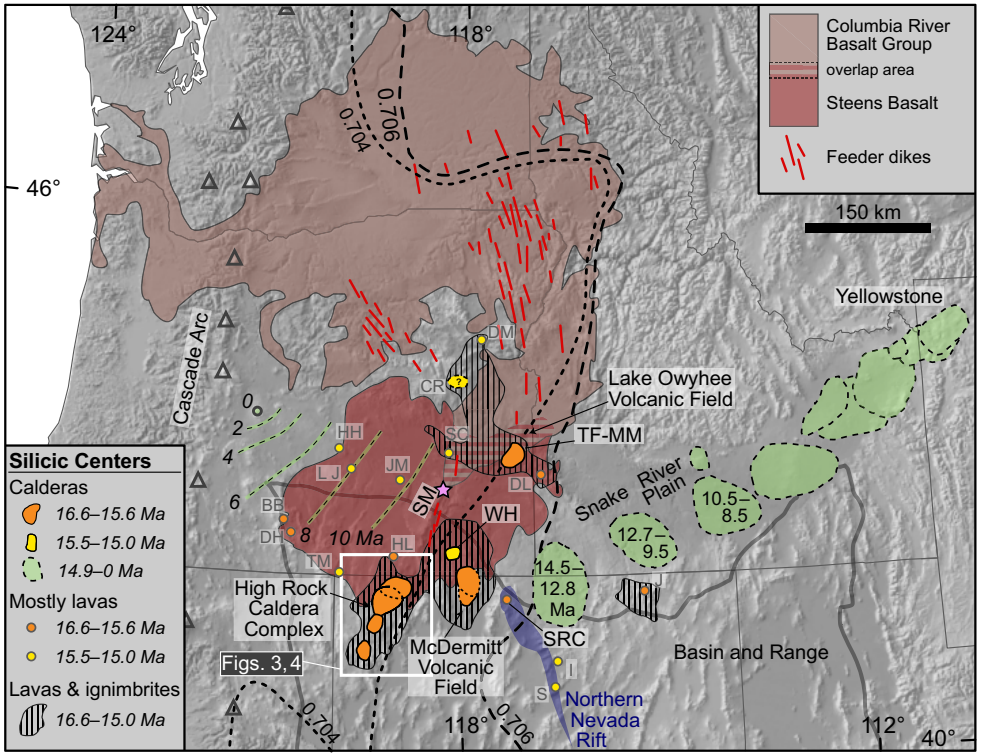

Figure 1. Location map showing the relationship of mid-Miocene silicic centers to contemporaneous Steens and Columbia River Flood Basalt lavas and to the younger rhyolite caldera complexes of the Snake River Plain–Yellowstone trend. SM—Steens Mountain, the site of the thickest accumulation of Steens flood basalt. The largest mid-Miocene caldera centers occur near the $^{87}Sr/^{86}Sr_i = 0.704$ and 0.706 isopleths on transitional crust (dotted, dashed lines; isopleths adapted from Kistler and Peterman, 1973; Armstrong et al., 1977). Lake Owyhee volcanic field contains the TF-MM—Three Fingers Rock–Mahogany Mountain calderas) and a postulated eruptive center at Castle Rock (CR; Streck et al., 2015). The McDermitt volcanic field contains the McDermitt and Whitehorse (WH) calderas. Lava-dominated mid-Miocene rhyolite centers: BB—Bald Butte, DH—Drum Hill, DL—DeLamar–Silver City, DM—Dooley Mountain, HH—Horsehead Mountain, HL—Hawks Valley–Lone Mountain, I—Ivanhoe, J—Jarbidge Rhyolite, JM—Jackass Mountain, LJ—Little Juniper Mountain, S—Sheep Creek Range, SC—Swamp Creek Rhyolite, SRC—Santa Rosa–Calico volcanic field, TM—Twenty Mile Creek. Green dashed lines are 2 Ma isochrons for the inception of rhyolitic volcanism in the High Lava Plains province. Large green centers are inferred silicic calderas beneath the Snake River Plain. Modified from Coble and Mahood (2012); BB, DH, TM centers are from Ford et al. (2013).

Detailed work on caldera-forming silicic magmatism contemporaneous with Steens and Columbia River Basalt volcanism has been published only for the McDermitt volcanic field (MVF) on the Oregon-Nevada border (Rytuba and McKee, 1984; Conrad, 1984). As a result, the McDermitt caldera has tended to be the mid-Miocene silicic center most discussed in petrogenetic models for the flood basalt province and the eastward-younging silicic volcanism of the Snake River Plain (e.g., Hooper et al., 2007; Leeman et al., 2008). In many published models, the initial impingement of a proposed Yellowstone mantle plume head on North American lithosphere is located on the Oregon-Nevada border near the McDermitt caldera (Fig. 1) (e.g., Parsons et al., 1994; Pierce et al., 2002; Hooper et al., 2007; Leeman et al., 2008). The McDermitt caldera is also commonly cited as the starting point for the time-transgressive trend of silicic calderas along the Snake River Plain (e.g., Christiansen and Yeats, 1992; Pierce and Morgan, 1992; Perkins and Nash, 2002; Christiansen et al., 2002; Brueseke et al., 2007; Shervais and Hanan, 2008), and a trend of smaller silicic centers that generally young to the northwest away from McDermitt in the High Lava Plains province in eastern Oregon (Jordan et al., 2004; Ford et al., 2013) (Fig. 1). However, numerous workers have suggested that mid-Miocene silicic volcanism is more widespread (e.g., Christiansen and Yeats, 1992; Pierce and Morgan, 1992; Brueseke and Hart, 2008; Shervais and Hanan, 2008; Coble and Mahood, 2012; Camp et al., 2013; Streck et al., 2015). A compilation by Coble and Mahood (2012) documented that a minimum of 3900 km^3 of rhyolite dense rock equivalent (DRE) erupted over a wide region between 16.5 and 15.0 Ma, contemporaneous with the main phase of Steens and Columbia River Basalt activity, the bulk of it at three major caldera complexes (Fig. 1): the MVF (1665 km^3), Lake Owyhee volcanic field (~1115 km^3), and High Rock caldera complex (HRCC) (~700 km^3).

This paper presents the results of our study of the HRCC, which was named by Ach and Swisher (1990) for a northeast-trending set of 4 calderas ~70 km west-southwest of the McDermitt caldera (Fig. 2). It is part of an effort to genetically link the timing, volume, and distribution of rhyolitic volcanism to models for the origin of flood basalts. Given the prolonged aridity and minimal local extension since the mid-Miocene (Wolfe et al., 1997; Colgan et al., 2006; Mulch et al., 2008), the HRCC has undergone only minor erosion and minimal sedimentation, making it among the best-preserved examples of the original morphology of silicic volcanism related to flood basalt eruptions anywhere on Earth. These centers are also better exposed than the hotspot-related silicic centers in the Snake River Plain, most of which are largely buried by younger Snake River Plain basalts, or, as is the case for the younger than 2.2 Ma volcanism at Yellowstone, are heavily forested.

Supplemental Material Text:
Coble and Mahood – Geosphere

Part 1: PREVIOUS STUDIES AT HIGH ROCK CALDERA COMPLEX
Part 2: DETAILED METHODOLOGY
Part 3: PETROLOGIC AND FIELD EVIDENCE FOR DISTINGUISHING HRCC IGNIMBRITES AND LAVAS
Part 4: ADDITIONAL DESCRIPTIONS FOR GEOLOGIC UNITS IN THE HIGH ROCK CALDERA COMPLEX
Part 5: ADDITION DETAILS ON CALDERAS OF HIGH ROCK CALDERA COMPLEX

Part 1:
PREVIOUS STUDIES AT HIGH ROCK CALDERA COMPLEX

Our efforts at creating a complex-wide understanding of the calderas and major eruptive units that constitute the HRCC are built on more than a century of geologic studies. These began with Merriam (1910, 1911) who identified mammalian fossils of mid-Miocene age within opal-bearing lacustrine sediments at Virgin Valley, and correlated these thick sedimentary sequences with similar deposits near High Rock Canyon and south of Little High Rock Canyon (Figs. 3 and 4) in what are now known to be sediments deposited in caldera lake environments (Hilton et al., 2008; this study).

[1]Supplemental Text File. Discussion of methods, previous studies, and additional descriptions of volcanic units and calderas in the High Rock caldera complex. Please visit http://dx.doi.org/10.1130/GES01162.S1 or the full-text article on www.gsapubs.org to view the Supplemental Text File.

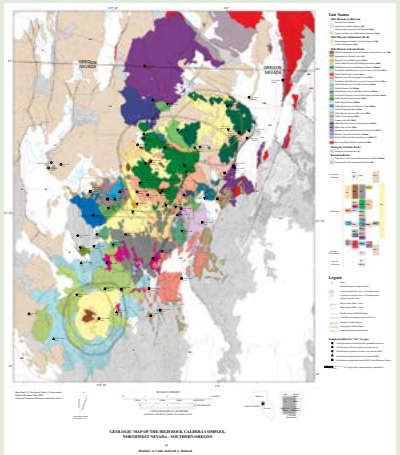

[2]Plate 1. 1:200,000 scale detailed geologic map of the High Rock caldera complex. Please visit http://dx.doi.org/10.1130/GES01162.S2 or the full-text article on www.gsapubs.org to view Plate 1.

[3]Plate 2. Compilation of quadrangle maps for the Bear Buttes, Badger Mountain SE, Nut Mountain, and Massacre Creek 7.5′ quadrangles. Please visit http://dx.doi.org/10.1130/GES01162.S3 or the full-text article on www.gsapubs.org to view Plate 2.

Ours is the first caldera complex–wide study of the HRCC; we delineate individual calderas, establish the stratigraphy of the major ignimbrites, and assign rhyolitic and trachytic lavas to caldera centers. Through regional- and 1:24,000-scale geologic mapping, geochemical correlation, and high-precision $^{40}Ar/^{39}Ar$ geochronology, we have developed a tightly constrained stratigraphy for a 1 m.y. interval in the mid-Miocene. By demonstrating the extraordinary rate of activity concentrated at ca. 16.4–15.5 Ma, and the overlap in age with the outpouring of Steens Basalt and earliest Columbia River Basalt and with similar silicic volcanism at the MVF, we provide a more accurate understanding of the silicic magmatism associated with flood basalt eruptions and the inception of the Snake River Plain–Yellowstone caldera trend.

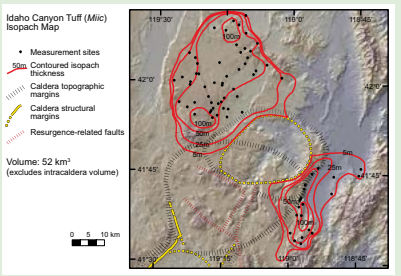

[4]Supplemental Figure 1. Isopach maps for ignimbrites in the High Rock caldera complex. Please visit http://dx.doi.org/10.1130/GES01162.S4 or the full-text article on www.gsapubs.org to view Supplemental Figure 1.

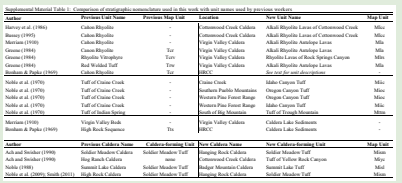

[5]Supplemental Table 1. Comparison of stratigraphic nomenclature used in this work with unit names used by previous workers. Please visit http://dx.doi.org/10.1130/GES01162.S5 or the full-text article on www.gsapubs.org to view Supplemental Table 1.

METHODS

In the Supplemental Text File[1] we discuss in detail our field mapping, sample collection strategy, sample preparation methods, whole-rock major and trace element analyses, Nd and O isotopic analyses, and paleomagnetic work. We also summarize the analytical methods for $^{40}Ar/^{39}Ar$ geochronology, and discuss precision, accuracy, and geologic sources of inaccuracy in the ages.

Field Mapping

We conducted new 1:100,000-scale mapping (Plate 1[2]) of the area shown in Figures 3 and 4 between 2006 and 2012 in order to delineate calderas, correlate individual ignimbrites, and assign ignimbrites and lavas to specific calderas or centers. We also conducted 1:24,000-scale mapping of 4 contiguous quadrangles (Bear Buttes, Badger Mountain SE, Nut Mountain, and Massacre Creek) to investigate a complicated area of overlapping calderas (Figs. 3 and 4; Plate 2[3]). All volume estimates (Table 1) are calculated from mapped extracaldera eruptive exposures (Fig. 5; see Supplemental Fig. 1[4] for isopach maps) and expressed as DRE. Intracaldera deposits are not exposed due to the lack of incision and large-magnitude normal faulting in the HRCC.

Stratigraphic Nomenclature for Eruptive Units

For the major ignimbrites we have used the formal and informal unit names of Noble et al. (1970), except where our new mapping requires they be revised. We draw upon unit names for lavas from Greene (1984) and Korringa (1973), modifying the place names as necessary to be more representative. See Supplemental Table 1[5] for a comparison of the nomenclature used by previous workers with our revised and standardized unit names.

The convention we have followed in forming abbreviations for rhyolitic units on maps, figures, tables, and in the text is as follows: all have the prefix M for Miocene or P for Paleogene, followed by an i for an ignimbrite that is considered a single eruptive unit, t for a tuffaceous unit that represents more than a geologic instant in time because it consists of some combination of multiple ignimbrites, fall and surge deposits, reworked pumice deposits, and minor lavas, or an l for a lava unit, which generally consists of multiple flows that are chemically related and of similar age. These are followed by a one- or two-letter abbreviation for the unit name or location (e.g., sl for Summit Lake Tuff, Misl). In addition, mid-Miocene postcaldera mafic lavas and trachytic intermediate lavas are indicated by Mm and Mt, respectively.

Silicic Rock Classification

The total alkalies versus silica (TAS) classification diagram of LeBas et al. (1986) is of limited utility for rocks with >63 wt% SiO_2 because many different rocks are subsumed under the rhyolite field. We have informally modified the traditional TAS diagram to add fields to provide for greater specificity in naming silicic rocks at the HRCC (Fig. 6). Our modification was prepared by comparing the names applied previously and the compositions of felsic rocks worldwide using the EarthChem Portal (http://www.earthchem.org/portal; accessed August 2013). It explicitly captures the fact that total alkalies generally begin to decline at silica contents >~74 wt% SiO_2 due to the large proportion of alkali feldspar in the fractionating assemblage in a rhyolitic magma approaching minimum-melt composition.

$^{40}Ar/^{39}Ar$ Geochronology

We obtained 70 new $^{40}Ar/^{39}Ar$ ages for rhyolitic lavas and ignimbrites and intermediate and mafic lavas associated with the HRCC employing a Nu-Instruments Noblesse noble gas mass spectrometer at Stanford University (Stanford, California) in multicollector mode using methods described in Coble et al. (2011). Single sanidine grains or individual groundmass fragments were fused using a 10W CO_2 laser. No step-heating analyses were performed. Analyses were conducted during consecutive analytical sessions under the same instrument conditions; the circumstances in which the $^{40}Ar/^{39}Ar$

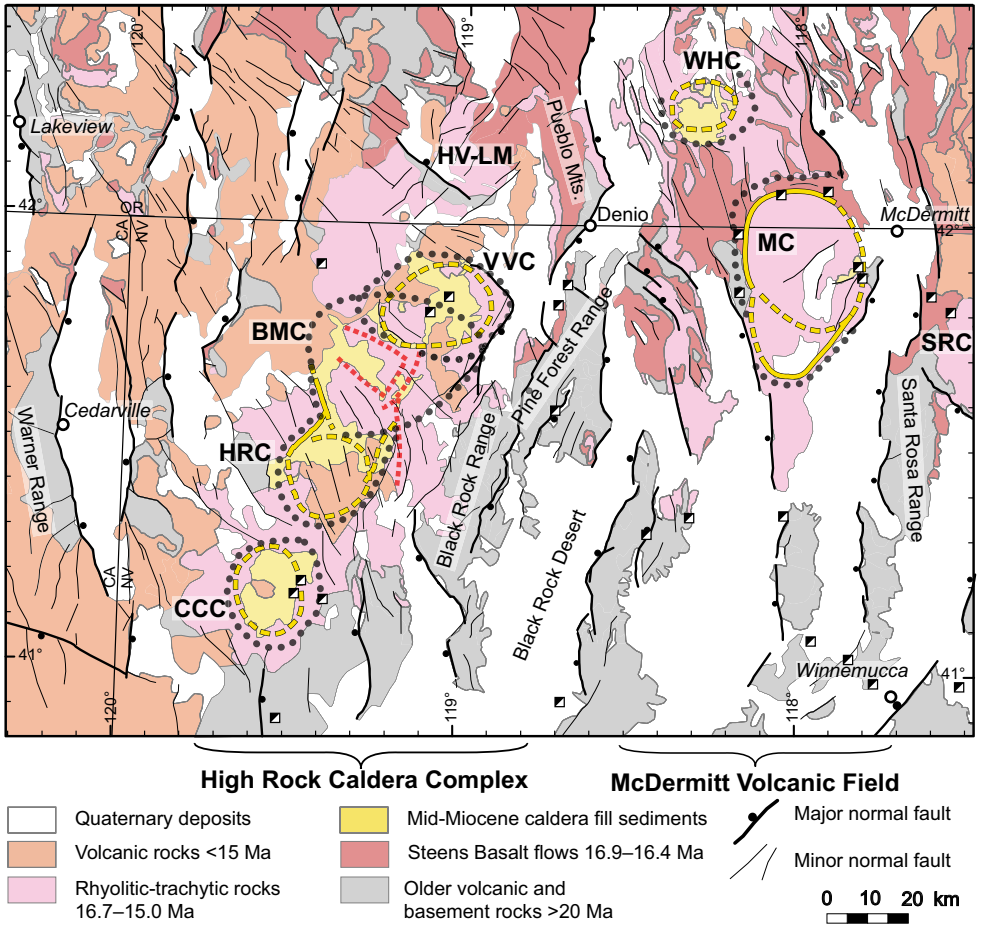

Figure 2. Regional geologic map showing the High Rock caldera complex (HRCC) and McDermitt volcanic field with known extent of the mid-Miocene rhyolitic ignimbrites and lavas from these centers (pink). Locations of caldera topographic margins are shown as dotted black lines; structural margins are shown in yellow; and trapdoor uplift–related faults are indicated by red dashed lines. Mines are shown as half-filled boxes. Four major calderas make up the HRCC: Virgin Valley caldera (VVC), Badger Mountain caldera (BMC), Hanging Rock caldera (HRC), and Cottonwood Creek caldera (CCC). The McDermitt volcanic field (Rytuba and McKee, 1984) contains the McDermitt caldera (MC) and the Whitehorse caldera (WHC), both of which may have undergone multiple collapse events. Hawks Valley–Lone Mountain center (HV-LM) and the Santa Rosa—Calico center (SRC) contain lavas of similar age (Wypych et al., 2011; Brueseke et al., 2007) and may represent extensions of the HRCC and MVF trends, respectively.

method has the greatest precision in distinguishing between the ages of units.

Total-fusion sanidine and groundmass ages are reported as weighted means and 2σ standard errors. Inverse-isochron ages are the calculated York fit intercept and 2σ error (York, 1968). Reported 2σ standard errors for total-fusion model ages are multiplied by the square root of the mean square of weighted deviates (MSWD) when the latter exceeded the range expected for a homogeneous population based upon Monte Carlo simulations (Mahon, 1996). All reported ages are calculated relative to a model age of 28.02 Ma for Fish Canyon sanidine (Renne et al., 1998).

Our preferred ages for eruptive units are listed in Table 1. Representative results for single-grain analyses of alkali and feldspar are illustrated in Figure 7 and results for devitrified groundmass of rhyolite lava and microcrystalline groundmass of trachyte and basalt lavas are in Figure 8. (Full information for all the analyses is available in Supplemental Table 2[6] and a discussion of analytical methods in the Supplemental Text File.)

PREVIOUS STUDIES AT THE HRCC

Our work reconstructing the geologic history of the calderas and major eruptive units that constitute the HRCC builds on more than a century of geologic studies. These began with Merriam (1910), who identified mammalian fossils of mid-Miocene age within what are now known to be sediments deposited in caldera lake environments (Hilton et al., 2008; this study). Noble et al. (1970) were the first to assign names to ignimbrites in northwest Nevada, obtain K-Ar dates that established their mid-Miocene ages, and propose potential sources. Subsequent work by Noble and colleagues (e.g., Korringa, 1973; Park, 1983; Noble et al., 2009; Smith et al., 2010; Smith, 2011) elucidated the volcanology and petrology of the Soldier Meadow Tuff and tuff of Trough Mountain and their relationship to possible calderas. Geologic mapping by the U.S. Geological Survey that focused on assessing resources in lands set aside as the Sheldon National Wildlife Refuge and as potential wilderness areas (e.g., Greene, 1984; Greene and Plouff, 1981; Ach, 1988, Ach and Swisher, 1990; Ach et al., 1991) furthered the understanding of the stratigraphy and the location of calderas. In particular, Ach and Swisher (1990) were the first to recognize the presence of four major calderas. Investigations of mineralization at the Virgin Valley caldera (Castor and Henry, 2000; Rytuba et al., 2010) and Cottonwood Creek caldera (Harvey et al., 1986; Bussey, 1996) (Fig. 4) have shown a strong correlation between the location of postcaldera ring-fracture rhyo-

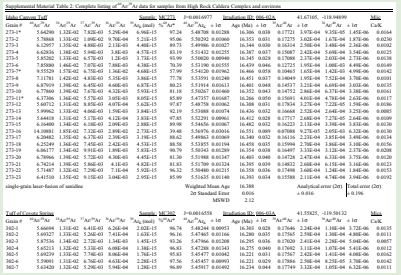

[6]Supplemental Table 2. Complete listing of $^{40}Ar/^{39}Ar$ data for samples from the High Rock caldera complex and environs. Please visit http://dx.doi.org/10.1130/GES01162.S6 or the full-text article on www.gsapubs.org to view Supplemental Table 2.

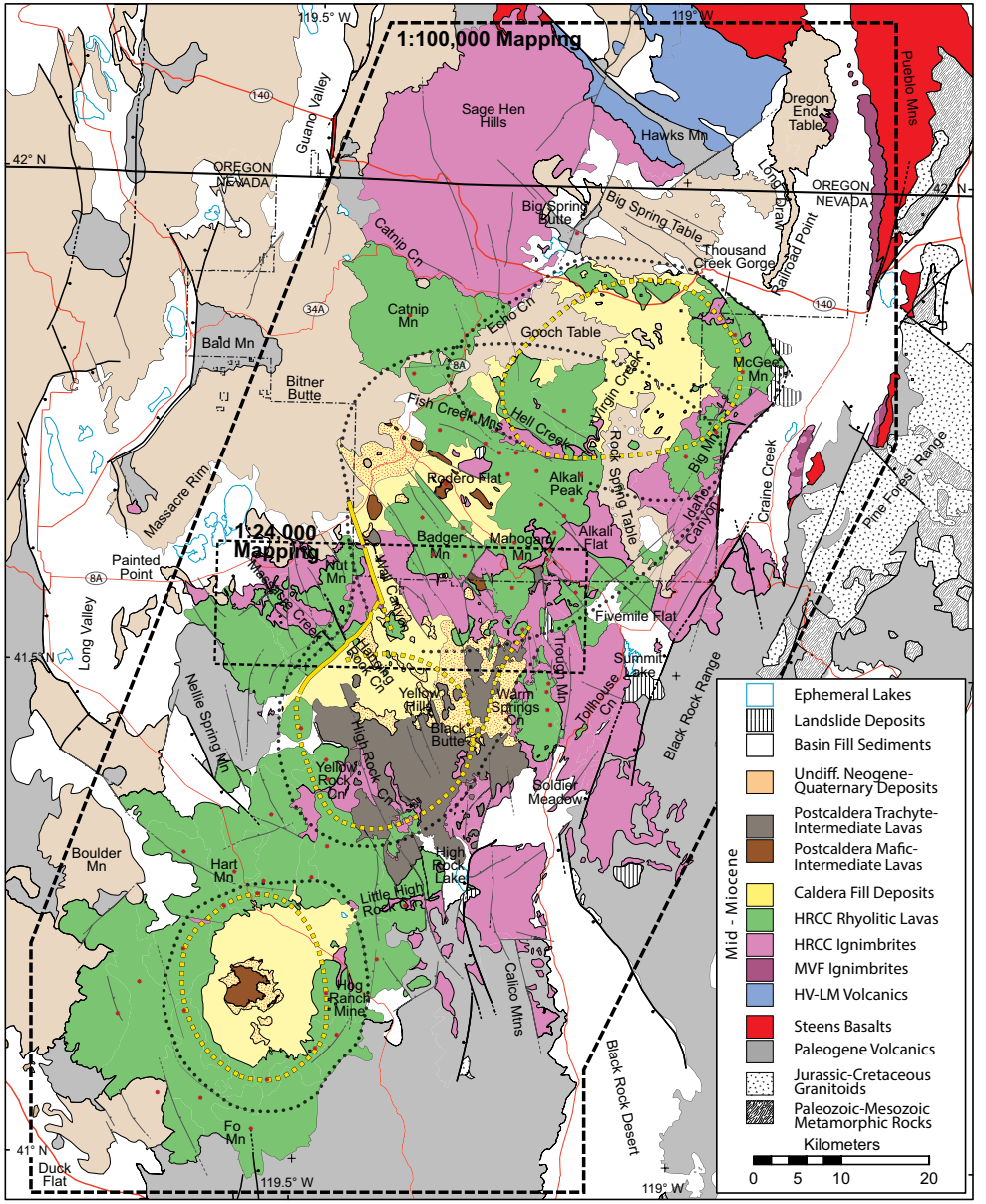

Figure 3. Generalized geologic map of High Rock caldera complex (HRCC) and surrounding region. Location names referred to in the text are shown here or appear on U.S. Geological Survey 1:100,000-scale topographic maps (Mn—mountain). The Sheldon National Antelope Refuge is outlined with a black dash-dot line. The locations of 1:100,000- and 1:24,000-scale maps in Plates 1 and 2 are outlined with the bold and fine black dashed lines, respectively. Paved and maintained dirt roads are shown with thin red lines. Normal faults with >50 m of offset are shown as thick black lines; smaller faults are shown as thin black lines. Individual silicic lavas and ignimbrites are grouped together for simplicity, but are differentiated in Figure 4 and Plates 1 and 2. MVF—McDermitt volcanic field; HV-LM—Hawks Valley–Lone Mountain center. Caldera structures are shown as dotted black, dashed yellow, and dashed red lines as in Fig. 2.

litic intrusions with mineralization by gold, silver, uranium, lithium, gallium, and mercury. For a more extensive discussion of how our study builds on previous work, see the Supplemental Text File.

Summary of Eruptive History of the HRCC

The results of our mapping, geochronology, geochemistry, and paleomagnetic measurements indicate that the HRCC consists of eruptive products associated with 4 calderas that erupted over a period of ~1 m.y. starting ca. 16.6 Ma (Figs. 2 and 4). We summarize that history (Table 1; Fig. 5 [see Supplemental Fig. 2[7] for a printable version of interactive Fig. 5]) and discuss the detailed geology of individual units and calderas in the following sections. Unit abbreviations in parentheses are referenced on maps (Fig 4; Plates 1 and 2) and throughout the text. All volume estimates for ignimbrites (calculated as DRE) are for outflow sheets, as the lack of incision makes accurate estimates of intracaldera volumes impossible.

We have delineated four major calderas, which decrease in age from northeast to southwest (Figs. 2, 4, and 5). The oldest, the Virgin Valley caldera, formed at 16.38 Ma on eruption of the mineralogically and chemically zoned alkali rhyolite Idaho Canyon Tuff (Miic), which has a minimum calculated volume of 52 km^3 (Table 1). Within only a few tens of thousands of years, eruption of the strongly porphyritic, low-silica rhyolite Summit Lake Tuff (Misl), dated as 16.34 Ma, caused collapse of the

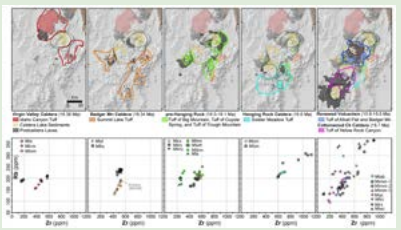

[7]Supplemental Figure 2. Printable version of Figure 5 (not interactive) showing the schematic summary of the volcanic evolution of the High Rock caldera complex. Please visit http://dx.doi.org/10.1130/GES01162.S7 or the full-text article on www.gsapubs.org to view Supplemental Figure 2.

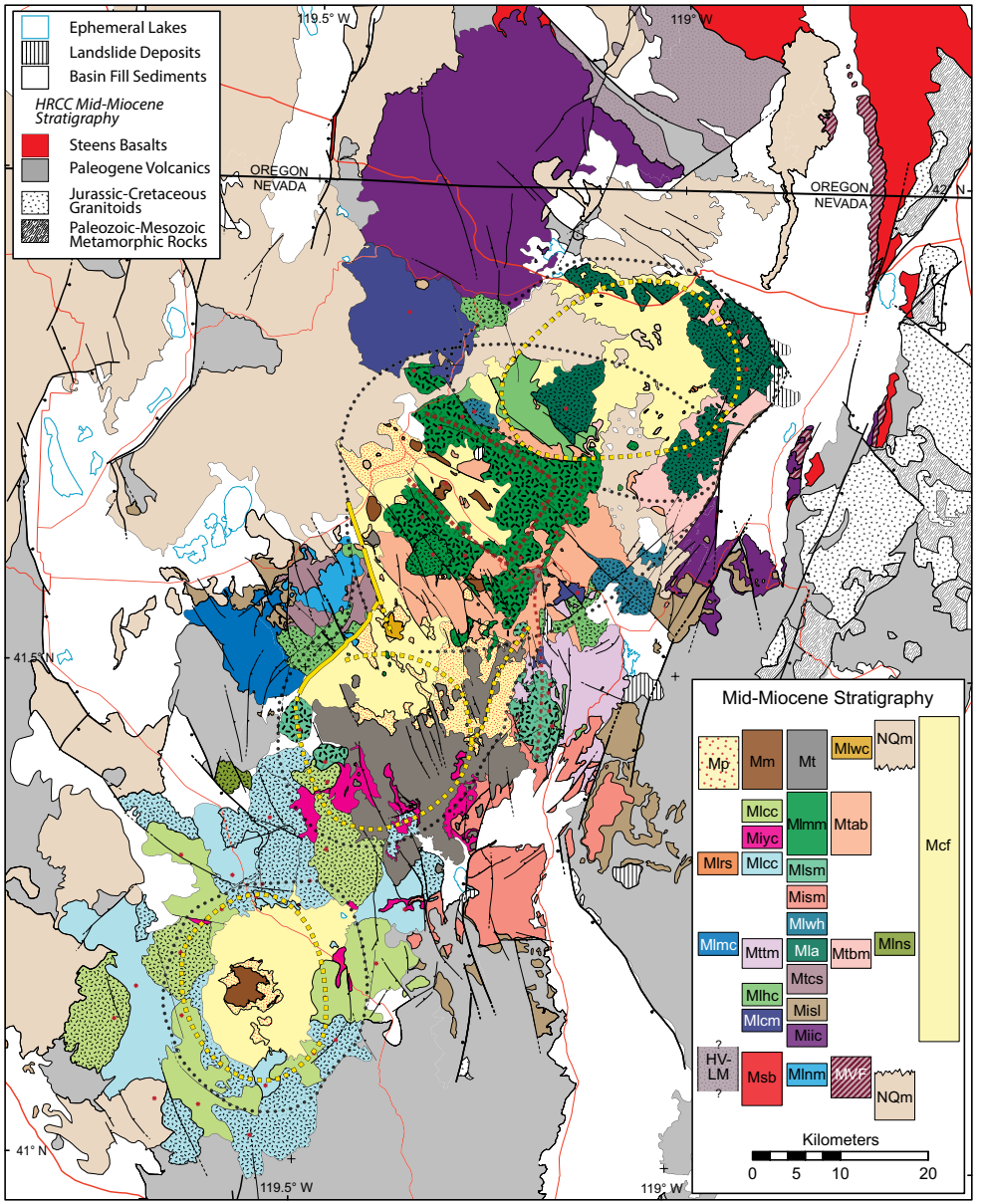

Figure 4. Geologic map of the High Rock caldera complex (HRCC). Mid-Miocene caldera-forming ignimbrites are in shades of purple, pink, and brown, and lavas are shown in blue and green. Caldera topographic margins are shown as dotted black lines, structural margins as yellow dashed lines, and trapdoor uplift–related faults as red dashed lines; all other line symbols are as in Figure 3. See text or Table 1 for unit abbreviations. See Plate 1 for a version of this map at 1:200,000 scale that includes locations for dated samples. Line patterns on silicic lavas reflect phenocryst content: coarse pattern: >10% phenocrysts; fine pattern: <10% phenocrysts; no pattern: aphyric.

Badger Mountain caldera, which overlapped the southern margin of the Virgin Valley caldera. Approximately 100 k.y. after eruption of the Summit Lake Tuff, >55 km^3 of crystal-poor alkali rhyolite Antelope lavas (Mla) and compositionally similar small-volume pyroclastic units referred to as the tuff of Big Mountain (Mtbm) vented along reactivated ring faults of the Virgin Valley caldera.

South of the Badger Mountain caldera, there are curvilinear faults and vent alignments for 16.3–16.2 Ma crystal-poor alkali rhyolite lavas. Adjacent to these are exposures of densely welded ignimbrites of similar compositions, the newly identified 16.27 Ma tuff of Coyote Spring (Mics) and the 16.25–16.15 Ma tuff of Trough Mountain (Mttm). We suggest that these ignimbrites erupted from areas now preserved as scallop-shaped collapse features that represented migration of the caldera focus southwestward. The tuffs of Coyote Spring and Trough Mountain now form high-standing massifs (Figs. 3 and 4) due to magmatic uplift that culminated in eruption of more strongly alkalic rhyolite lavas along the northern ring fracture of the next major caldera, the Hanging Rock caldera. It formed at 16 Ma as a result of eruption of an estimated volume of ~65 km^3 of strongly porphyritic, alkali rhyolite of the Soldier Meadow Tuff (Mism). It is the most peralkaline of the major ignimbrites erupted at the HRCC. Shortly following collapse of the Hanging Rock caldera, the Soldier Meadow alkali rhyolite lavas (Mlsm), which are petrographically and chemically similar to the Soldier Meadow Tuff, erupted within the caldera and along an arcuate, north-south–trending vent array sympathetic to the eastern caldera margin.

TABLE 1. SUMMARY OF GEOLOGIC HISTORY OF THE HIGH ROCK CALDERA COMPLEX AND $^{40}Ar/^{39}Ar$ AGES FOR MAJOR UNITS

Caldera name and size (km)	Unit name	Map unit	Volume (km^3)	Phenocryst content (%)	Rock composition*	Rock sample type†	Material dated§	WM age ±2σ SE** (Ma)	n	MSWD	Sample no.	Analysis type**
Precaldera	Precaldera mafic and intermediate lavas	–	n.d.	4–8	B	L	MM	16.6 ± 0.6	10	6.65	AT6	WM
		–			T	L	MM	16.75 ± 0.39	10	2.65	AT31	II
	Nut Mountain lavas	Mlnm	14	0	HSR	D	DM	16.59 ± 0.15	9	8.88	MC341	II
Virgin Valley (24 × 34)	**Idaho Canyon Tuff**	$Miic_b$	52	15–20	HAR	DW	S	16.37 ± 0.02	12	0.28	MC274	WM
						DW	S	16.40 ± 0.04	8	1.04	H95-74 (C)	WM
		$Miic_a$		4–8	HAR	DW	S	16.37 ± 0.02	10	0.49	MC502	WM
						DW	S	16.39 ± 0.02	20	2.12	MC273	WM
	Catnip Mountain lavas	Mlcm	38	0	HAR	D	DM	16.33 ± 0.12	10	3.16	MC317	WM
						D	DM	16.31 ± 0.13	11	5.54	MC504	II
Badger Mountain (30 × 40)	**Summit Lake Tuff**	Misl	31	25–32	LAR	DW	A	16.35 ± 0.02	10	0.46	MC611	WM
						DW	A	16.34 ± 0.02	12	0.68	MC85	WM
						V	A	16.31 ± 0.03	12	1.06	MC365	WM
						DW	A	16.29 ± 0.03	11	0.66	MC263	WM
Pre–Hanging Rock	**Tuff of Big Mountain**	Mtbm	23	2–5	HAR	V	S	16.23 ± 0.03	9	1.01	H95-72 (C)	WM
						V	S	16.13 ± 0.03	10	1.36	MC326	WM
	Antelope lavas	Mla	57	8–15	HAR	D	S	16.27 ± 0.04	9	1.55	H95-63 (C)	WM
						D, S	S	16.25 ± 0.03	10	2.19	MC413	WM
						D	S	16.20 ± 0.04	7	1.28	H95-71 (C)	WM
	Tuff of Coyote Spring	Mics	5	4–9	HAR	DW	S	16.27 ± 0.04	12	0.26	MC302	WM
						DW	S	16.27 ± 0.02	11	0.87	MC302	WM
	Tuff of Trough Mountain	Mttm	13	2–6	HAR	MW	S	16.25 ± 0.03	10	2.06	MC212	WM
						DW	S	16.15 ± 0.02	11	1.30	MC124	WM
	Hell Creek lavas	Mlhc	12	0–11	HAR	D, E	S	16.31 ± 0.03	10	1.99	MC430	WM
					HAR	D	S	16.29 ± 0.02	10	0.72	MC244	WM
					HAR	D	S	16.22 ± 0.02	9	0.66	MC433	WM
	Nellie Spring Mountain lavas	Mlns	1	3–7	LAR	D	S	16.21 ± 0.02	10	1.93	MC271	WM
	Massacre Creek lavas	Mlmc	22	0	HAR	D	DM	16.20 ± 0.03	18	1.50	MC308	II
	Wild Horse Pasture lavas	Mlwh	4	2–5	HAR	D	S	16.10 ± 0.02	12	0.62	MC423	WM
Hanging Rock (25 × 30)	**Soldier Meadow Tuff**	Mism	65	35–48	HAR	DW	S	16.00 ± 0.02	10	1.71	MC121	WM
						DW	S	16.01 ± 0.02	12	1.06	MC369	WM

(*continued*)

TABLE 1. SUMMARY OF GEOLOGIC HISTORY OF THE HIGH ROCK CALDERA COMPLEX AND $^{40}Ar/^{39}Ar$ AGES FOR MAJOR UNITS (*continued*)

Caldera name and size (km)	Unit name	Map unit	Volume (km^3)	Phenocryst content (%)	Rock composition*	Rock sample type†	Material dated§	WM age ±2σ SE** (Ma)	n	MSWD	Sample no.	Analysis type**
Renewed magmatism at Rodero Flat	**Tuff of Alkali Flat**	Mtab	20	32–42	HAR	V	S	15.84 ± 0.02	10	1.03	MC429B	WM
						V	S	15.80 ± 0.03	9	0.58	MC217	WM
	Tuff of Badger Mountain			35–45	HAR	V	S	15.71 ± 0.02	10	0.94	MC314	WM
	Soldier Meadow lavas	Mlsm	9	33–43	HAR	D, S	S	[16.12 ± 0.02]	11	1.07	MC376	WM
					HAR	D	S	15.96 ± 0.02	10	0.96	MC213	WM
					HAR	D	S	15.89 ± 0.02	11	0.92	MC315	WM
	Mahogany Mountain lavas	Mlmm	53	2–55	HAR	D	S	15.89 ± 0.02	9	1.76	MC505	WM
					HAR	D	S	15.79 ± 0.03	7	0.19	H95-57 (C)	WM
					HAR	D, S	S	15.72 ± 0.04	10	2.04	MC346	WM
					HAR	D	S	15.71 ± 0.02	9	1.16	MC357	WM
					HAR	D	S	15.67 ± 0.02	11	0.61	MC513	WM
					HAR	D	S	15.67 ± 0.02	12	0.71	MC421	WM
					HAR	D	S	15.56 ± 0.02	11	1.56	MC333	WM
					HAR	D	S	15.51 ± 0.02	13	1.31	MC420	WM
					HAR	D, S	S	[15.59 ± 0.02]	11	1.10	MC238	WM
					HAR	D, S	S	15.97 ± 0.02	10	1.33	MC230	WM
Cottonwood Creek (24 × 28)	Precaldera Cottonwood Creek lavas	Mlcc	136	0–8	HAR	D	DM	15.91 ± 0.04	11	1.21	MC137	II
					HAR	D	DM	15.82 ± 0.03	13	0.54	MC415	II
					HAR	D	S	15.75 ± 0.02	11	1.02	MC254	WM
	Tuff of Yellow Rock Canyon	Miyc	50	7–16	HAR	P	S	15.69 ± 0.01	12	1.44	MC256	WM
					HAR	P	S	15.71 ± 0.03	12	1.90	MC428	WM
					T	P	A	[15.81 ± 0.03]	10	3.84	MC364	WM
	Postcaldera Cottonwood Creek lavas	Mlcc	84	0–8	HAR	D	DM	15.78 ± 0.07	12	2.71	MC370	II
					HAR	D	S	15.69 ± 0.02	11	1.45	MC385	WM
					HAR	P	S	15.66 ± 0.02	11	0.90	MC138	WM
Post–HRCC mafic to intermediate magmatism	Intermediate lavas	Mt	n.d.	1–5	T	L	MM	15.44 ± 0.07	12	3.56	MC249	II
	Alkali olivine basalt, basalt, and trachybasaltic andesite lavas	Mm	n.d.	1–5	B	L	MM	15.55 ± 0.06	12	1.12	MC89	WM
					TA	L	MM	15.08 ± 0.05	11	1.74	MC506	II
					TBA	L	MM	14.84 ± 0.03	11	0.95	MC237	WM
					TA	L	MM	14.5 ± 0.8	10	6.58	MC390	II
					B	L	MM	14.21 ± 0.04	9	1.28	MC266	WM
Post–HRCC metaluminous rhyolites	Rock Springs lavas	Mlrs	<1	8–11	TR	D	B	15.85 ± 0.15	11	1.25	H95-106 (C)	PL
	Wall Canyon lavas	Mlwc	<1	0–3	HSR	D	DM	14.68 ± 0.29	10	4.45	MC330	II
Late Miocene to Pleistocene basalts	Low-K olivine tholeiite lavas	NQm	n.d.	1–4	B	L	MM	10.1 ± 1.2	6	1.04	MC381	II
					B	L	MM	7.5 ± 0.9	9	4.89	MC358	II
					B	L	MM	4.7 ± 0.8	6	1.42	AT26	II
			n.d.	4–8	B	L	MM	4.4 ± 0.7	6	0.15	AT13	II

Note: HRCC—High Rock Caldera Complex; MSWD—mean square of weighted deviations; (C) indicates age from Castor and Henry (2000); n.d.—not determined; dash indicates no map unit.
*Rock composition: B—basalt, TBA—trachybasaltic andesite, TA—trachyandesite, T—trachyte, TR–trachyrhyolite, LAR—low-Si alkali rhyolite, HAR—high-Si alkali rhyolite, HSR—high-Si rhyolite.
†Sample type: P—pumice lapilli in tuff, V—vapor phase–altered ignimbrite, MW—moderately welded ignimbrite, DW—densely welded ignimbrite, S—silicified, D—devitrified rhyolitic lava, E—enclave in lava, L—lava.
§Material dated: S—sanidine, A—anorthoclase, B—biotite, DM—devitrified matrix, MM—microcrystalline matrix.
**Age calculation: WM—weighted mean age; SE—standard error; II—inverse isochron age; PL—plateau age. New and published ages are calculated using $\lambda = 5.543e^{-10}$ yr^{-1} (Steiger and Jäger; 1977) and referenced to an age of 28.02 Ma for the Fish Canyon Tuff (Renne et al., 1998). Ages in brackets are obtained from strongly altered samples and/or samples interpreted to have contained extraneous radiogenic ^{40}Ar and are interpreted to be inaccurate (see text).

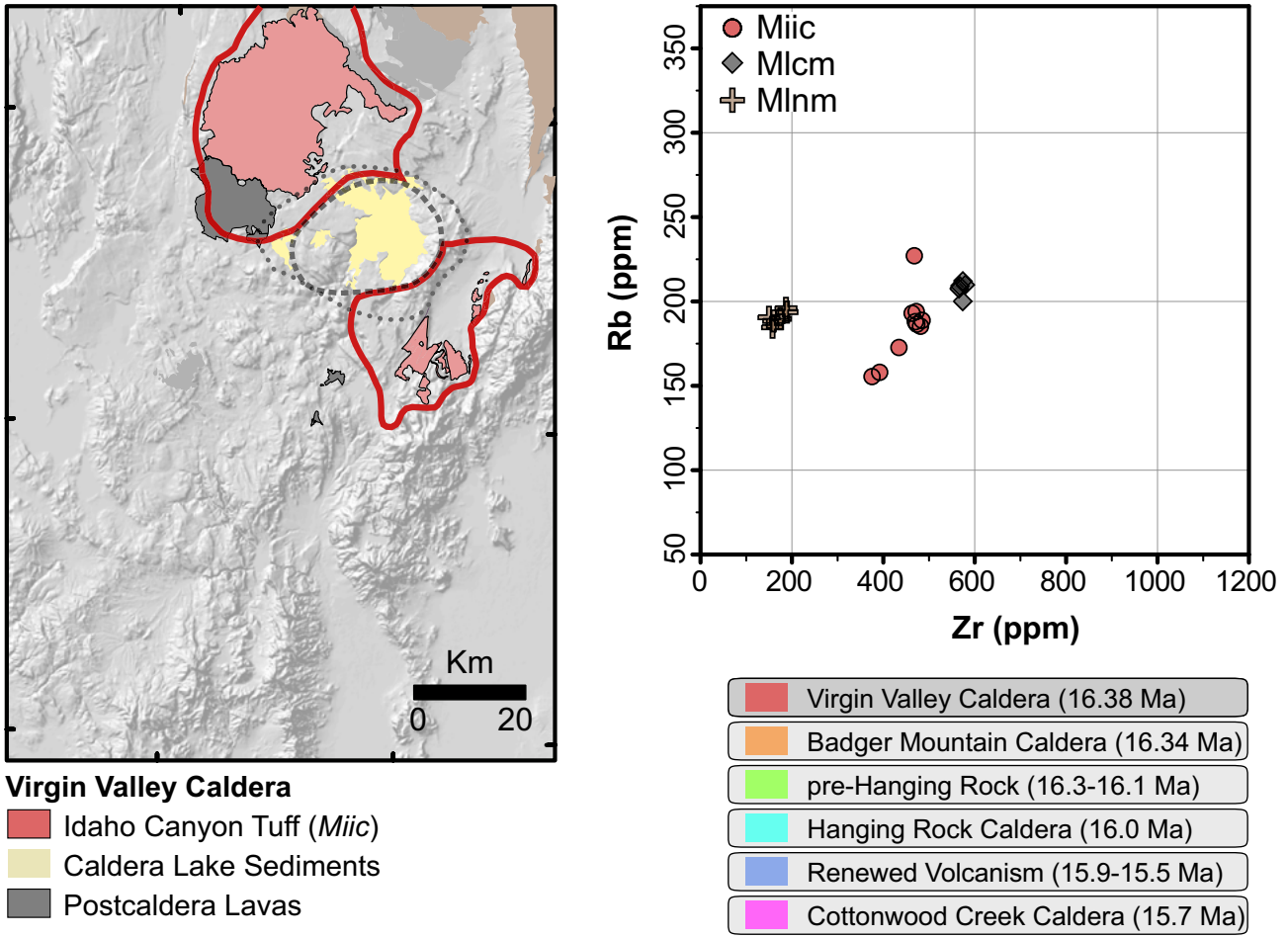

Figure 5. Schematic summary of the volcanic evolution of the High Rock caldera complex. Left panel illustrates how the focus of silicic volcanism and calderas initially migrated south with time. Outcrops of ignimbrites for each time interval are shown outlined in black, with estimated original distributions outlined in thick, solid, colored lines. Right panel plots Rb versus Zr for rhyolitic ignimbrites, tuffs, and lavas as a function of time, and illustrates how lavas associated with calderas have compositions similar to trends defined by caldera-forming ignimbrites. To activate the interactive image and display different eruptive units, roll over caldera names. A printable version of this figure is available as Supplemental Figure 2. See text or Table 1 for unit abbreviations.

Beginning ca. 15.95 Ma, shortly following eruption of the Soldier Meadow Tuff, renewed magma influx focused beneath the Badger Mountain caldera resulted in uplift and eruption of three chemically distinct generations of alkali rhyolite lavas of Mahogany Mountain (Mlmm); these lavas erupted over a period of 0.4 m.y. (Fig. 5). Vents were focused along the inferred ring fracture for the buried southern margin of the Virgin Valley caldera and along northwest- and north-northeast–trending faults related to trapdoor uplift within the Badger Mountain caldera. Associated with these lavas are small-volume crystal-rich, alkali rhyolite ignimbrites and fall deposits, the tuffs of Alkali Flat and Badger Mountain (Mtab), which erupted between ca. 15.85 and 15.7 Ma, and mostly ponded within the Badger Mountain caldera.

Contemporaneous with renewed magmatism in the Badger Mountain caldera, aphyric and weakly porphyritic alkali rhyolite magmas were erupting at the youngest and southernmost major caldera in the HRCC, the Cottonwood Creek caldera (Fig. 5). We propose that it collapsed on eruption of the newly identified tuff of Yellow Rock Canyon (Miyc) at 15.70 Ma. The tuff of Yellow Rock Canyon is the most strongly zoned ignimbrite in the HRCC, ranging from crystal-poor, high-silica alkali rhyolite to trachyte with ~10% phenocrysts. In contrast to other calderas at the HRCC, the volume of aphyric and crystal-poor precaldera and postcaldera ring-fracture alkali rhyolite lavas of Cottonwood Creek (Mlcc), ~220 km^3, greatly exceeds the estimated volume of the outflow ignimbrite, ~50 km^3, though the latter is a minimum estimate due to its poor preservation.

The youngest eruptions of alkali rhyolite lavas along the Cottonwood Creek caldera ring fracture

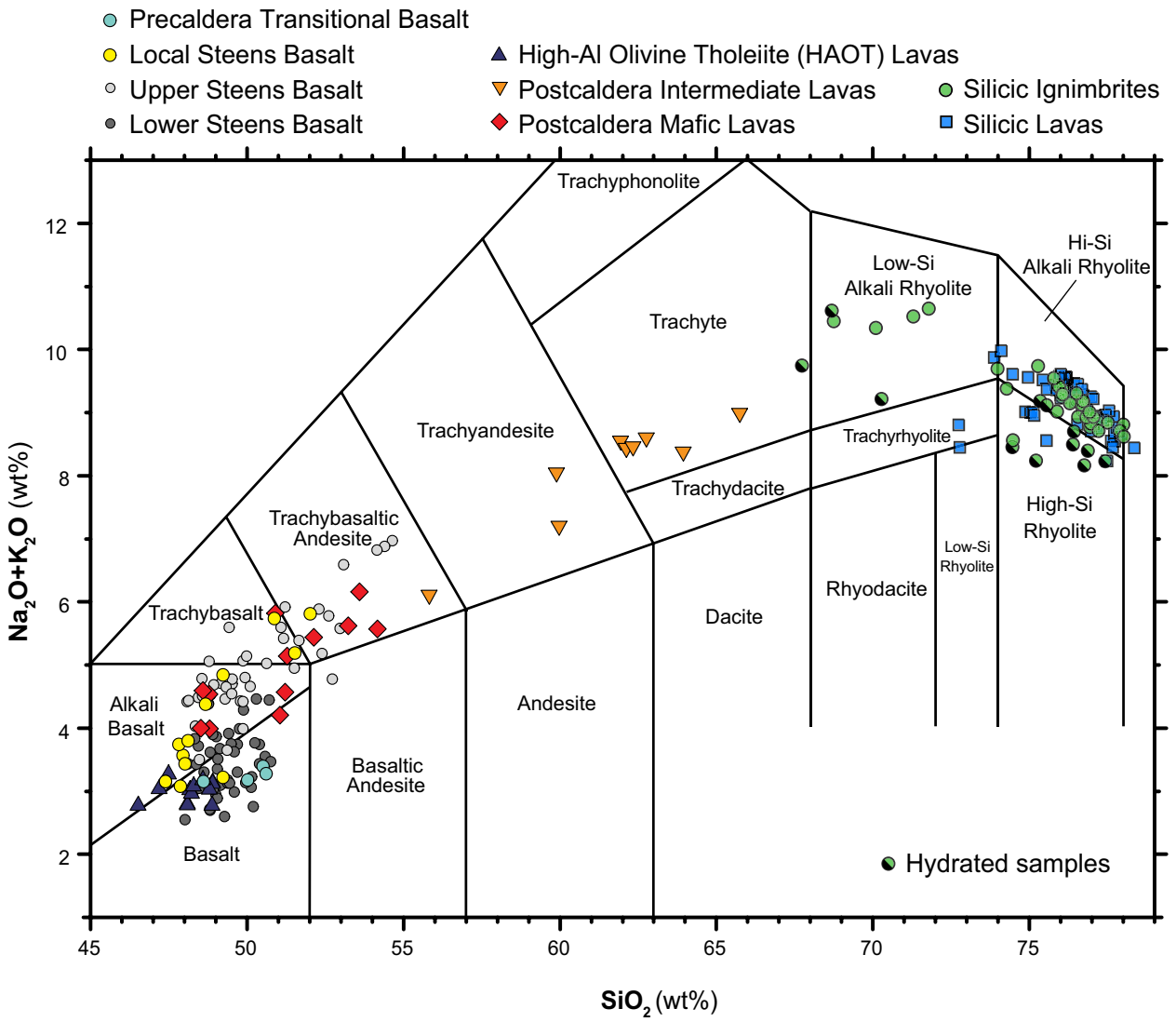

Figure 6. Total alkalies versus silica (TAS) classification of rocks in and adjacent to High Rock caldera complex (HRCC). The diagram was modified from Le Bas et al. (1986) at >63 wt% SiO_2 to allow greater specificity in naming silicic rocks (see text for discussion), and a boundary between the basalt and alkali basalt fields was added based on Macdonald (1986). We plot silicic rocks that are strongly hydrated (loss on ignition >3%, mostly pumice lapilli) with a half-darkened symbol because such rocks are subject to alkali loss sufficient to cause erroneous classification on the TAS diagram. Data for upper and lower Steens Basalt are from Johnson et al. (1998); Steens Basalt in areas around HRCC (shown as local Steens Basalt) are from Hart et al. (1989), Colgan et al. (2006), and this study.

occurred a few tens of thousands of years after caldera collapse, and ceased by ca. 15.6 Ma; the youngest of the uplift-related rhyolitic lavas in the Badger Mountain caldera are ca. 15.5 Ma. These eruptions marked the cessation of peralkaline rhyolitic volcanism in the HRCC, followed by eruption between ca. 15.5 and 14.2 Ma of alkalic mafic lavas inside the Cottonwood Creek and Badger Mountain calderas and trachytic intermediate lavas along the southern ring fracture of the Hanging Rock caldera. Also during this interval, chemically distinct, small-volume metaluminous rhyolite lavas erupted within the Hanging Rock and Virgin Valley calderas.

Erosion due to draining of three lakes that occupied the overlapping Hanging Rock and Badger

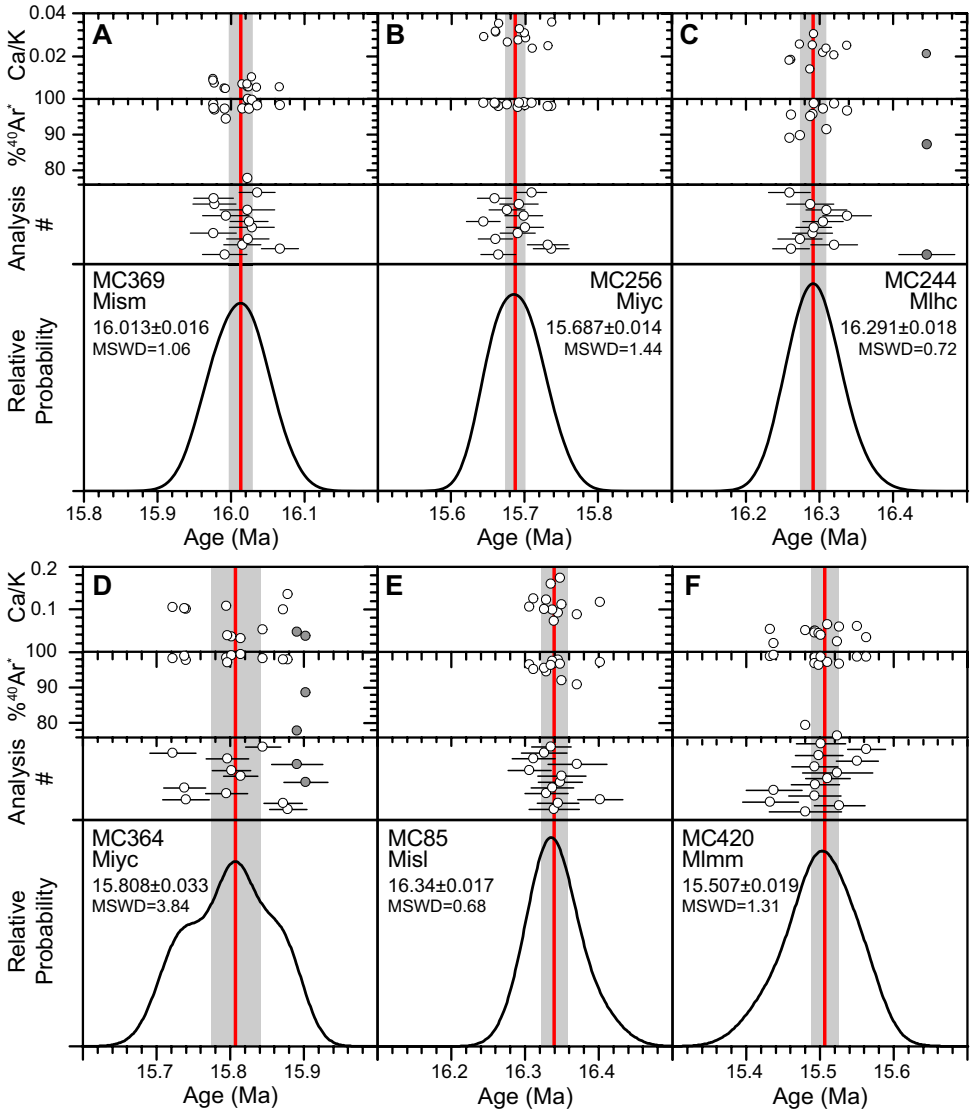

Figure 7. Representative $^{40}Ar/^{39}Ar$ age distributions for single-grain analyses of sanidine and anorthoclase and calculated weighted mean model ages from representative rhyolitic ignimbrite and lavas samples. The top panel of each diagram is the Ca/K of the grains, with values <0.1 reflecting sanidine and >0.1 reflecting anorthoclase. The second panel from the top is the radiogenic yield (%$^{40}Ar^*$) for individual analyses. The third row of panels shows calculated $^{40}Ar/^{39}Ar$ ages and 1σ errors for individual grains in consecutive order with the first analysis on the bottom. The bottom panels show weighted mean ages (red line), 2σ standard error (gray bars), mean square of weighted deviations (MSWD), and probability density curve from the individual ages. Individual $^{40}Ar/^{39}Ar$ analyses shown in gray were omitted from the calculated age and probability density functions. See text or Table 1 unit for abbreviations.

Mountain calderas, the Cottonwood Creek caldera, and the Virgin Valley caldera removed most of the caldera fill deposits, and carved striking gorges through ring-fracture lavas at High Rock Canyon (of emigrant trails fame), Little High Rock Canyon, and Thousand Creek Gorge, respectively. In the northern part of the HRCC the mid-Miocene volcanic and sedimentary rocks are covered and preserved by mesas capped by nearly flat-lying late Miocene high-Al olivine tholeiite lavas.

GEOCHEMISTRY AND PETROGRAPHY

Silicic Lavas and Ignimbrites

Mineralogy of Silicic Units

The phenocryst contents and assemblages of the major silicic units are summarized in Table 2. The vast majority of the silicic rocks are moderately peralkaline alkali rhyolites (Fig. 6) characterized by a single feldspar, sodic sanidine, as a near-liquidus phase. Rhyolites with >5%–8% crystals also contain phenocrystic quartz, with the ratio of sanidine to quartz decreasing with increasing abundance of phenocrysts. Trachytes either lack quartz or have feldspar:quartz > 10. In the low-silica alkali rhyolite of the Summit Lake Tuff, the alkali feldspar phenocrysts are anorthoclase (Fig. 9), with small amounts of resorbed plagioclase visible in thin sections (Fig. 10). In many of the ignimbrites, alkali feldspar and quartz phenocrysts are transparent in nonwelded to partially welded exposures, but in densely welded and devitrified specimens the feldspars are adularescent blue and the quartz is gray, dark gray, to nearly black.

Mafic phenocryst phases are sparse and difficult to see in hand specimen in the silicic rocks, except in pumiceous specimens, and are commonly strongly altered in vapor phase or silicified rocks; thus, they are only rarely diagnostic for mapping purposes. In thin section (Fig. 10), the porphyritic rhyolitic samples contain some combination of sodic clinopyroxene, sodic amphibole, and/or opaque Fe-Ti oxides (typically oxidized and exsolved). Sodic clinopyroxene is aegirine augite in

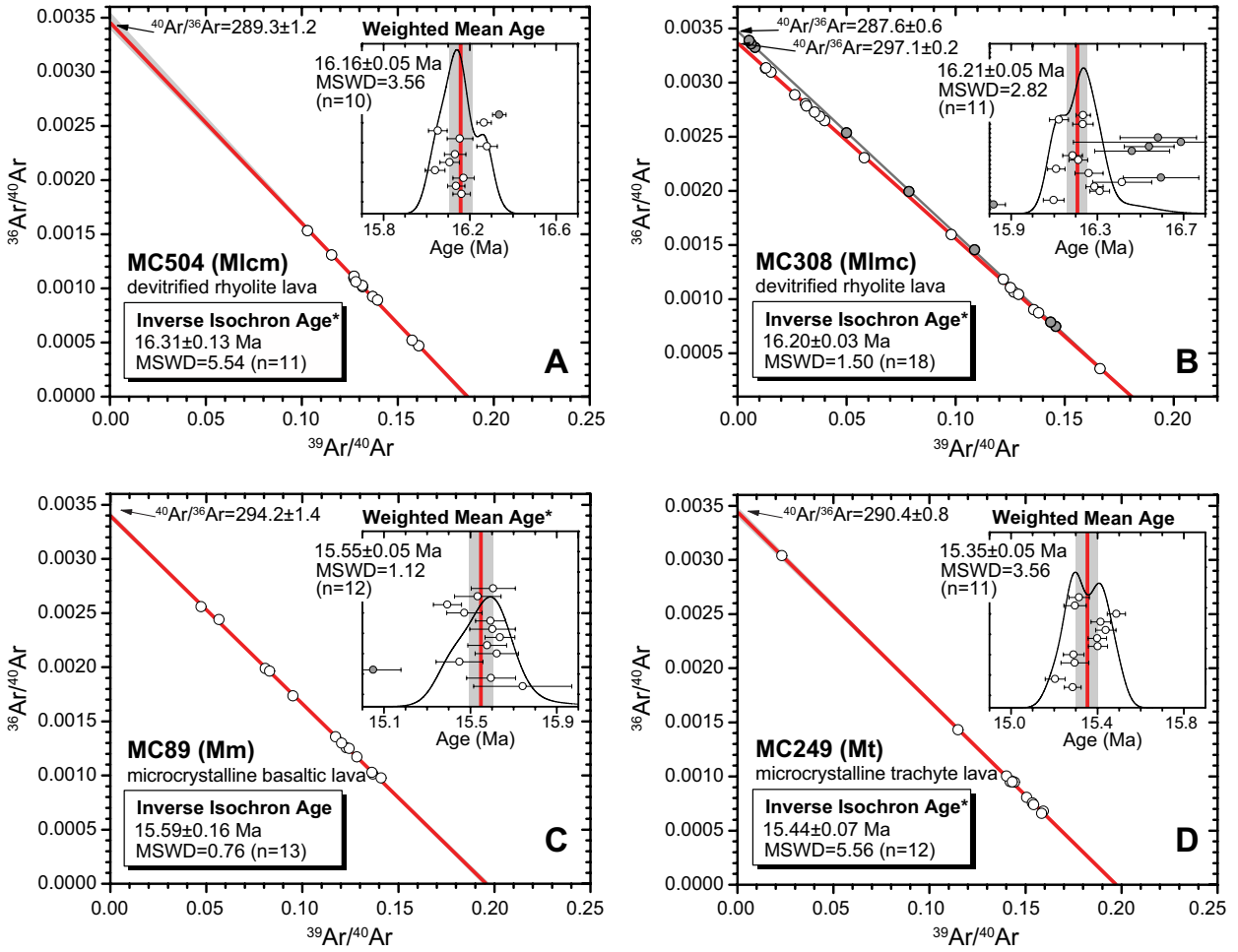

Figure 8. Representative $^{40}Ar/^{39}Ar$ inverse isochrons and (inset) weighted mean age distributions for total-fusion analyses of groundmass concentrates. (A, B) Devitrified aphyric rhyolitic samples. (C) Microcrystalline groundmass of basalt. (D) Microcrystalline groundmass of trachyte lava. Red lines on the inverse-isochron diagrams represent the York linear regression (York, 1968), and gray bands are the 95% confidence level. In the insets, the red lines are the weighted mean model age, and the gray bands are the 2σ standard error (MSWD—mean square of weighted deviations). Individual $^{40}Ar/^{39}Ar$ analyses shown in gray were omitted from the calculated ages. Sample MC308 of devitrified high-silica alkali rhyolite matrix appears to have two compositions of extraneous argon, possibly due to the presence of vapor-phase minerals in some matrix fragments. Ages with superscript (*) represent the preferred age for each sample. See text or Table 1 for unit abbreviations.

rhyolitic compositions and sodic augite in trachytic compositions, where it can occur with fayalitic olivine. The more evolved alkali rhyolites contain phenocrysts of Ca-Na amphibole (Fig. 9). Chevkinite is prominent in a few rhyolitic samples, and zircon is present in most units as inclusions within or surrounding Fe-Ti oxides or clinopyroxene. Biotite phenocrysts occur in small amounts in the low-silica alkali rhyolite of the Summit Lake Tuff, were reported in the Soldier Meadow Tuff by Korringa (1973), and are relatively abundant in the late-stage metaluminous rhyolite lavas.

The most common vapor-phase minerals are tridymite, alkali feldspar, and Na amphibole (Fig. 9). Vapor-phase tridymite can be distinguished from phenocrystic quartz by its purple color and/or bipyramidal form. Vapor-phase hematite and zircon have also been found.

TABLE 2. SUMMARY OF PHENOCRYST ASSEMBLAGES OF SILICIC IGNIMBRITES AND LAVAS AT THE HIGH ROCK CALDERA COMPLEX

Name	Total phenocryst (%)	Quartz volume (%)	Feldspar volume (%)	Feldspar length (mm)	Mafic phases
Ignimbrites and tuffs					
Idaho Canyon Tuff					
$Miic_a$	5–10	1–2	4–8	<1	tr. px, amph, ox, zr, chev
$Miic_b$	15–20	0–3	12–15	0.5–4	1% px + ox
Summit Lake Tuff	20–30	0 (xeno)	20–25	3–4	ox (1%); tr. bi, px, amph, zr
Tuff of Big Mountain	1–4	<2	1–3	0.5–2.5	tr. oxidized mafics
Tuff of Coyote Spring	5–9	0–tr.	5–9	<1	tr. px (to 1 mm), amph, ox, zr, chev
Tuff of Trough Mountain	1–7	0–2	1–5	0.5–2.5	tr. px, ox
Soldier Meadow Tuff	35–45	15–20	25–30	1–2	amph (1%–2% , <1 mm); tr. ox, zr, resorbed px
Tuffs of Alkali Flat and Badger Mountain	35–45	20–25	15–20	1–2	tr. amph, ox
Tuff of Yellow Rock Canyon					
Early rhyolite	3–8	1–3	2–5	<2	tr. mafics
Late trachyte	7–10	<2	5–7	1–4	tr. amph, ox
Rhyolitic lavas					
Nut Mountain	0	–	–	–	–
Catnip Mountain	0	–	–	–	tr. ox
Hell Creek	0 or 5	tr.	1–2	1–5	ox (1%), tr. amph
Antelope	8–15	3–5	5–10	0.5–3	tr. px, amph, zr, ox
Big Dike	~20	10	7–10	1–3	ox (2%); tr. px
Nellie Springs Mountain	3–7	0	3–7	up to 6	tr. chev (0.05–0.2 mm), ox, amph
Massacre Creek	0	–	–	–	–
Wild Horse Pasture	2–5	0	2–5	up to 4	tr. ox, amph
Soldier Meadow	30–45	10–15	20–25	1–4	amph (2%–3%, 1–5 mm); tr. ox, zr
Cottonwood Creek	0 or 3–7	0–2	2–7	up to 4	ox (1%); tr. amph
Mahogany Mountain (highly variable between flows and domes; examples here are illustrative)					
Rock Spring Table	~35	30	5	2–6	tr. px, ox
Blowout Mountain	~55	25	30	1–3	tr. mafics
Fish Creek Mountain	~12	6	6	0.5–3	tr. amph
Badger Mountain	1–3	0	1–3	1–4	tr. ox
Rodero Flat	~15	0	15	3–8	3% px + amph + bi + ox
Rock Springs Canyon	10–15	0	7–10	0.5–2	bi (3%–4%, <1 mm), resorbed px (1%–2%), ox (1%)
Wall Canyon	1–2	tr.	<2	0.5–1	tr. mafics

Note: tr.—trace, xeno—trace xenocrystic, px—sodic Fe-rich clinopyroxene, amph—sodic amphibole (except in Mlrs, where it is hornblende), ox—Fe-Ti oxide, zr—zircon, chev—chevkinite, bi—biotite. Dash indicates mineral absent.

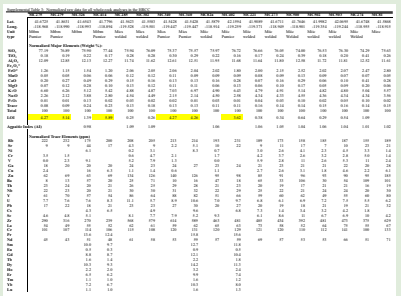

[8]Supplemental Table 3. Normalized data for all whole-rock analyses in the High Rock caldera complex. Please visit http://dx.doi.org/10.1130/GES01162.S8 or the full-text article on www.gsapubs.org to view Supplemental Table 3.

Fine-grained sodic clinopyroxene in the groundmass of devitrified lavas and densely welded ignimbrites can make fresh surfaces have a greenish tinge. This is most prominent in the Mahogany Mountain lavas. Similarly, the presence of fine-grained Na amphibole (riebeckite) causes a bluish cast, most obvious in the moderately peralkaline Soldier Meadow Tuff. In contrast, most of the weathered surfaces of devitrified rhyolitic rocks are dark reddish-brown due to oxidation of the abundant iron that characterizes these peralkaline compositions.

Whole-Rock Compositions of Silicic Units

Rhyolitic rocks in the HRCC range from metaluminous to moderately peralkaline. None are as strongly peralkaline or as rich in iron as pantellerites (Table 3; Supplemental Table 3[8]). The usual indicator of magma peralkalinity, the agpaitic index (mol $[Na_2O + K_2O]/Al_2O_3$), is not an accurate measure in most of the silicic rocks due to vapor-phase crystallization in ignimbrites and lavas, widespread weak silicification of ring-fracture lavas, and hydration of pumice lapilli. Instead, we estimate the peralkalinity based on the concentration of Zr, a high field strength element (HFSE) that is relatively re-

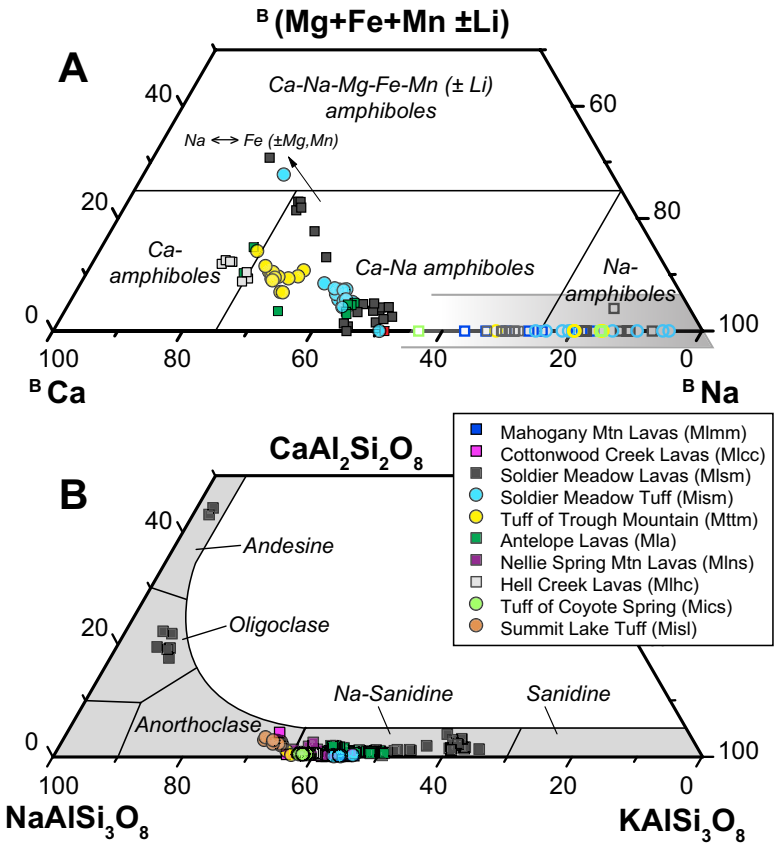

Figure 9. Composition of amphibole and feldspar in rhyolites and trachytes of High Rock caldera complex. (A) Phenocrysts of alkali amphibole are mostly Ca-Na amphiboles, whereas groundmass and vapor-phase amphiboles (open symbols), encompassed by gray band, are Na-amphiboles. Amphibole classification diagram is from Hawthorne and Oberti (2007). (B) High-silica alkali rhyolites contain sodic sanidine, whereas the low-silica alkali rhyolite of the Summit Lake Tuff contains anorthoclase. The highly evolved, phenocryst-rich Soldier Meadow lava has the most potassic sanidine and also contains resorbed plagioclase. See text or Table 1 for unit abbreviations.

sistant to the effects of hydration, weathering, and weak hydrothermal alteration. Zr behaves as an incompatible element because zircon is not abundant due to the large solubility of zircon in peralkaline melts (Watson and Harrison, 1983). We characterize as mildly peralkaline those rhyolites that have ~240–500 ppm Zr, because fresh, unaltered samples with these values typically have agpaitic indices of 1.01–1.05. Those rhyolites with ~500–1100 ppm Zr are moderately peralkaline, with agpaitic indices of 1.05–1.15.

The most abundant rocks in the HRCC are mildly to moderately peralkaline alkali rhyolite ignimbrites and lavas (Fig. 6), although both the youngest and oldest rhyolitic lavas are metaluminous. Late in the history of the complex, after nearly all the volume of rhyolitic magmas had been erupted, crystal-poor intermediate lavas ranging from trachyte to trachyandesite erupted in the Hanging Rock and Badger Mountain calderas.

Due to the fact that many of the rhyolitic magmas approach minimum-melt compositions in the Q-Ab-Or system, SiO_2 is not a good measure of degree of magma differentiation. Incompatible trace elements (e.g., Zr, Rb, and Th) are a better measure. Declining TiO_2 is a good proxy for degree of differentiation except in the most evolved silicic rocks, where the tiny proportion of mafic phenocrysts results in TiO_2 being buffered at a near-constant value (Fig. 11A). FeO* has a variable behavior at the HRCC because the inverse covariation of fO_2 and peralkalinity among suites results in it being incompatible, weakly compatible, or a strongly compatible element (Fig. 11A).

On a plot of Zr versus Rb (Figs. 11B and 12), two incompatible elements in these zircon-poor rocks, the HRCC ignimbrites form arrays with different slopes. Although some fraction of the dispersion along the arrays can be explained by crystal concentration in densely welded ignimbrites, the fact that different units have very different slopes on some bivariate plots (e.g., TiO_2 versus FeO* or Ba versus Zr) (Figs. 11 and 12B) proves that most of the arrays are a result of compositional zoning in magma bodies prior to eruption. Although most of the HRCC ignimbrites display a range in trace element concentrations on bivariate plots, we have identified systematic variations in composition with stratigraphic height and sectoral emplacement for only two: (1) the Idaho Canyon Tuff is zoned from crystal-poor to crystal-rich high-silica rhyolite in the later erupted, stratigraphically higher part; and (2) the tuff of Yellow Rock Canyon is zoned from crystal-poor high-silica rhyolite to trachyte with 10% phenocrysts (Table 2; Figs. 6, 11, and 12).

The presence of compositional zoning that results in different slopes and offsets of elemental ratios on bivariate plots makes it possible to distinguish similar-looking ignimbrites and correlate far-flung exposures. These plots were also used to assign lavas to eruptive groups and to calderas. Bivariate plots using Zr, Rb, Th, Zn, Ba, FeO*, and TiO_2 proved to be the most useful, with the caveats that anomalously high Rb values can occur in strongly hydrated pumice lapilli

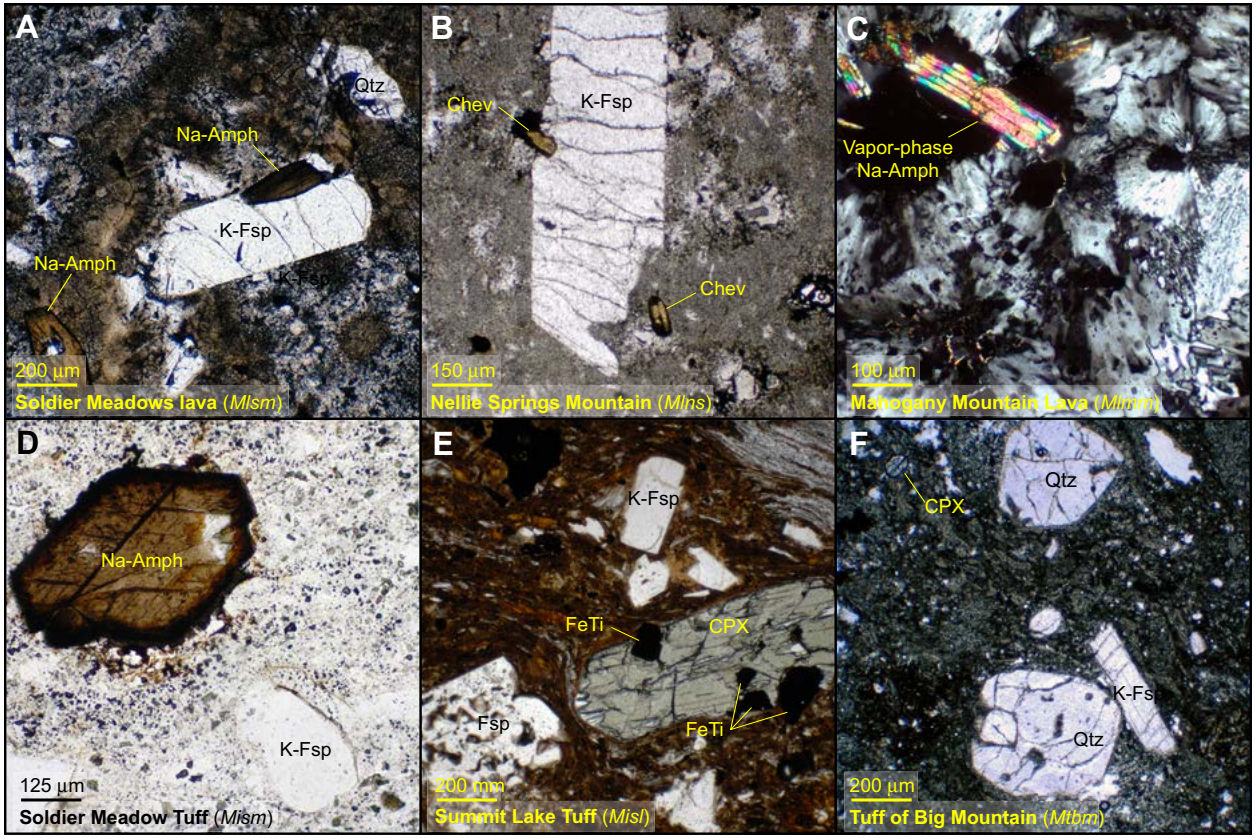

Figure 10. Photomicrographs illustrating textures and phenocryst relationships in rhyolites of High Rock caldera complex. (A) Coarsely devitrified Soldier Meadow high-silica alkali rhyolite lava (MC376) with phenocrysts of sanidine (K-Fsp), sodic amphibole (Na-Amph), and quartz (Qtz). (B) Finely devitrified crystal-poor low-silica alkali rhyolite of Nellie Springs Mountain (MC271) showing a large anorthoclase (K-Fsp), two chevkinite (Chev) phenocrysts, and anhedral, opaque, Fe-Ti oxides. Groundmass devitrification textures are cryptocrystalline. (C) Coarse radiating devitrification texture in the groundmass of crystal-rich high-silica alkali rhyolite lava of Mahogany Mountain (MC87). Large, strongly pleochroic, vapor-phase sodic amphiboles are present in vesicles. (D) Strongly welded high-silica alkali rhyolite Soldier Meadow Tuff (MC121) with distinctive sodic amphibole phenocrysts. In the groundmass are <15 µm vapor-phase Na-amphibole crystals that give the welded ignimbrite its blue-green color. (E) Partially welded low-silica alkali rhyolite Summit Lake Tuff (MC146) with abundant anorthoclase (K-Fsp), aegirine-augite (clinopyroxene, CPX), Fe-Ti oxides (FeTi), and resorbed feldspar. The matrix is composed of glass fragments and small pumice lapilli. (F) High-silica alkali rhyolite tuff of Big Mountain (MC326) with resorbed, rounded quartz (Qtz) and euhedral sanidine (K-Fsp) phenocrysts. Small clinopyroxene (CPX) phenocrysts are also present. All images are plain-polarized light, except C, which is cross-polarized. See text or Table 1 for unit abbreviations.

sampled from ignimbrites and fall deposits, and that the Ba analyses are neither accurate nor precise at concentrations below ~50 ppm. In addition, we found that analyses of Ba, Th, Nb, Y, and the light rare earth elements (REE) are subject to nugget effects due to the high concentration of Ba in alkali feldspar and the other elements in accessory phases.

Mafic and Intermediate Lavas

Mafic and intermediate lavas are greatly subordinate in the HRCC. Pre-HRCC mafic lavas of known mid-Miocene age include the Steens Basalt in small volume on the east side of the complex and transitional olivine basalts and intermediate lavas and associated phreatomagmatic deposits on the northwest and southwest side. Postcaldera alkalic mafic and intermediate lavas erupted in the Cottonwood Creek, Hanging Rock, and Badger Mountain calderas for ~1 m.y. following cessation of main-stage silicic volcanism. Much later, high-Al olivine tholeiite lavas that erupted from vents north of the HRCC flowed over parts of the Virgin Valley and Badger Mountain calderas.

TABLE 3. REPRESENTATIVE ANALYSES OF RHYOLITIC IGNIMBRITES AND LAVAS FROM THE HIGH ROCK CALDERA COMPLEX

	MC341*	MC502*	MC273*	MC274*	MC504*	MC85*	MC352B*	MC426†	MC244*	MC430†	MC326†	MC135*	MC413†
Lat (°N)	41.5588	41.9982	41.6711	41.6748	41.8883	41.5689	41.5818	41.4147	41.5251	41.8725	41.6543	41.7599	41.7909
Long (°W)	119.4699	119.3544	118.9490	118.9547	119.3160	119.0213	119.5780	119.0694	119.4965	119.2505	118.9929	118.9308	118.8889
Unit	Mlnm	Miic-a	Miic-a	Miic-b	Mlcm	Misl	Misl	Misl	Mlhc	Mlhc	Mtbm	Mla	Mla
Type	devitrified lava	welded, WR ig	welded, WR ig	welded, WR ig	devitrified lava	welded, WR ig	nonwelded pumice	welded, WR ig	devitrified lava	devitrified lava	nonwelded pumice	devitrified lava, dike	devitrified lava
Composition	HSR	HAR	HAR	HAR	HAR	LAR	LAR	LAR	HAR	HAR	HAR	HAR	HAR
Age (Ma)	16.59±0.15	16.37±0.02	16.39±0.02	16.37±0.02	16.31±0.13	16.34±0.02	16.41±0.03	n.a.	16.29±0.02	16.31±0.03	16.13±0.03	n.a.	16.25±0.03
Normalized major elements (wt%)													
SiO_2	75.04	76.53	76.05	74.29	76.20	70.11	68.70	71.31	77.80	76.70	75.90	77.14	77.55
TiO_2	0.19	0.18	0.24	0.41	0.27	0.55	0.70	0.48	0.25	0.26	0.22	0.19	0.17
Al_2O_3	13.42	11.72	11.80	12.52	11.53	14.87	15.27	14.69	11.24	11.88	12.13	12.01	12.15
FeO*	1.12	2.02	2.15	2.47	1.91	2.60	2.80	1.90	1.54	1.58	1.54	1.35	0.84
MnO	0.04	0.09	0.09	0.07	0.12	0.16	0.21	0.03	0.08	0.09	0.06	0.05	0.03
CaO	0.86	0.06	0.16	0.41	0.12	0.72	0.84	0.56	0.03	0.06	0.49	0.14	0.12
MgO	0.13	0.05	0.10	0.20	0.10	0.37	0.47	0.26	0.08	0.11	0.28	0.07	0.04
K_2O	5.23	4.82	4.91	5.04	4.87	4.99	6.74	5.28	4.91	4.89	5.12	5.02	4.92
Na_2O	3.77	4.36	4.33	4.34	4.69	5.34	3.86	5.24	3.85	4.25	3.88	3.92	4.10
P_2O_5	0.04	0.02	0.03	0.10	0.01	0.08	0.13	0.08	0.07	0.02	0.13	0.04	<0.01
Trace	0.17	0.15	0.14	0.14	0.18	0.19	0.27	0.17	0.15	0.16	0.24	0.07	0.07
Total	100.00	100.00	100.00	100.00	100.00	100.00	100.00	100.00	100.00	100.00	100.00	100.00	100.00
LOI	0.38	0.29	0.34	1.09	n.a	n.a	4.35	0.71	0.60	0.36	1.39	n.a	n.a
Normalized trace elements (ppm)													
Rb	190	185	173	155	210	152	126	169	229	239	175	202	205
Sr	86	7	11	23	0.2	51	18	44	2.1	12	44	6.1	17
Ni	2.2	2.3	2.6	3.3	1.9	7.0	b.d.	b.d.	2.3	b.d.	6.1	b.d.	b.d.
Cr	3.1	3.2	3.7	5.0	3.7	6.5	3.8	b.d.	3.3	b.d.	b.d.	2.7	b.d.
V	9	2.6	2.8	11	4.2	17.9	2.4	11	8	5.0	9.1	4.0	
Ga	17	21	23	20	22	22	22	24	24	25	20	18	20
Cu	4.4	1.8	2.6	2.2	b.d.	8.3	1.5	b.d.	0.7	b.d.	16	1.1	b.d.
Zn	31	93	91	95	131	117	152	77	117	106	63	59	49
Ba	616	30	33	109	5.9	724	1587	631	15	22	57	16	28
Th	26	21	19	16	26	16	14	19	26	28	20	22	23
Nb	17	24	22	20	30	22	20	25	30	31	20	21	22
Y	39	49	60	60	91	74	79	72	74	87	57	45	59
U	11.3	7.2	6.1	5.5	8.8	5.2	3.5	7.9	9.0	9.3	7.6	7.4	8.6
Pb	18	21	19	21	27	18	13	12	19	21	18	12	14
Cs	9.6	3.2	1.4	1.8	10.2	b.d.	b.d.	5.1	4.3	4.6	4.3	b.d.	4.2
Sc	3.3	6.7	8.6	10	7.4	13	16	9	6.9	5.0	5.1	4.6	b.d.
Zr	175	481	434	375	579	469	361	490	502	502	270	266	255
La	44	64	58	55	59	56	50	58	33	44	55	53	53
Ce	69	112	120	100	124	105	106	102	67	96	114	94	107
Pr								15.2		14.1	13.6		12.8
Nd	38	53	57	51	55	62	63	62	40	57	51	45	49
Sm								12.6		13.8	10.0		9.8
Eu								2.3		1.0	0.5		0.4
Gd								12.1		13.6	8.8		9.3
Tb								2.0		2.4	1.6		1.6
Dy								12.7		15.3	10.3		10.6
Ho								2.7		3.4	2.2		2.2
Er								8.1		10.0	6.5		6.8
Tm								1.3		1.6	1.1		1.1
Yb								8.5		10.6	7.2		7.2
Lu								1.2		1.5	1.1		1.1

(*continued*)

TABLE 3. REPRESENTATIVE ANALYSES OF RHYOLITIC IGNIMBRITES AND LAVAS FROM THE HIGH ROCK CALDERA COMPLEX (*continued*)

	MC302*	MC124†	MC212*	MC271†	MC308*	MC423†	MC121*	MC369*	MC213†	MC315*	MC380*	MC513*	MC505*
Lat (°N)	41.5583	41.4902	41.5349	41.3931	41.5046	41.5665	41.3045	41.2687	41.5360	41.4567	41.72099	41.7569	41.6753
Long (°W)	119.5013	119.0852	119.1804	119.6136	119.5615	119.0773	119.1693	119.3094	119.2026	119.1721	119.117	119.3477	119.3399
Unit	Mics	Mttm	Mttm	Mlns	Mlmc	Mlwh	Mism	Mism	Mlsm	Mlsm	Mlmm-1	Mlmm-2	Mlmm-2
Type	welded, WR ig	welded, WR ig	welded, WR ig	devitrified lava	devitrified lava	devitrified lava	welded, WR ig	welded, WR ig	devitrified lava	devitrified lava	devitrified lava	devitrified lava	devitrified lava
Composition	HAR	HAR	HAR	LAR	HAR	HAR	HAR	HAR	HAR	HAR	HAR	HAR	HAR
Age (Ma)	16.27±0.02	16.15±0.02	16.25±0.03	16.21±0.02	16.20±0.03	16.10±0.02	16.00±0.02	16.01±0.02	15.96±0.02	15.89±0.02	n.a.	15.67±0.02	15.89±0.02
Normalized major elements (wt%)													
SiO_2	76.09	74.49	76.74	73.88	76.07	75.88	76.98	77.06	76.98	77.07	77.20	77.22	77.11
TiO_2	0.28	0.27	0.27	0.44	0.27	0.28	0.24	0.25	0.16	0.17	0.24	0.12	0.11
Al_2O_3	11.62	11.79	11.40	12.77	11.60	11.68	10.42	10.43	10.64	10.59	10.68	11.11	10.97
FeO*	2.05	1.89	1.76	2.34	2.07	2.00	2.61	2.75	2.72	2.80	2.58	2.36	2.42
MnO	0.12	0.10	0.11	0.12	0.12	0.13	0.15	0.13	0.13	0.12	0.11	0.05	0.04
CaO	0.16	2.12	0.29	0.27	0.11	0.18	0.40	0.11	0.15	0.15	0.09	0.07	0.07
MgO	0.12	0.49	0.10	0.17	0.11	0.25	0.12	0.10	0.10	0.04	0.08	0.01	0.03
K_2O	4.87	4.50	4.79	5.24	4.98	4.88	4.58	4.56	4.56	4.47	4.63	4.53	4.50
Na_2O	4.49	4.06	4.39	4.63	4.46	4.48	4.24	4.37	4.14	4.35	4.23	4.22	4.42
P_2O_5	0.02	0.08	0.03	0.03	0.04	0.02	0.06	0.04	0.12	0.03	0.03	0.05	0.04
Trace	0.18	0.20	0.13	0.10	0.17	0.21	0.20	0.21	0.30	0.22	0.14	0.27	0.28
Total	100.00	100.00	100.00	100.00	100.00	100.00	100.00	100.00	100.00	100.00	100.00	100.00	100.00
LOI	0.26	2.68	0.72	2.47	0.39	0.46	0.55	0.20	0.70	n.a.	n.a.	n.a.	n.a.
Normalized trace elements (ppm)													
Rb	205	217	220	167	206	196	220	227	308	303	228	362	365
Sr	9	47	13	10	4.3	18	13	3.4	25	8	1.6	5.3	5.3
Ni	3.1	6.2	2.9	b.d.	2.7	b.d.	2.9	3.3	b.d.	b.d.	b.d.	2.7	3.6
Cr	4.7	b.d.	4.8	b.d.	2.6	b.d.	4.8	3.2	b.d.	1.0	0.5	3.5	3.8
V	7.9	11	6.1	5.1	6.6	b.d.	6.1	11	5.1	5.9	3.7	10	13
Ga	23	26	24	26	23	25	24	24	27	23	23	27	29
Cu	1.4	11	3.3	b.d.	1.0	b.d.	3.3	2.0	b.d.	4.1	1.0	5.2	3.8
Zn	126	119	171	106	129	115	171	168	171	183	179	200	226
Ba	71	180	38	19	18	62	38	28	39	27	5	18	22
Th	25	26	28	21	24	24	28	29	40	41	24	46	44
Nb	30	30	33	28	29	28	33	33	55	53	32	65	62
Y	64	91	95	44	67	66	95	105	90	101	101	202	176
U	5.7	10.7	6.5	4.8	8.5	5.8	6.5	7.0	6.9	6.0	4.8	16.4	13.8
Pb	23	22	33	17	20	23	33	31	47	44	21	53	68
Cs	4.9	6.9	9.5	2.6	4.6	4.4	9.5	5.7	3.0	b.d.	b.d.	7.2	5.5
Sc	7.7	7.2	10	8	9	8	10	10	b.d.	2.8	10	1.6	0.4
Zr	579	519	628	427	538	518	628	702	1043	1137	657	807	910
La	61	55	69	69	71	67	69	62	51	76	46	77	49
Ce	108	99	145	128	108	119	145	137	125	155	129	138	132
Pr		16.8		17.0		16.2			14.6				
Nd	58	68	64	63	71	60	64	66	56	75	46	80	61
Sm		15.2		11.2		12.0			13.4				
Eu		1.2		0.9		1.0			0.6				
Gd		15.0		9.2		10.6			12.2				
Tb		2.4		1.5		1.9			2.4				
Dy		15.9		9.5		12.2			15.3				
Ho		3.5		1.9		2.6			3.4				
Er		10.6		5.7		7.9			11.0				
Tm		1.7		0.9		1.2			1.8				
Yb		11.4		6.0		8.3			13.3				
Lu		1.8		1.0		1.3			2.1				

(*continued*)

TABLE 3. REPRESENTATIVE ANALYSES OF RHYOLITIC IGNIMBRITES AND LAVAS FROM THE HIGH ROCK CALDERA COMPLEX (*continued*)

	MC429B*	MC314†	MC421†	MC333*	MC256*	MC428†	MC373†	MC137*	MC385*	MC254*	MC330†	MC132†
Lat (°N)	41.5846	41.5755	41.6505	41.6111	41.3499	41.2583	41.4188	41.3467	41.2381	41.39881	41.5421	41.79443
Long (°W)	119.3734	119.3260	119.1604	119.3616	119.4960	119.4976	119.4318	119.6078	119.6223	119.5539	119.3713	118.977
Unit	Mtab	Mtab	Mlmm-3	Mlmm-3	Miyc	Miyc	Miyc	Mlcc	Mlcc	Mlcc	Mlwc	Mlrs
Type	VP WR ig	welded, WR ig	devitrified lava	devitrified lava	nonwelded pumice	nonwelded pumice	nonwelded pumice	devitrified lava	devitrified lava	devitrified lava	devitrified lava	devitrified lava
Composition	HAR	HAR	HAR	HAR	HAR	HAR	T	HAR	HAR	HAR	HSR	TR
Age (Ma)	15.84±0.02	15.71±0.02	15.67±0.02	15.56±0.02	15.69±0.01	15.71±0.03	n.a.	15.91±0.04	15.69±0.02	15.75±0.02	14.68±0.29	15.85±0.15
Normalized major elements (wt%)												
SiO_2	76.71	77.90	77.91	76.85	75.80	76.44	67.75	76.01	77.15	77.44	77.46	72.79
TiO_2	0.13	0.14	0.09	0.09	0.13	0.14	0.45	0.15	0.12	0.11	0.16	0.30
Al_2O_3	11.30	11.50	11.55	12.36	11.96	12.15	14.35	12.32	11.76	11.59	12.53	14.42
FeO*	1.66	1.48	1.45	1.31	1.90	1.83	5.19	2.00	1.82	1.51	0.62	1.63
MnO	0.03	0.01	0.04	0.03	0.05	0.04	0.21	0.02	0.03	0.01	<0.01	<0.01
CaO	0.59	0.06	0.06	0.18	0.45	0.37	1.79	0.06	0.04	0.08	0.78	1.78
MgO	0.12	0.05	0.02	0.02	0.07	0.12	0.19	0.07	0.02	0.12	0.10	0.29
K_2O	5.02	4.76	4.48	4.77	6.85	6.92	5.90	4.92	4.79	4.66	4.62	4.66
Na_2O	4.10	3.94	4.23	4.28	2.69	1.77	3.84	4.31	4.14	4.30	3.60	3.79
P_2O_5	0.17	0.02	0.03	0.02	0.01	<0.01	0.05	0.02	0.01	0.03	0.03	0.12
Trace	0.17	0.14	0.14	0.08	0.10	0.24	0.27	0.12	0.12	0.16	0.10	0.22
Total	100.00	100.00	100.00	100.00	100.00	100.00	100.00	100.00	100.00	100.00	100.00	100
LOI	1.93	0.29	0.36	n.a.	4.46	4.28	5.40	0.69	0.37	0.40	0.68	0.96
Normalized trace elements (ppm)												
Rb	204	198	335	218	178	229	96	155	166	181	129	132
Sr	24	15	14	8	28	19	21	6.0	2.6	8	72	326
Ni	2.8	5.0	b.d.	b.d.	b.d.	b.d.	b.d.	3.6	2.1	2.9	b.d.	7.1
Cr	3.0	b.d.	b.d.	1.3	2.4	b.d.	b.d.	2.9	2.9	3.0	b.d.	b.d.
V	7.7	7.0	b.d.	3.0	b.d.	b.d.	b.d.	5.9	2.6	4.4	7	26
Ga	26	26	28	21	23	25	22	24	23	23	15	17
Cu	4.7	0.0	b.d.	2.0	1.3	b.d.	0.0	4.4	3.3	2.4	b.d.	19
Zn	133	114	122	54	134	128	113	115	115	123	23	31
Ba	25	36	16	48	4.8	15	759	79	12	89	488	1159
Th	20	21	37	24	18	18	9	15	18	19	17	12
Nb	30	30	57	33	19	20	15	18	20	20	13	11
Y	90	86	129	69	66	57	37	51	37	65	18	15
U	8.5	8.2	10.1	8.5	6.0	7.4	3.6	3.9	5.4	6.3	6.9	4.8
Pb	40	31	36	22	29	29	22	17	19	38	21	16
Cs	8.0	5.1	6.8	b.d.	b.d.	15.1	5.0	5.7	2.3	6.0	5.1	3.2
Sc	1.6	b.d.	b.d.	2.1	1.3	b.d.	16	b.d.	0.4	1.1	b.d.	b.d.
Zr	491	435	330	263	395	373	202	328	414	446	96	200
La	53	67	51	54	63	55	33	45	37	54	26	32
Ce	121	129	99	104	115	112	71	63	72	104	48	57
Pr		17.5	13.3			13.8	8.9				5.0	6.3
Nd	55	66	48	44	59	53	36	45	32	53	17	21
Sm		14.2	12.5			10.4	7.5				3.0	3.5
Eu		0.3	0.2			0.1	1.4				0.4	0.6
Gd		14.0	13.5			9.9	7.2				2.5	3.0
Tb		2.4	2.8			1.6	1.2				0.4	0.5
Dy		16.0	19.5			10.4	7.1				2.7	2.6
Ho		3.4	4.5			2.2	1.5				0.6	0.5
Er		10.0	14.8			6.7	4.4				1.8	1.6
Tm		1.6	2.4			1.0	0.7				0.3	0.2
Yb		10.4	16.1			6.5	4.4				2.2	1.6
Lu		1.6	2.3			1.1	0.8				0.4	0.3

Note: Loss on ignition (LOI) was measured only on those samples that appeared hydrated or altered in hand sample. n.a.—not analyzed; b.d.—below detection limit. HAR—high-Si alkali rhyolite, LAR—low-Si alkali rhyolite, HSR—high-Si rhyolite, TR—trachyrhyolite, T—trachyte. VP—vapor phase altered, WR ig—whole-rock ignimbrite; pumice, scoria—lapilli from pyroclastic deposit. Age for MC132 from Castor and Henry (2000).

*Sample numbers were analyzed at Washington State University Geoanalytical Labs (Pullman) by wavelength-dispersive X-ray fluorescence (XRF).

†Samples were analyzed by the U.S. Geological Survey for major elements by XRF and for trace elements by inductively coupled plasma atomic emission spectroscopy.

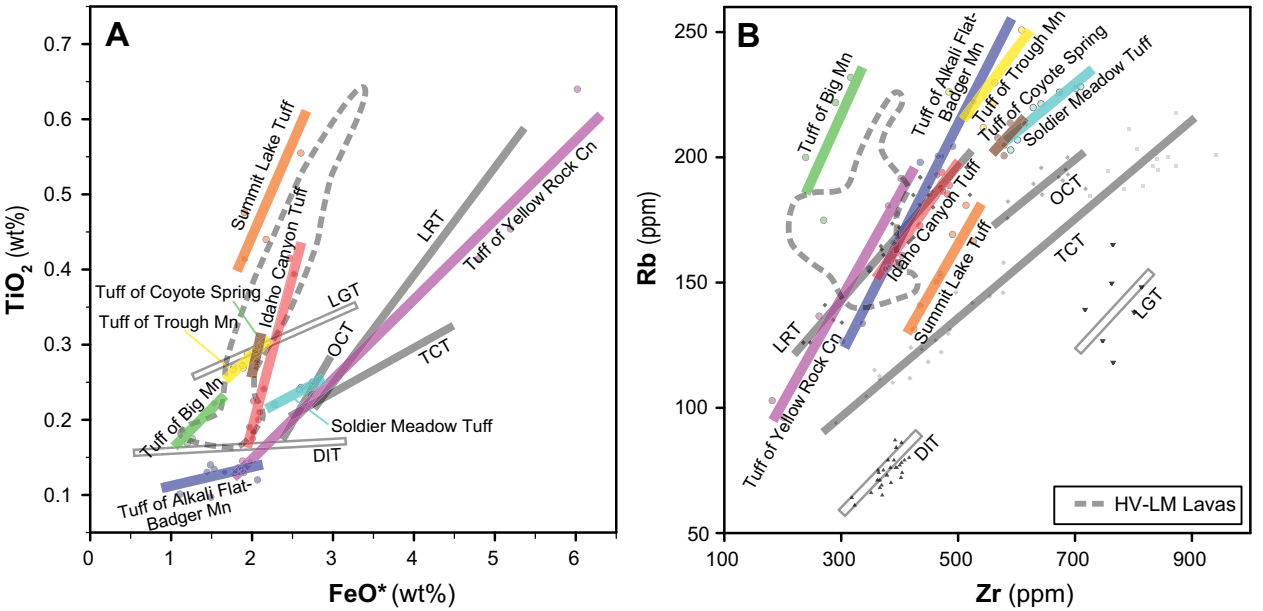

Figure 11. Compositions of rhyolitic units of High Rock caldera complex (HRCC), illustrating how they can be distinguished from units erupted at nearby mid-Miocene centers by different average trends on bivariate plots of minor and trace elements. Long Ridge tuff (LRT), Trout Creek tuff (TCT), and Oregon Canyon Tuff (OCT) are peralkaline ignimbrites from the McDermitt volcanic field (MVF). Dinner Creek tuff (DIT) and Leslie Gulch tuff (LGT) are ignimbrites from Lake Owyhee volcanic field. Mn—mountain. (A) In silica-rich rocks, declining TiO_2 can serve as a proxy for increasing degree of differentiation. At any given degree of differentiation, the rocks from the MVF have higher concentrations of FeO* than HRCC rocks. (B) Reflecting their less alkalic composition, rocks from Hawks Valley–Lone Mountain (HV-LM) have lower concentrations of Zr than HRCC and MVF rhyolites. Data for HV-LM are from Wypych et al. (2011); data for the MVF are from Rytuba and McKee (1984) and Conrad (1984); data for LGT are from T.R. Benson and Mahood (personal data); data for DIT are from Camp et al. (2003) and Binger (1997).

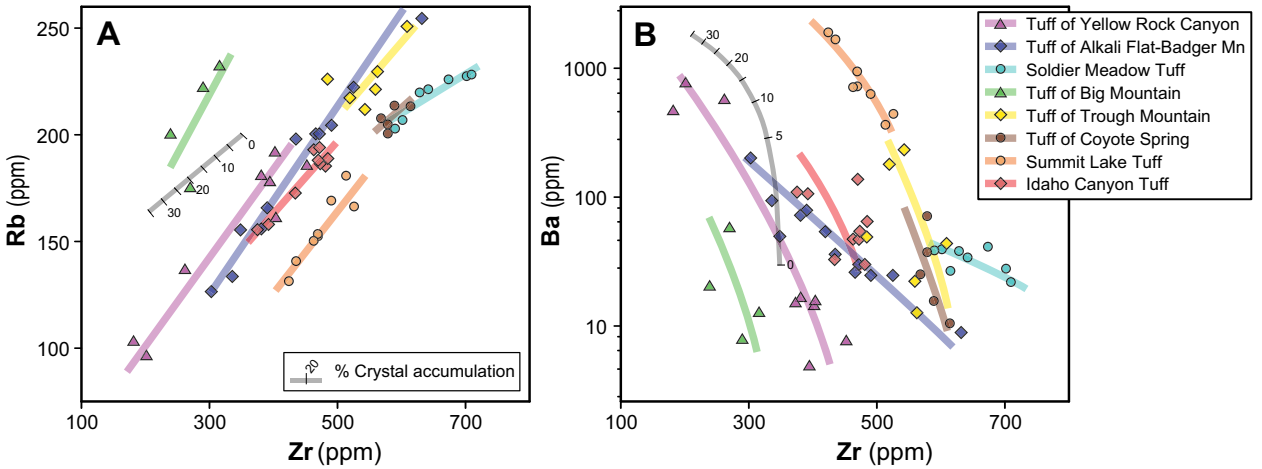

Figure 12. (A) Plot of Rb versus Zr illustrating compositional trends defined by ignimbrites and tuffs from High Rock caldera complex (HRCC; Mn—mountain; Cn—canyon). (B) Plot of log Ba versus Zr. Gray bar illustrates the potential effect of crystal accumulation in whole-rock ignimbrite samples due to elutriation of glassy ash during eruption and emplacement, based on simple mass-balance addition of a typical phenocryst assemblage using the partition coefficients of Bachmann et al. (2005). HRCC units defining a low Rb/Zr trend are plotted as circles; units with a high Rb/Zr trend are plotted as diamonds. See text for discussion of chemical trends for tuff of Big Mountain (Mtbm) and tuff of Yellow Rock Canyon (Miyc) shown as triangles.

Steens Basalt

On many published and unpublished maps, isolated exposures of mid-Miocene basaltic lavas in and around the HRCC have been mapped as the Steens Basalt. We adopted the suggestion of Camp et al. (2013) that the term Steens Basalt be restricted to lavas in physical continuity with the thick sections at Steens Mountain and in the Pueblo Mountains. In the area around the HRCC, most of the Steens Basalt lavas are phenocryst-poor, dense, microcrystalline rocks, which makes it easy to distinguish them from mid-Miocene olivine basalts that contain conspicuous olivine and plagioclase phenocrysts, and the younger 10–1 Ma high-Al olivine tholeiites, which are uniformly diktytaxitic and less weathered.

In Figures 6 and 13–15 we plot compositions of Steens Basalt lavas that are immediately adjacent to the HRCC as local Steens Basalt in order to distinguish them from the compositions of samples collected to the north and closer to the type section (e.g., Hart et al., 1989; Johnson et al., 1998; Camp et al., 2013). The Steens Basalt has been informally subdivided into two compositionally distinct members (Johnson et al., 1998; Camp et al., 2003, 2013): lower Steens lavas are olivine tholeiites, whereas upper Steens lavas are generally more evolved and more alkalic, including transitional basalts, alkali basalt, trachybasalt, and trachybasaltic andesite. The Steens Basalt lavas adjacent to the HRCC belong to the more alkalic upper member.

Precaldera Transitional Olivine Basalts and Intermediate Lavas

Silicic volcanic rocks of the HRCC overlie mafic and intermediate lavas widely at the edges of the complex, but only a few of these lavas have been dated precisely. The transitional olivine basalts adjacent to the HRCC that we interpret based on the available ages and on stratigraphic relationships to be mid-Miocene in age are easily distinguished chemically from Oligocene basalts and intermediate lavas, which have much higher ratios of large ion lithophile elements/HFSE. The known and presumed mid-Miocene lavas we have analyzed overlap the field of Steens Basalt on the TAS diagram (Fig. 6), but their concentrations of Zr and TiO_2 (Figs. 13 and 14) are too low to be considered Steens Basalt.

Immediately Postcaldera Alkalic Mafic and Intermediate Lavas

Mafic lavas that erupted in the calderas between ca. 15.5 and 14.2 Ma, shortly following cessation of most of the silicic volcanism, are

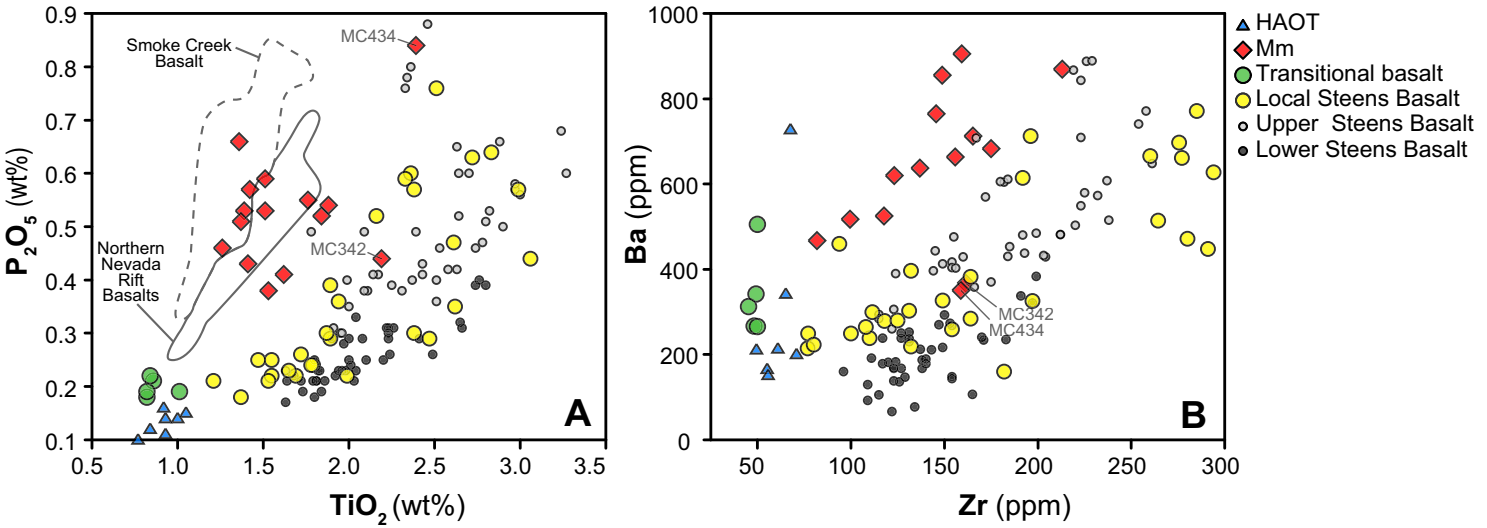

Figure 13. Comparison of the composition of mafic lavas in and around High Rock caldera complex (HRCC) to the Steens Basalt and other Miocene basalts of northern Nevada. Postcaldera mafic lavas (Mm) have lower concentrations of high field strength elements than Steens Basalt. The two exceptions are samples MC434 and MC342, which have compositions similar to Steens Basalt. These small volumes of basalt erupted on ring-fracture faults of the Hanging Rock and Summit Lake calderas, and we believe represent small volumes of Steens Basalt magma that penetrated the HRCC silicic focus to erupt at the surface. The HRCC postcaldera mafic lavas have chemical similarities to the 16.6–16.0 Ma basalts erupted in the nearby Buffalo Hills–Smoke Creek area and to 16.5–15.0 Ma basalts of the northern Nevada Rift. Precaldera transitional olivine tholeiites at HRCC have similarities to late Miocene high-Al olivine tholeiites (HAOT) erupted millions of years after silicic volcanism ceased. Data for the type section at Steens Mountain are from Johnson et al. (1998); for Steens Basalt in areas around HRCC (shown as local Steens Basalt) are from Hart et al. (1989), Colgan et al. (2006), and this study; and for northern Nevada rift and Buffalo Hills–Smoke Creek basalts are from Camp et al. (2013).

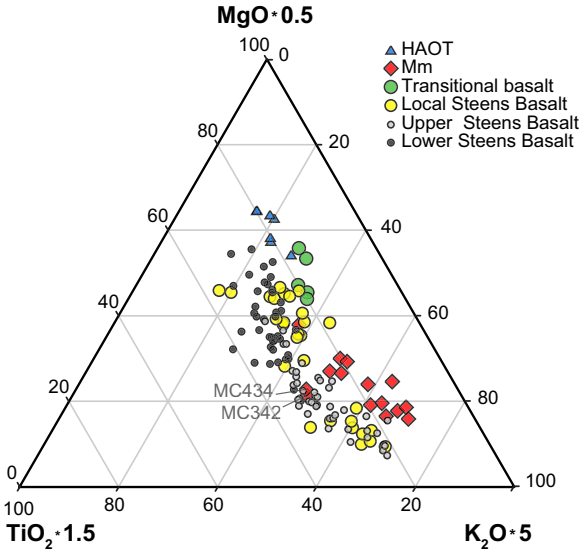

Figure 14. Ternary plot comparing High Rock caldera complex (HRCC) mafic lavas with Steens Basalt. Postcaldera lavas (Mm) are more alkalic and more evolved than most Steens Basalt. Postcaldera basalts MC434 and MC342 plot in the field for Steens Basalt, suggesting they represent Steens Basalt that penetrated the silicic focus. Precaldera transitional olivine tholeiite basalts are similar to late Miocene high-Al olivine tholeiites (HAOT), though slightly enriched in incompatible elements. Data sources as in Figure 13.

exclusively alkalic, ranging from alkali basalt to trachybasaltic andesite. Most are phenocryst poor (0%–8%) with an aphanitic or microcrystalline groundmass. Alkali basalts typically contain small (~1 mm) olivine phenocrysts, whereas more evolved compositions have 1%–5% clinopyroxene and/or plagioclase phenocrysts with only trace olivine.

The mafic lavas overlap the range of the alkalic upper Steens Basalt on the TAS diagram (Fig. 6), but contain higher P_2O_5, Ba, and Sr and lower Zr and TiO_2 and lower Zr/Ba than Steens Basalt (Fig. 14; Table 4). They have chemical similarities to a stack of somewhat older alkalic basalts that erupted 16.6–16.0 Ma in the Buffalo Hills and Smoke Creek region of northwestern Nevada, southwest of the HRCC, and to the small volumes of basalt in the northern Nevada rift (Camp et al., 2013) that erupted between 16.5 and 15.0 Ma (John et al., 2000).

Intermediate lavas, ranging in composition from trachyandesite to trachyte (Fig. 6), erupted along trapdoor uplift–related faults in the Badger Mountain caldera and in relatively large volumes from vents within and along the southern ring fracture of the Hanging Rock caldera (Fig. 4). The trachytic lavas are weakly porphyritic with 2%–8% total phenocrysts of feldspar, clinopyroxene, fayalitic olivine, and Fe-Ti oxides in variable proportions in an aphanitic or microcrystalline groundmass. Feldspar phenocrysts are typically resorbed, which along with the presence of quartz phenocrysts, suggests that there was magma mixing involving entrainment of rhyolitic magma. Despite being crystal poor, all four of the intermediate rocks we analyzed for REEs (MC248, MC300, MC321, and MC390 in Table 4) have pronounced positive Eu anomalies (Fig. 14), suggesting that their current phenocryst-poor state and exceedingly fine grained groundmass comes from a preeruptive heating by hotter magma that caused cumulate feldspars to be resorbed. That these lavas represent mobilization of feldspar-rich cumulates is supported by their extremely high concentrations of Ba, to nearly 10,000 ppm (Table 4).

Late Miocene to Quaternary High-Al Olivine Tholeiite Lavas

Thin, flat-lying lavas of olivine basalt form mesas in the northern part of the HRCC, and postdate all the mid-Miocene volcanism (shown in Figs. 3 and 4 as part of NQm: undifferentiated Neogene–Quaternary deposits). Chemically, they are similar to other lavas in the region that have been termed high-alumina olivine tholeiite (HAOT of Hart et al., 1984) or low-K olivine tholeiite (e.g., Carmichael

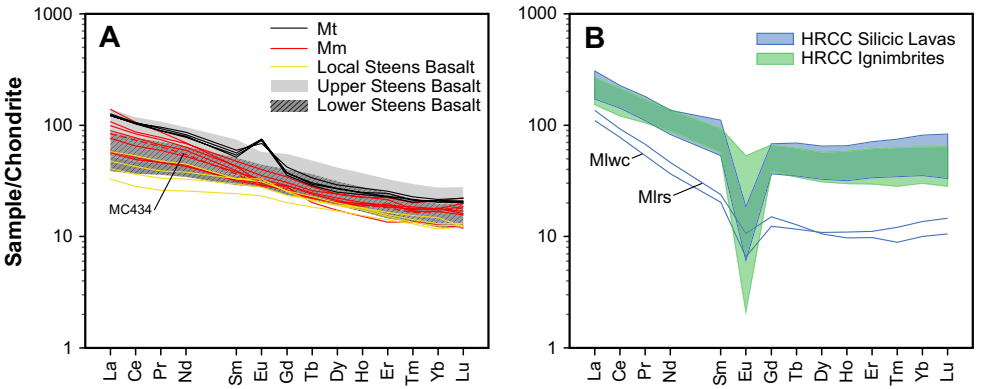

Figure 15. (A) Chondrite-normalized rare earth element (REE) plots for representative postcaldera mafic lavas (Mm) and trachyte lavas (Mt). (B) Range of values for rhyolitic lavas and ignimbrites from High Rock caldera complex (HRCC). Trachyte lavas (Mt), despite being phenocryst poor, have positive Eu anomalies, indicating they interacted with feldspar-rich cumulates. The two rhyolite lavas with lower REE abundances, Mlwc and Mlrs, are metaluminous lavas that postdate main-stage rhyolitic volcanism at their respective locations. Data sources as in Figure 13. REE values are normalized to primitive mantle per McDonough (1991). See text or Table 1 for unit abbreviations.

TABLE 4. REPRESENTATIVE ANALYSES OF MAFIC AND INTERMEDIATE LAVAS IN AND AROUND THE HIGH ROCK CALDERA COMPLEX

	MC409†	AT2*	AT6*	MC434†	MC342*	MC89†	MC312†	MC266†	MC237*	MC383†
Lat (°N)	41.69341	41.1667908	41.1734617	41.5100	41.5650	41.7389	41.5956	41.1655	41.5899	41.7096
Long (°W)	118.8469	119.8340	119.8276	119.3788	119.4431	119.3767	119.3181	119.5236	119.2638	119.3130
Unit	Msb	NQm	NQm	Mm	Mm	Mm	Mm	Mm	Mm	Mm
Composition	AB	B-transitional	B-transitional	AB	AB	AB	AB	AB	TB	TBA
Age (Ma)	n.a.	n.a.	16.6 ± 0.6	n.a.	n.a.	15.55 ± 0.06	n.a.	14.21 ± 0.04	14.84 ± 0.03	n.a.
Normalized major elements (wt %)										
SiO_2	47.83	50.04	50.62	48.68	49.25	48.81	48.78	51.05	51.28	52.14
TiO_2	1.89	0.82	0.84	2.39	2.19	1.53	1.84	1.39	1.88	1.51
Al_2O_3	16.70	17.54	18.35	17.14	18.31	17.05	16.60	16.98	16.16	16.81
FeO*	11.87	8.68	9.02	10.69	10.97	11.49	11.95	9.94	10.50	10.11
MnO	0.20	0.18	0.22	0.19	0.16	0.18	0.19	0.18	0.18	0.18
CaO	9.43	10.63	11.31	10.18	9.14	9.27	9.13	9.15	8.60	7.79
MgO	7.77	8.55	5.91	5.35	4.51	7.08	6.27	6.37	5.53	5.22
K_2O	0.70	0.50	0.41	1.09	1.00	0.70	1.14	1.12	1.78	1.69
Na_2O	3.03	2.66	2.86	3.28	3.84	3.29	3.40	3.09	3.36	3.75
P_2O_5	0.39	0.18	0.22	0.84	0.44	0.38	0.52	0.53	0.54	0.53
Trace	0.18	0.21	0.23	0.17	0.18	0.22	0.18	0.20	0.19	0.28
Total	100.00	100.00	100.00	100.00	100.00	100.00	100.00	100.00	100.00	100.00
LOI	1.59	n.a.	n.a.	3.71	n.a.	0.79	n.a.	1.41	n.a.	0.34

	MC506*	MC390†	MC200	MC249*	MC321†	MC358*	MC381*	AT26	AT13*
Lat (°N)	41.6847	41.3915	41.5935	41.4436	41.5118	41.7744	41.7366	41.6509	41.666571
Long (°W)	119.3175	119.2565	119.1888	119.4184	119.2778	119.3502	119.1030	119.7533	119.7090
Unit	Mm	Mt	Mt	Mt	Mt	MQb	MQb	MQb	MQb
Composition	TBA	TBA	TA	T	T	B-HAOT	B-HAOT	B-HAOT	B-HAOT
Age (Ma)	15.08 ± 0.05	14.5 ± 0.8	n.a.	15.44 ± 0.07	n.a.	7.5 ± 0.9	10.1 ± 1.2	4.7 ± 0.8	4.4 ± 0.7
Normalized major elements (wt %)									
SiO_2	54.16	55.83	59.89	61.94	62.34	48.91	48.89	48.10	48.18
TiO_2	1.41	2.29	1.68	1.38	1.41	0.93	0.77	0.93	1.05
Al_2O_3	15.91	15.07	15.58	15.50	15.41	17.52	17.65	17.67	17.51
FeO*	9.72	9.19	5.65	6.11	5.77	9.33	9.24	9.43	9.62
MnO	0.17	0.21	0.70	0.25	0.19	0.18	0.18	0.17	0.17
CaO	7.27	6.50	4.50	3.63	3.62	11.34	11.85	11.60	11.35
MgO	5.10	3.24	1.98	1.52	1.61	8.37	8.40	9.04	8.77
K_2O	1.94	2.23	3.60	4.00	3.88	0.43	0.27	0.22	0.34
Na_2O	3.63	3.88	4.45	4.55	4.58	2.71	2.49	2.57	2.69
P_2O_5	0.43	1.22	0.76	0.57	0.61	0.14	0.10	0.11	0.15
Trace	0.26	0.33	1.21	0.53	0.58	0.16	0.16	0.17	0.18
Total	100.00	100.00	100.00	100.00	100.00	100.00	100.00	100.00	100.00
LOI	n.a.	0.29	1.26	n.a.	0.79	n.a.	n.a.	n.a.	n.a.

Note: MC200 and AT26 were analyzed by X-ray fluorescence (XRF) at Franklin & Marshall College (Lancaster, Pennsylvania; Stan Mertzman). LOI—loss on ignition; n.a.—not analyzed. B—basalt, AB—alkali basalt, TB—trachybasalt, TBA—trachybasaltic andesite, TA—trachyandesite, T—trachyte, Msb—Steens Basalt, HAOT—high-Al olivine tholeiitic, NQm—Quaternary Undifferentiated Volcanics.

*Sample numbers were analyzed at Washington State University (Pullman) Geoanalytical Labs by wavelength-dispersive XRF.

†Samples were analyzed by the U.S. Geological Survey for major elements by XRF and for trace elements by inductively coupled plasma–atomic emission spectroscopy.

et al., 2006) (Table 4; Fig. 14). The high-alumina olivine tholeiites contain a distinctive diktytaxitic groundmass texture in which angular vesicles occur between groundmass grains of olivine, augite, plagioclase, and minor oxides. Phenocryst content varies between flows, but most contain very small (<0.5 mm) subhedral to anhedral olivine (1%–8% vol%) and plagioclase (0–4 vol%).

LANDSCAPE PRIOR TO DEVELOPMENT OF THE HRCC

Based on the distribution of Miocene ignimbrites and lavas, the landscape prior to eruptions at the HRCC does not appear to have been one of great relief. The current generation of Basin and Range faulting and tilting that created the steep eastern scarp of the Pueblo Mountains and the elevation of the Pine Forest Range postdates volcanism at the MVF and HRCC, based on exposures of Steens Basalt and ignimbrites from the MVF in the tilted section on the west sides of these ranges (Figs. 3 and 4). Our mapping and geochronology suggest that HRCC lavas and ignimbrites and the immediately preceding Steens Basalt erupted onto a hilly topography developed on Paleogene volcanic rocks, and that Paleogene volcanic edifices influenced the distribution pattern of the mid-Miocene ignimbrites (Figs. 3 and 4).

The oldest Cenozoic rocks in the region surrounding the HRCC are Eocene to Oligocene volcanic and volcaniclastic units. West of the HRCC, the Warner Mountains and Hays Canyon Range (Fig. 2) contain andesite and basaltic lavas with subduction-related chemical affinities, along with thick sections of volcaniclastic sediments and lahars, indicative of an ancestral Cascades arc setting (Duffield and McKee, 1986; Carmichael et al., 2006; Colgan et al., 2011; Egger and Miller, 2011). Paleogene volcanic rocks are present immediately south of the complex (Fig. 3), where they are extensively exposed in the Calico Mountains (Bonham and Papke, 1969; this study). To the east in the Pine Forest Range, they consist of rhyolitic ignimbrites, subordinate silicic lavas, and rare basalt and basaltic andesite lava flows (Noble et al., 1970; Colgan et al., 2006; Lerch et al., 2008). Most are calc-alkaline to alkali-calcic in composition, characterized by the presence of plagioclase and biotite phenocrysts in felsic rocks. There are, however, mildly peralkaline Oligocene rhyolites similar in composition to the rhyolites of the HRCC: the Ashdown Tuff and tuff of Alder Creek (Colgan et al., 2006; Lerch et al., 2008).

On the east side of the HRCC, mid-Miocene ignimbrites appear to have been influenced by a north-northeast–trending basin in what is now the area of Bog Hot Valley, Craine Creek Valley, and the northern Black Rock Desert (Fig. 3). We interpret the thick section of Idaho Canyon Tuff in the northern Black Rock Range and the tuff of Trough Mountain to have ponded in this north-northeast–trending paleobasin, which also seems to have controlled the distribution of the Summit Lake Tuff and Soldier Meadow Tuff (Fig. 4). We interpret the sediments in this north-northeast–trending basin, now largely removed by erosion, to have formed the eastern topographic wall for the Virgin Valley caldera. The presence of an active alluvial channel in the mid-Miocene west of what is now the southern Pueblo Mountains and northern Pine Forest Range may account for the relative lack of exposures of the caldera-forming unit, the Idaho Canyon Tuff , northeast of the caldera (Fig. 4).

Preexisting topography, albeit of low relief, also influenced the distribution of the Oregon Canyon Tuff and other ignimbrites from the MVF. They overtopped a low divide between what is now the southern Pueblo Mountains and the northern Pine Forest Range, but most of the volume of these units was confined to the east (Figs. 3 and 4).

Although the presence of a north-northeast–trending paleobasin and the partial confinement of MVF outflow ignimbrites are consistent with post-Oligocene, pre–16.5 Ma normal faulting, the magnitude of such faulting must have been small. Early Miocene sediments preserved beneath high-alumina olivine tholeiite lavas at Oregon End Table and Big Springs Table and on both sides of Craine Creek Valley (Fig. 4) consist of silt- to pebble-sized clasts, indicating that the relief was not great enough to generate coarse debris. Most of the identifiable clasts are silicic volcaniclastic rocks derived from mid-Miocene and Paleogene volcanic rocks. Modern Craine Creek Valley, in contrast, contains coarser deposits of sand- to cobble-sized clasts that include granitic and metamorphic rocks in addition to volcaniclastic debris, presumably due to the relief produced by late Miocene to Holocene uplift of the Pine Forest and Black Rock Ranges that exposed the basement. This faulting may have reactivated pre–16.5 Ma faults, particularly in the Black Rock Range.

GEOLOGIC HISTORY OF THE HRCC

Precaldera Volcanism

Overall, there is a paucity of precaldera volcanism at the HRCC. This statement has to be qualified by the fact that there may be precaldera volcanism covered on the north and west by late Miocene high-Al olivine tholeiite lavas and obscured in the interior of the complex by successive caldera collapse.

Steens Basalt

The nearest exposures of known Steens Basalt are east of the HRCC in the southern Pueblo Mountains (Hart et al., 1989) and the northern Pine Forest Range (Colgan et al., 2010). There are undated lavas mapped as Steens Basalt that underlie outflow ignimbrites further south in the Pine Forest Range, Idaho Canyon, and in the northern Black Rock Range (Figs. 3 and 4), but this correlation has been confirmed chemically only on the east side of Craine Creek Valley and in Idaho Canyon (Figs. 3 and 4), where both have chemical similarities to upper Steens Basalt (Figs. 13–15).

The section of Steens Basalt lavas thins abruptly south of the Oregon-Nevada border (Lerch et al., 2008) from nearly 1 km in the northern Pueblo Mountains (Hart et al., 1989) to ~550 m in the northern Pine Forest Range (Colgan et al., 2010). In a fault scarp on the east side of Idaho Canyon (Figs. 3, 4, and 16), ~80 m of Steens Basalt is present; the base is unexposed. In the northern Black Rock Range, the Steens Basalt is ~150 m thick. South of ~41.55°N (Figs. 2 and 3), however, the Steens

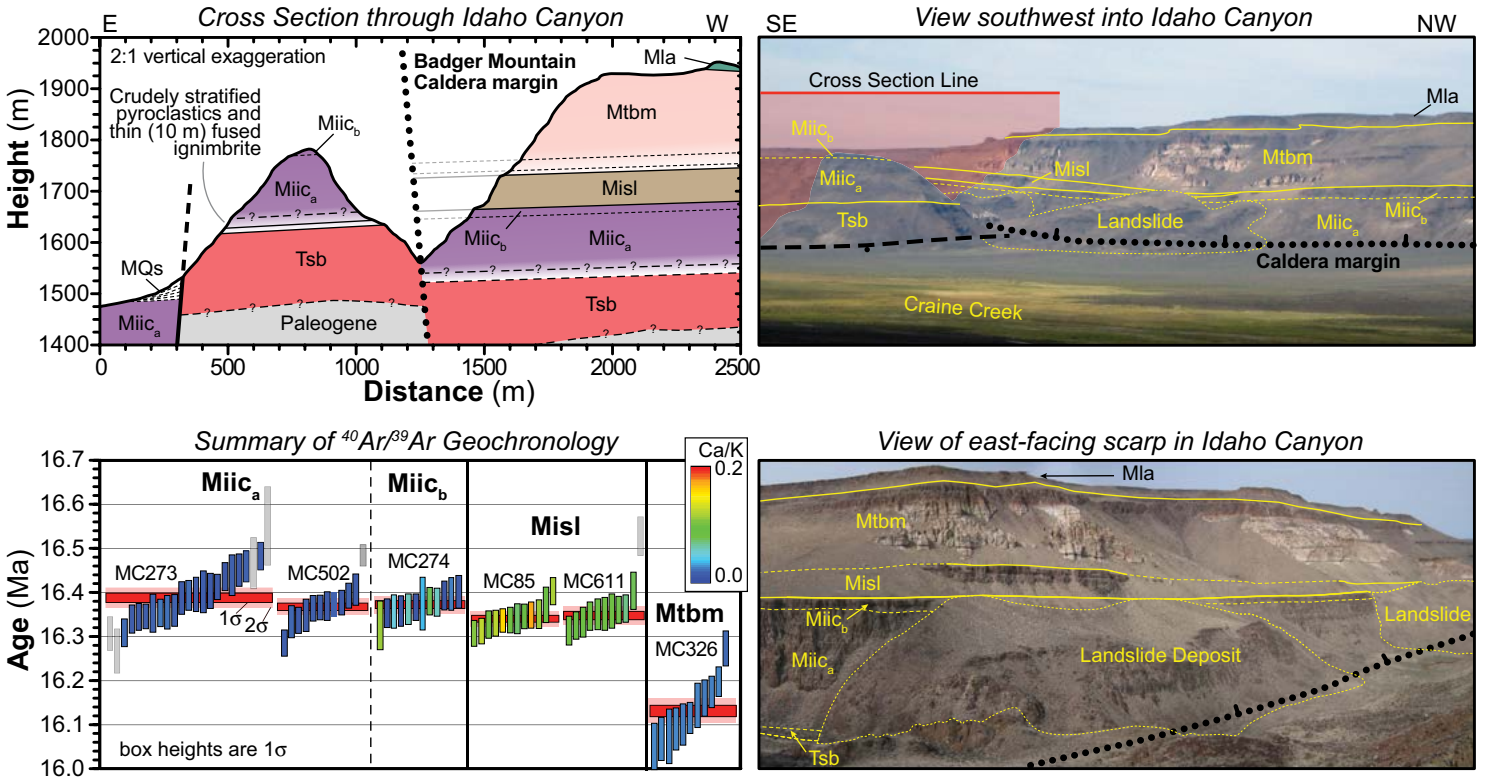

Figure 16. Photos and stratigraphic relationships exposed near the mouth of Idaho Canyon. Basalt lavas we have chemically correlated with the Steens Basalt (Tsb) are at the base of the exposed section. In the cross section we indicate the presence of older Paleogene volcanic rocks at a shallow depth based on their exposure nearby. Outflow Idaho Canyon Tuff is zoned from crystal poor (Miic$_a$) to strongly porphyritic (Miic$_b$). The Summit Lake Tuff (Misl) is overlain by reworked and primary pyroclastic deposits, which are in turn overlain by the tuff of Big Mountain (Mtbm), which is preserved where it accumulated within the Badger Mountain caldera and was covered by cogenetic Antelope lavas (Mla). The color of the boxes for the $^{40}Ar/^{39}Ar$ analyses are keyed to the Ca/K of the individual feldspar grains analyzed; blue is sodic sanidine and orange is anorthoclase. Gray boxes are analyses that were not included in the weighted mean age. Red bands are weighted mean age at 1σ and 2σ. MQs—Miocene-Quarternary Basin-fill Deposits. See text or Table 1 for unit abbreviations.

Basalt is, to our knowledge, absent, and outflow ignimbrites from the HRCC and MFV directly overlie Paleogene sedimentary and volcanic rocks (Lerch et al., 2008; this study) in the Black Rock Range and Calico Mountains (Fig. 3).

Mid-Miocene Mafic and Intermediate Lavas

Mafic and intermediate lavas that are not petrographically Steens Basalt directly underlie HRCC rhyolitic lavas near Massacre Creek, Wall Canyon Reservoir, and Nellie Spring Mountain, and are found beneath outflow ignimbrites in the Calico Mountains (Figs. 3 and 4). Based on the available chemistry and their petrography and geologic occurrence, we believe that all of these lavas except those near Wall Canyon Reservoir are Paleogene, although this remains to be proved. We obtained a $^{40}Ar/^{39}Ar$ age of 16.55 ± 0.56 Ma from a transitional olivine basalt lava near Wall Canyon Reservoir (AT6 in Table 4; Fig. 4). It underlies lavas from the Cottonwood Creek caldera, which our dating indicates erupted between 15.9 and 15.6 Ma. See the Supplemental Text File for new $^{40}Ar^{39}Ar$ ages and a discussion of other precaldera mafic and intermediate units in Nellie Spring Mountain and at Massacre Rim.

Silicic Lavas

Hawks Valley—Lone Mountain volcanic center 16.5–16.3 Ma. There is significant silicic activity of mid-Miocene age 10 km north of Virgin Valley caldera at the Hawks Valley–Lone Mountain center (Figs. 3 and 4), for which Wypych et al. (2011) reported $^{40}Ar/^{39}Ar$ plateau ages for trachydacitic

and rhyolitic lavas that range from 16.51 ± 0.25 to 16.33 ± 0.17 Ma. It remains to be demonstrated through further mapping and more precise geochronology whether this center contains a caldera and how it relates to the HRCC. We include it within precaldera volcanism because distal outflow of the first major ignimbrite from the HRCC, the 16.38 Ma Idaho Canyon Tuff, banks in against silicic lavas at the Hawks Mountain massif (Fig. 3). This age relationship is consistent with the southward younging of the initiation of activity within the HRCC.

Rhyolite lavas of Nut Mountain (Mlnm) 16.6 Ma. The oldest rhyolitic unit in the HRCC proper is the rhyolite lavas of Nut Mountain (Mlnm), which emanated from a large cumulodome centered at Nut Mountain (Figs. 3 and 4). The lavas are aphyric and typically finely devitrified and strongly flow foliated. Obsidian nodules to 25 cm in diameter are ubiquitous in talus at the base of outcrops or as subcrop, and the dark gray, opaque, and slightly resinous luster of the obsidian is unique at the HRCC. Mlnm are metaluminous high-silica rhyolite in composition, setting them apart from the alkali rhyolites that dominate the main stage of silicic volcanism at the HRCC. As such, they contain the lowest measured concentrations of HFSE elements and have relatively elevated Ba and Sr (Table 3).

A sample of aphyric devitrified lava (MC341) from Nut Mountain yielded an inverse isochron age of 16.59 ± 0.15 Ma. Nut Mountain is one of the few units in the HRCC that has a normal paleomagnetic polarity (Fig. 17). This age is consistent with Nut Mountain lavas having erupted during the C5Cr chron. The 25 × 15 km positive aeromagnetic anomaly centered on Nut Mountain (Fig. 18) suggests that Nut Mountain lavas extend west beneath younger eruptive units to cover an area at least twice that of the current 7-km-diameter exposure.

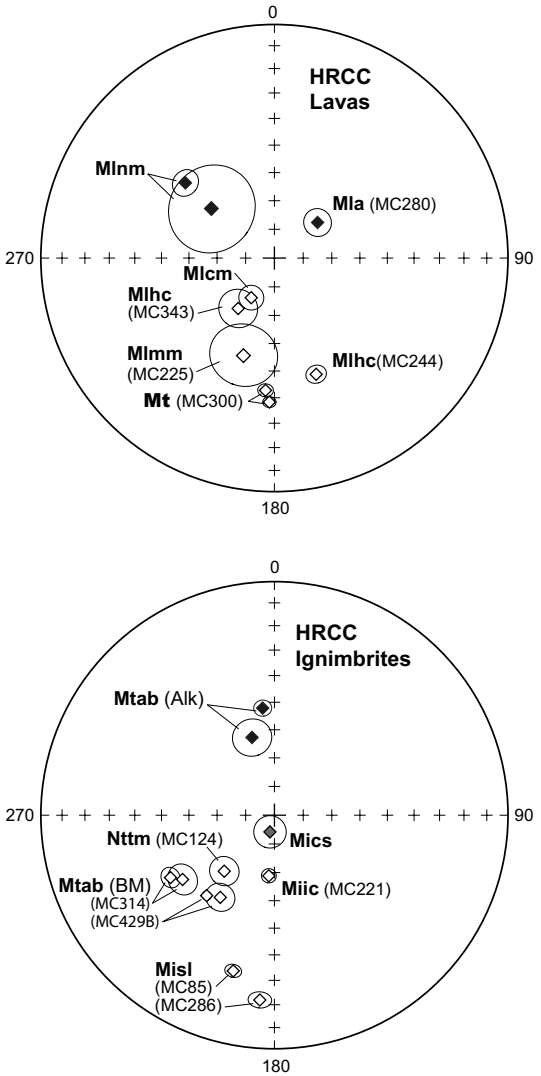

Figure 17. Equal-area projections showing paleomagnetic directions for lavas (top) and ignimbrites (bottom) from High Rock caldera complex (HRCC). Mean directions are shown by a black diamond for normal polarity, gray diamond for transitional, and white diamond for reversed. The black line surrounding the mean direction indicates 95% confidence limits. The tuff of Alkali Flat and Badger Mountain (Mtab) records both normal and reversed directions, confirming the results of Park (1983) and demonstrating that it is a composite unit separate from the petrographically similar Soldier Meadow Tuff. Paleomagnetic drill-site locations and results are shown in Supplemental Table 4. The tuff of Alkali Flat (Alk) and tuff of Badger Mountain (BM) are plotted separately after Park (1983). See text or Table 1 for unit abbreviations.

Idaho Canyon Tuff (Miic) 16.38 Ma

The first major ignimbrite known to erupt from the HRCC is the Idaho Canyon Tuff, which resulted in collapse of the Virgin Valley caldera. It was named formally by Noble et al. (1970) for exposures in Idaho Canyon (Figs. 3, 4, and 16). The ignimbrite is typically strongly welded and devitrified, with distinctive well-developed postdepositional revesiculation cavities 5–30 cm in diameter (Fig. 19). Lithics are rare, but are most abundant near Virgin Valley, where they are mostly devitrified rhyolite or mafic lava fragments <2 cm in size.

The Idaho Canyon Tuff is zoned from crystal-poor (~4–8 vol%) high-silica alkali rhyolite ($Miic_a$) to slightly more mafic, crystal-rich (~15–20 vol%), high-silica alkali rhyolite ($Miic_b$) (Figs. 11 and 12; Table 2). The zoning is best displayed at the mouth of Idaho Canyon (Figs. 16 and 19), where the strongly welded ignimbrite overlies crystal-poor Steens Basalt and ~25 m of pyroclastic deposits. Approximately 125 m of crystal-poor, pur-

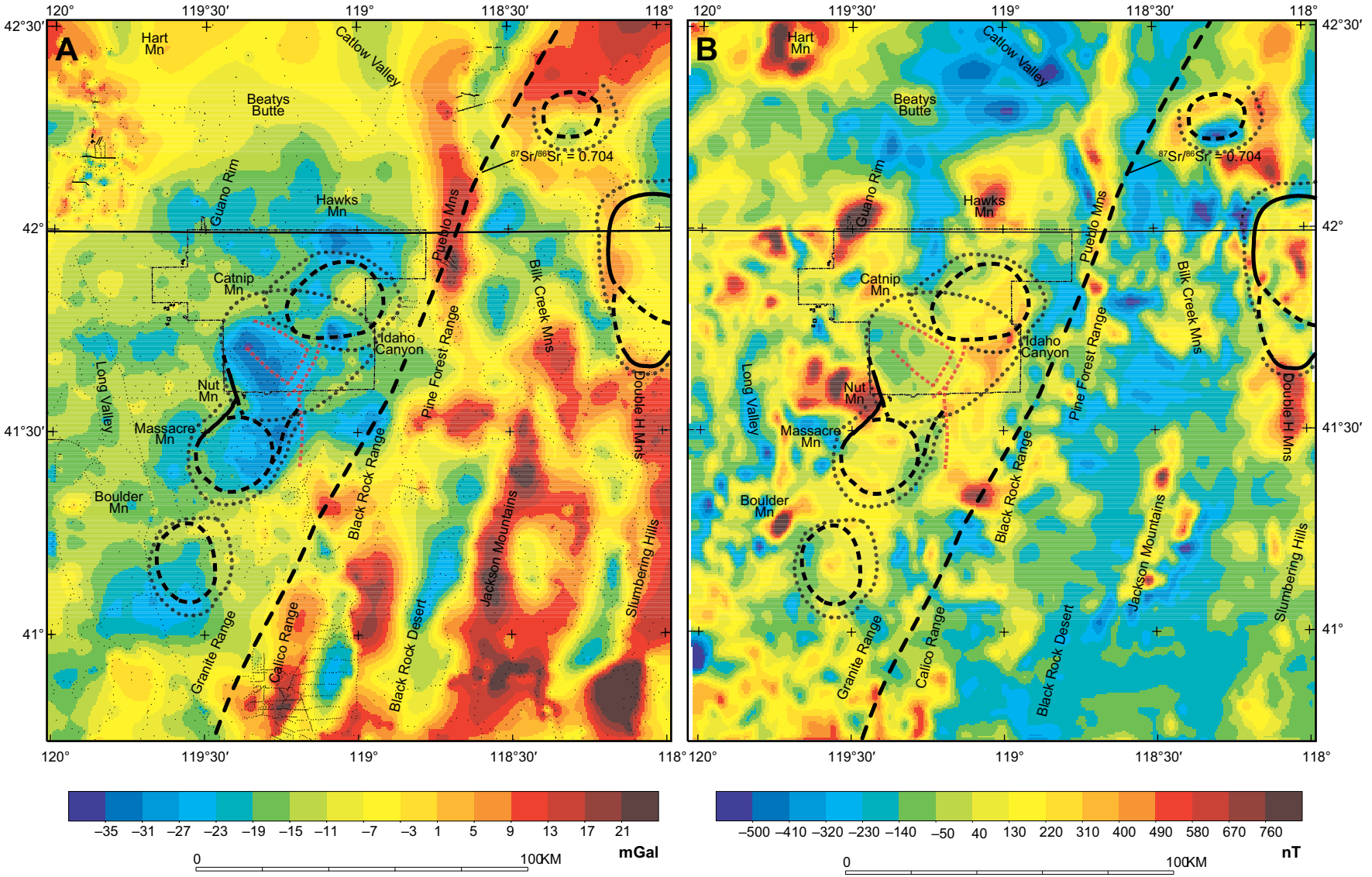

Figure 18. Regional gravity and reduced to pole magnetic maps of the region around High Rock caldera complex (HRCC). Prominent physiographic features and line symbols for mid-Miocene calderas and the Sheldon National Antelope Refuge are the same as in Figure 3. Mn—mountain; Mtns—mountains. (A) Isostatic residual gravity map for northwest Nevada and southern Oregon. Small black dots are individual gravity stations. The HRCC is well expressed regionally by large gravity lows that are interpreted to be the result of thick accumulations of low-density sediments and/or nonwelded ignimbrite deposits, as well as subjacent plutons or buried Paleogene calderas. The individual mid-Miocene calderas, however, generally do not coincide with gravity lows due to overlapping collapse structures, renewal of magmatism within the Badger Mountain caldera, and younger mafic magmatism in HRCC. (B) Reduced to pole aeromagnetic map for northwest Nevada and southern Oregon. Features of the mid-Miocene calderas of the HRCC are expressed in the aeromagnetic map locally where lava edifices are truncated by caldera collapse (e.g., Nut Mountain), but generally there is not a strong correlation of calderas and magnetic signature due to the complicated distribution of postcaldera rhyolitic, trachytic, and mafic lavas and alteration zones in the lavas and caldera lake sediments producing variations in magnetic properties over short distances.

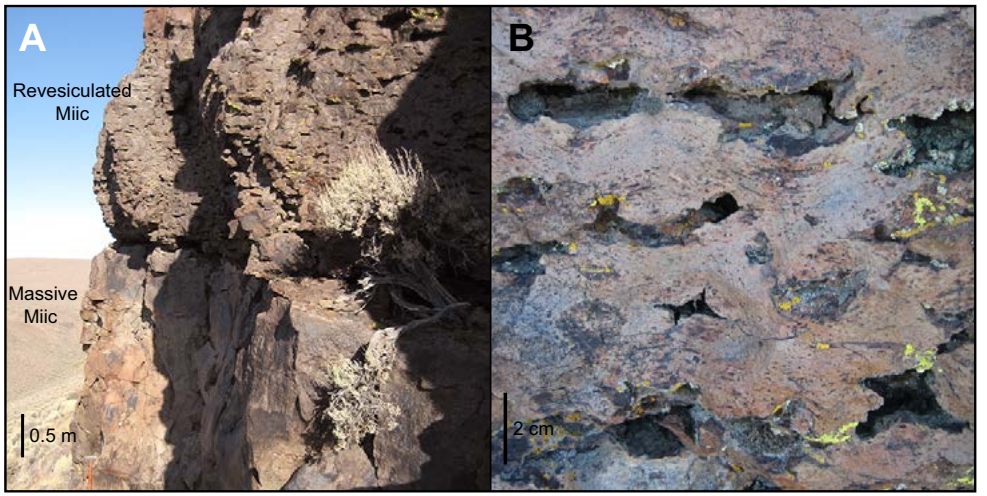

Figure 19. Photographs of outcrops of the Idaho Canyon Tuff (Miic; see text). (A) Densely welded and revesiculated Idaho Canyon Tuff. (B) Close-up of revesiculation and resulting lithophysal structures.

plish-gray $Miic_a$ grades sharply at the top of the section into an ~11-m-thick section of crystal-rich, dark gray to dark brown $Miic_b$. Lithics are more abundant (5%–8%) and slightly larger (1–5 cm) in $Miic_b$. Both $Miic_a$ and $Miic_b$ span a range of compositions (Fig. 12) and phenocryst abundance, but the obvious quartz and small feldspars of $Miic_a$ contrast with the larger and more abundant feldspar and the general absence of quartz characteristic of the slightly less evolved $Miic_b$.

The most extensive exposure of the ignimbrite, northwest of Virgin Valley (Figs. 3–5) consists entirely of $Miic_a$, where fresh surfaces are tan to pinkish-gray, and the densely welded and revesiculated portions weather to a deep reddish-brown. Exposures in Catnip Creek indicate that the outflow sheet is at least 80–100 m thick near the Virgin Valley caldera, where it consists of a single cooling unit with a characteristic tripartite massive-revesiculated-massive section (Fig. 19). To the north, several welding reversals become apparent, and where it laps against rhyolitic lavas of the Hawks Valley–Lone Mountain center, the ignimbrite is ~10 m thick. $Miic_b$ is best exposed in the scarp that extends from Idaho Canyon to south of McGee Mountain and in the northwesternmost Black Rock Range in the headwaters of Craine Creek, where it is densely welded. Thin, partially welded deposits occur locally in the westernmost Pine Forest Range.

We obtained $^{40}Ar/^{39}Ar$ ages on sanidine of 16.39 ± 0.02 Ma (MC273) and 16.37 ± 0.02 Ma (MC502) for densely welded samples of outflow $Miic_a$ collected at Idaho Canyon and near Sage Hen Hills ~12 km northwest of the Virgin Valley caldera, respectively, and 16.37 ± 0.02 Ma (MC274) on $Miic_b$ collected stratigraphically above $Miic_a$ at Idaho Canyon (Table 1). All 3 ages agree within 2σ error with the $^{40}Ar/^{39}Ar$ age of 16.40 ± 0.04 Ma reported by Castor and Henry (2000) for strongly welded Idaho Canyon Tuff exposed at the base of McGee Mountain (H95–74 in Fig. 4). We recollected the densely welded, crystal-rich exposure at their H95–74 locality (MC500), and, on analysis, found it to have the low Rb, Zr, Th, and Nb, and high Ti and Ba concentrations characteristic of $Miic_b$ (Figs. 11 and 12).

See the Supplemental Text File for a discussion of how we have distinguished Idaho Canyon Tuff $Miic_a$ from the slightly older Oregon Canyon Tuff sourced from the MVF (Rytuba and McKee, 1984), and $Miic_b$ from the similar looking, but slightly younger Summit Lake Tuff.

Summit Lake Tuff (Misl) 16.34 Ma

The Summit Lake Tuff (Misl) is a strongly porphyritic (25–32 vol%) low-silica alkali rhyolite ignimbrite, the eruption of which resulted in collapse of the proposed Badger Mountain caldera. The ignimbrite was described and named formally by Noble et al. (1970) for exposures near Summit Lake. Although exposures are generally thin (5–25 m), the Summit Lake Tuff has the largest areal distribution of the mid-Miocene ignimbrites in the HRCC (Fig. 5), and has an estimated volume of 31 km^3. It typically forms dark gray or dark brown rounded ledges of a single densely welded cooling unit (Fig. 20) with well-developed eutaxitic texture. Post-welding revesiculation cavities and lithophysae are common, and can be tens of centimeters in diameter. Lithic fragments typically make up 3%–5% of the rock, and are predominantly basaltic lava, with subordinate devitrified rhyolite and obsidian nodules. Talus and modern soils derived from the Summit Lake Tuff are distinctively crystal rich. The abundance of anorthoclase crystals, paucity of quartz (those present are xenocrystic), and dark color distinguish the Summit Lake Tuff from other HRCC ignimbrites.

We obtained a $^{40}Ar/^{39}Ar$ age of 16.34 ± 0.02 Ma on anorthoclase from the Summit Lake Tuff (MC85, Fig. 7) collected from near the type locality north of the Summit Lake Reservation (Figs. 3 and 4). We also obtained ages on 2 additional densely welded localities: 16.35 ± 0.02 Ma (MC611) from south of the summit of Nut Mountain, and 16.29 ± 0.03 Ma (MC263) from south of High Rock Lake. A sample of pumice lapilli from vapor-phase–altered, non-welded ignimbrite 5 km east of MC263 yielded an age of 16.31 ± 0.03 Ma (MC365).

Our preferred age of 16.34 Ma for the caldera-forming Summit Lake Tuff is based on the age for MC85, which was coirradiated and analyzed as an internal standard with all other eruptive units analyzed in this study. This age is stratigraphically consistent with the field observations that the Summit Lake Tuff directly overlies the 16.6 Ma lavas from Nut Mountain and the 16.38 Ma Idaho Canyon Tuff (Figs. 4 and 21). It is indistinguishable from the age of 16.33 ± 0.03 Ma (H06–18) reported in Smith

(2011) for a sample collected north of Summit Lake and analyzed at the New Mexico Geochronology Research Laboratory.

See the Supplemental Text File for a discussion of an ignimbrite with anomalously old ages tentatively mapped as Summit Lake Tuff in Massacre Creek and near Massacre Rim, and its possible correlation with the tuff of Big Basin of Swisher (1992).

Alkali Rhyolite Lavas of Catnip Mountain (Mlcm) 16.3 Ma

Catnip Mountain is a large composite lava dome consisting of aphyric, moderately peralkaline, high-silica alkali rhyolite lavas (Figs. 4 and 5). Greene (1984) informally named the lavas the Catnip rhyolite, and included within it the weakly porphyritic lava of Echo Canyon that we have assigned to the Hell Creek lavas. Devitrified exposures exhibit very strong millimeter- to centimeter-scale chaotic flow foliation. Poorly developed pressure ridges make it difficult to determine vent locations for individual flows. Black nodules of nonhydrated obsidian are locally abundant as a lag on surfaces. The obsidian is transparent on thin edges, whereas obsidian from the older Nut Mountain lavas is opaque.

We obtained an inverse isochron age of 16.31 ± 0.13 Ma from aphyric, devitrified, alkali rhyolite lava (MC504) sampled west of Catnip Mountain (Table 1; Fig. 8). Given the relatively large uncertainty on the age for the devitrified matrix of this aphyric lava, we cannot resolve it from the ages of the Idaho Canyon Tuff and Summit Lake Tuff or from the ages for the Hell Creek lavas (discussed in the following sections). We map the alkali rhyolite lavas of Catnip Mountain separately from aphyric Hell Creek lavas of similar age because the Catnip Mountain lavas are chemically distinct, with higher Zr/Rb ratios (Fig. 5). We interpret exposures along Nevada State Route 140 to indicate that Catnip Mountain lavas overlie the Idaho Canyon Tuff. The age relation relative to the Summit Lake Tuff is unknown because the two units are not exposed nearby. See the Supplemental Text File for a discussion of additional $^{40}Ar/^{39}Ar$ ages, unit correlations, and chemistry.

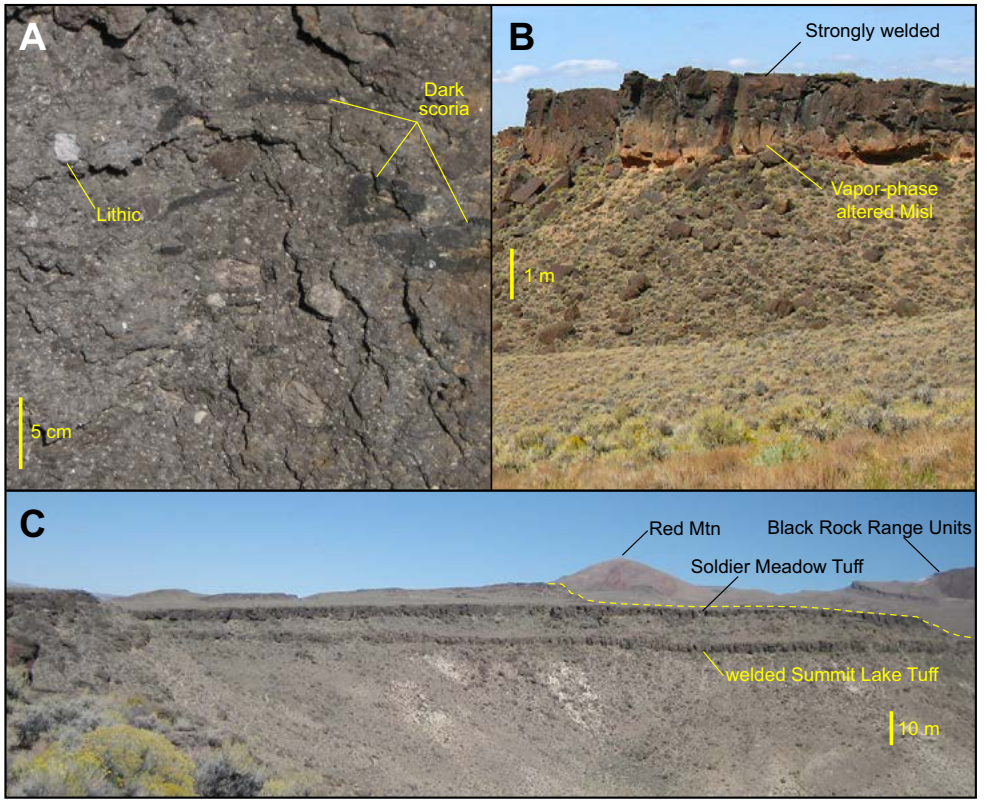

Figure 20. Photos of outcrops of the Summit Lake Tuff (Misl; see text). (A) Lithic-rich, moderately welded Summit Lake Tuff exposed south of Massacre Creek showing angular lithics of devitrified rhyolite and dark colored low-silica alkali rhyolite pumice lapilli and scoria. (B) Vapor-phase–altered nonwelded base grading upward into densely welded Summit Lake Tuff south of High Rock Lake. (C) Panoramic view looking northeast in the Black Rock Range. Lower bench of welded Summit Lake Tuff and upper bench of Soldier Meadow Tuff, banking in against Oligocene(?) volcanic rocks visible in the background.

Alkali Rhyolite Lavas of Hell Creek (Mlhc) 16.3–16.2 Ma

Aphyric and weakly porphyritic high-silica alkali rhyolite lavas that erupted in the western part of the Virgin Valley caldera and along the southern ring fracture and west of the Badger Mountain caldera (Figs. 4, 5, and 21) are newly recognized and informally named the alkali rhyolite lavas of Hell Creek (Mlhc). The total eruptive volume of these lavas is ~12 km^3. We obtained sanidine ages of 16.31 ± 0.03 Ma (MC430) and 16.29 ± 0.02 Ma (MC244, Fig. 7) for lavas at Hanging Rock Canyon and Echo Canyon, respectively. We also analyzed sanidine separated from a strongly porphyritic magmatic enclave slightly more mafic than its aphyric host near Hell Creek and obtained an age of 16.22 ± 0.02 Ma (MC433). We interpret the range of ages to reflect eruptions of chemically similar lavas over ~30–100 k.y. See the Supplemental Text File for a description of the distribution and field attributes of Mlhc lavas.

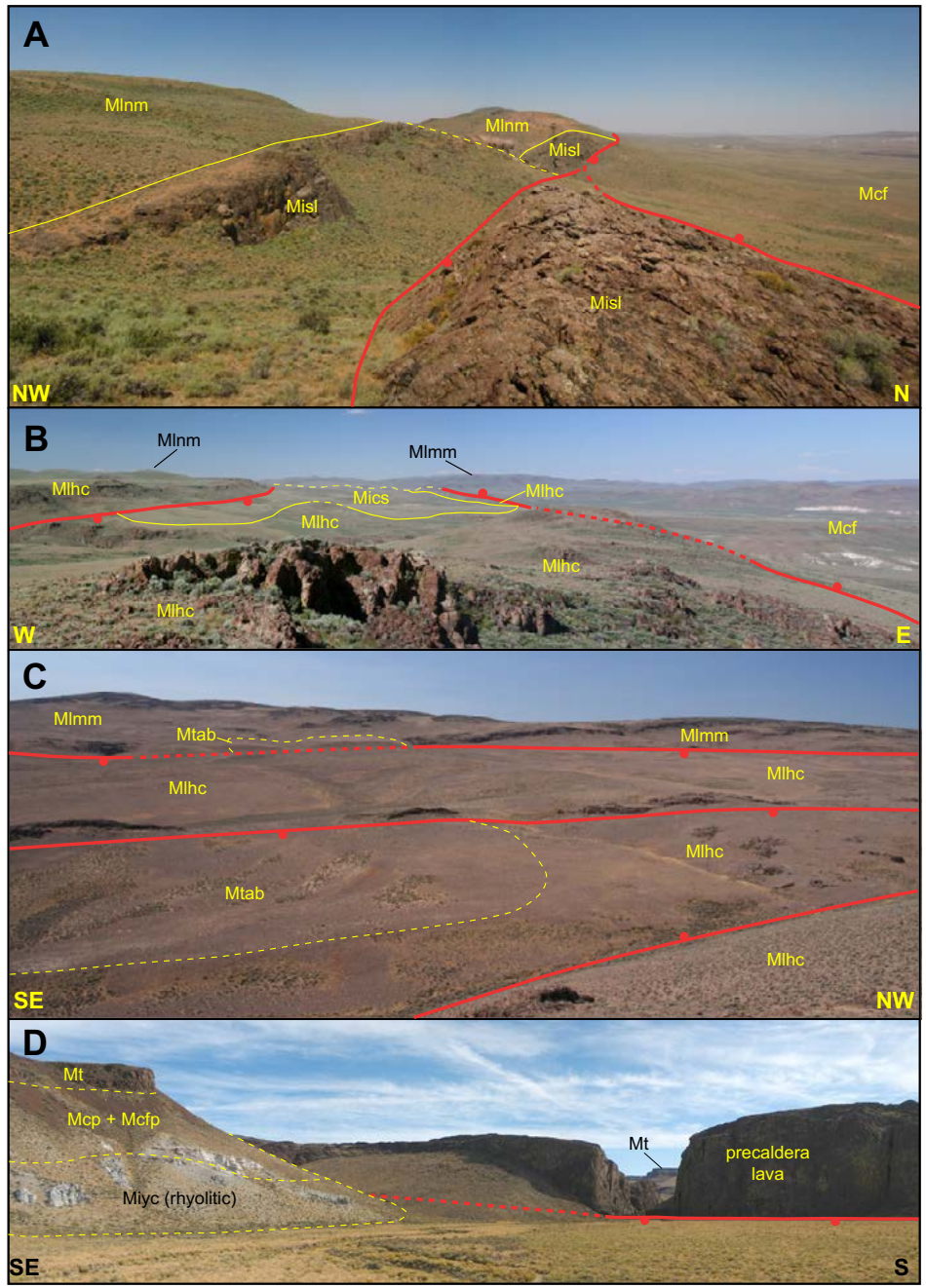

Figure 21. Panoramic photographs illustrating caldera margins and stratigraphic relationships between units. (A) View looking northwest along the margin of the Badger Mountain caldera in Wall Canyon. The 30–55-m-wide fault-bound blocks of strongly silicified and steeply dipping Summit Lake Tuff (Misl) were reactivated by later faults related to caldera collapse associated with eruption of the tuff of Coyote Spring and/or by renewed magmatism within the Badger Mountain caldera. (B) Panoramic view looking northeast at parallel benches of precaldera rhyolitic lavas of Nut Mountain (Mlnm), Hell Creek lavas (Mlhc), and the tuff of Coyote Spring (Mics), forming a 3–5-km-wide zone that defines the topographic margin of the Hanging Rock caldera. Caldera fill sediments (Mcf) bank against precaldera Mlhc. Younger lavas (Mlmm) related to renewal of volcanism in Badger Mountain caldera are visible at Badger Mountain in the background. (C) Benches of crystal-poor rhyolitic Hell Creek lavas (Mlhc) uplifted along Hell Creek, along what is interpreted as the reactivated structural margin of the Virgin Valley caldera. Crystal-rich rhyolitic lavas (Mlmm) erupted from vents focused along trapdoor uplift–related faults are locally onlapped by cogenetic tuff of Alkali Flat and Badger Mountain (Mtab). (D) View looking south in High Rock Canyon. A precaldera lava was truncated by collapse of the Hanging Rock caldera. The 15.70 Ma tuff of Yellow Rock Canyon (Miyc) flowed into this caldera and is exposed below caldera fill (Mcf) and trachytic lavas (Mt).

Tuff of Big Mountain (Mtbm) and Alkali Rhyolite Antelope Lavas (Mla) 16.3–16.1 Ma

Closely following and in part contemporaneous with eruption of the Catnip and Hell Creek lavas, less peralkaline lavas vented within the Virgin Valley caldera in association with eruptions of small ignimbrites, falls, and surges (Fig. 5). The weakly peralkaline, moderately porphyritic (8–10 vol%) alkali rhyolite lavas, which we have informally named the alkali rhyolite Antelope lavas, are interpreted as ring-fracture lavas (Castor and Henry, 2000), based on the arcuate pattern of vent locations partially encircling Virgin Valley (Fig. 4). Lava flows at lower elevations were covered by and interfingered with caldera lake sediments, resulting in highly silicified outcrops that weather rust-red or bright red. Antelope lavas exposed near the tops of McGee Mountain and Big Mountain have an appearance more typical of lavas in the HRCC. A large dike exposed in the east-facing fault scarp on the northeast side of Big Mountain (rhyolite dike, Tcrd, of Greene, 1984) has more phenocrysts than the typical Antelope lavas (~15% versus 5%–10%)

and is fresher; we interpret it as a feeder for the youngest lava capping Big Mountain.

Intercalated with the Antelope lavas are small ignimbrites, fall and surge deposits, and minor reworked volcaniclastic sedimentary intervals that make up the tuff of Big Mountain (Greene, 1984; Castor and Henry, 2000; this study). This unit name was originally applied by Noble et al. (1970) to the most conspicuous eruptive unit in the tuff, a crystal-poor (2–5 vol%) ignimbrite with a small areal extent near Big Mountain (Figs. 3, 4, 16, and 22). The ignimbrite is mostly nonwelded, with white pumice lapilli 3–15 cm in diameter, forming rounded light pink or light gray hoodoos and talus slopes; however, the upper 4–20 m is weakly to moderately welded, vapor-phase altered, salmon-colored on weathered surfaces, and incipiently columnar jointed (Fig. 22). It is relatively lithic rich (7%–12%), containing clasts to 6 cm in diameter of mafic lava, devitrified rhyolitic lava, and crystal-rich, densely welded ignimbrite, which are locally concentrated in layers.

We obtained an age of 16.25 ± 0.03 Ma (MC413) for a sample of alkali rhyolite Antelope lavas located low on the southeast side of McGee Mountain, which overlaps the $^{40}Ar/^{39}Ar$ age of 16.27 ± 0.04 Ma reported by Castor and Henry (2000) for a lava low on the northwest side. Castor and Henry (2000) reported a $^{40}Ar/^{39}Ar$ age of 16.20 ± 0.04 Ma for an Antelope lava high on McGee Mountain, and a similar age of 16.23 ± 0.03 Ma for ignimbrite below it. We obtained an age of 16.13 ± 0.03 Ma (MC326) for sanidine extracted from pumice lapilli in the main ignimbrite south of Big Mountain, which we interpret as the age of emplacement of the Antelope lava making up Big Mountain.

The compositions of Antelope lavas and pumice from the tuff of Big Mountain are similar regardless of age (Fig. 8), which suggests that the tuff of Big Mountain is composed of relatively small volume ignimbrites, falls, and surge deposits that erupted in association with emplacement of the Antelope lavas along the ring fracture of the Virgin Valley caldera over an extended period of time, perhaps 100 k.y.

The tuff of Big Mountain is ~150 m thick in the cliff west of Idaho Canyon, but it is absent immediately east of Idaho Canyon and south of Rock Spring Table, suggesting that it is preserved only where it is overlain by Antelope lavas. We interpret the tuff of Big Mountain as representing subaerial and minor littoral deposits at the margin of the caldera lake filling the Virgin Valley caldera; fine-grained, diatomaceous, ashy sediments indicative of a deep caldera lake environment accumulated in the depocenter in Virgin Creek (Fig. 3).

Our work suggests there are tuffs in the caldera fill section that are both older and younger than the Antelope lavas, and that the caldera fill records input from sedimentary and volcanic sources from the time of caldera collapse on eruption of the Idaho Canyon Tuff at 16.38 Ma until the end of most rhyolitic volcanism at 15.5 Ma. See the Supplemental Text File for further information on these tuffaceous deposits and the ages of units within them.

Tuff of Coyote Spring (Mics) 16.27 Ma

More or less simultaneously with ring-fracture eruption of the weakly peralkaline alkali rhyolite Antelope lavas and associated tuff of Big Mountain, more strongly peralkaline rhyolite lavas erupted along and near the southeastern ring fracture of the Badger Mountain caldera in a swath immediately north and northeast of the site of the future Hanging Rock caldera. Two ignimbrites that are similar in age and only slightly different in composition, the tuff of Coyote Spring and the tuff of Trough Mountain, also erupted in this area and may be related to scallop-shaped collapse features preserved between the older Badger Mountain caldera and the younger Hanging Rock caldera.

The tuff of Coyote Spring is a newly identified ignimbrite that is well exposed west of Wall Canyon and around Nut Mountain (Figs. 4, 5, and 21). The crystal-poor (5–9 vol%) ignimbrite is typically moderately to densely welded and devitrified, with a well-developed flattening foliation that causes exposures to weather into flaggy slabs. Outcrops are typically tan to gray, but can be light brown where intensely welded or silicified. Postdepositional revesiculation cavities 5–15 cm in diameter are common in more strongly welded sections. We estimate the exposed volume to be ~5 km^3 based on its restricted distribution and relatively thin exposures (~10–25 m); however, given the dense welding, we suspect that the volume is much greater and that it is buried beneath younger ignimbrites, lavas, and caldera fill to the south and east.

We obtained ages of 16.27 ± 0.04 Ma and 16.27 ± 0.02 Ma for aliquots of sodic sanidine from a densely welded exposure west of Nut Mountain (MC302). This age is consistent with the tuff overlying the 16.6 Ma lavas of Nut Mountain and the 16.29 ± 0.02 Ma Hell Creek lava at Hanging Rock Canyon.

Tuff of Trough Mountain (Mttm) 16.25–16.15 Ma

The tuff of Trough Mountain (Mttm) was named informally by Noble et al. (1970) for the thick section exposed at Trough Mountain (Figs. 3 and 4). Although the bulk of the exposure is lithic-poor, crystal-poor (<6 vol%), densely welded, devitrified alkali rhyolite ignimbrite, the tuff of Trough Mountain is a composite unit consisting of multiple cooling units of nonwelded to densely welded ignimbrite and intercalated welded fall deposits and lavas intruded by petrographically similar north-south–trending rhyolite dikes that are presumably feeders for the upper part of the tuff (Korringa, 1973; this study). The unit has a restricted areal distribution centered on Trough Mountain, where it exceeds 325 m in thickness, and thins rapidly to <50 m within 10 km in all directions (Korringa, 1973). The presence of variably welded fall deposits containing lithic fragments as large as 60 cm in diameter (Korringa, 1973) requires a nearby vent to produce welding in peralkaline fall deposits (Mahood, 1984) and to account for large ballistic lithic blocks. In Slumgullian Creek, densely welded Mttm ignimbrite is overlain by 30 m of chemically similar coarse fall deposit, indicating that the vents are nearby and that the great thickness of Mttm at Trough Mountain is not a result of a far-traveled ignimbrite ponding in a basin. The poorly sorted fall deposits are characterized by white or tan pumice lapilli and by distinctive thick, dark green bubble-wall glass shards as large as 6 mm in diameter that are lacking in other HRCC deposits.

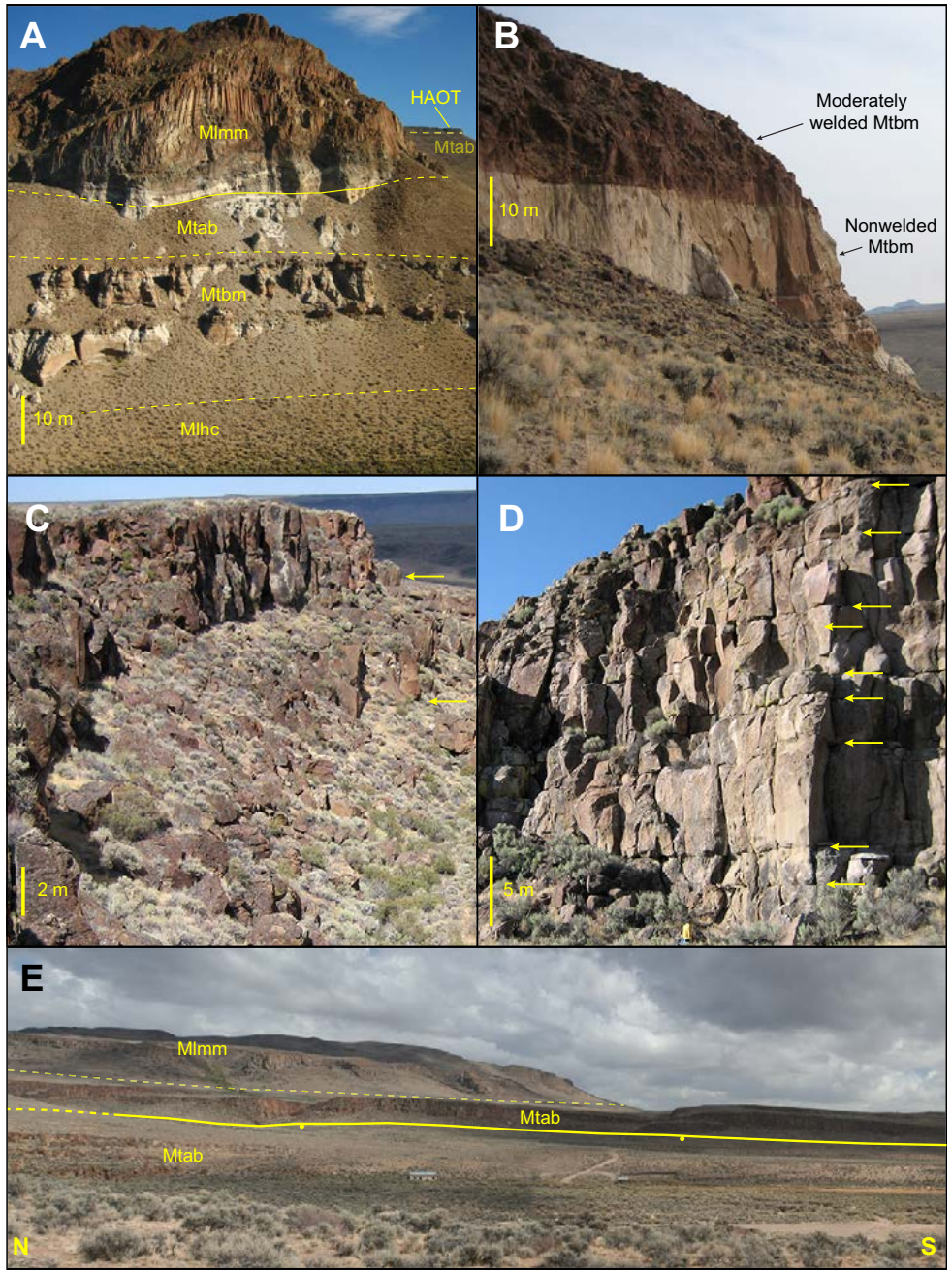

Figure 22. Photos of the tuff of Big Mountain, the tuff of Alkali Flat and Badger Mountain (Mtab), and the Mahogany Mountain lavas. (A) Columnar jointed Mahogany Mountain lava (Mlmm) overlying related thin surge and thicker ignimbrite deposits (Mtab), which overlie the tuff of Big Mountain (Mtbm) and a poorly exposed Hell Creek lava (Mlhc) in Virgin Creek. Thin flows of upper Miocene high-Al olivine tholeiite lavas (HAOT) overlie Mtab in the background. (B) View of ignimbrite component of tuff of Big Mountain (Mtbm) grading from nonwelded to moderately welded, located west of the mouth of Idaho Canyon. (C) Incipiently welded ignimbrite of tuff of Alkali Flat and Badger Mountain (Mtab) west of Fivemile Flat. (D) Strongly welded Mtab in Wall Canyon. Apparent breaks in deposition of the ignimbrite are indicated by yellow arrows, but all paleomagnetic samples collected through this section yielded the same direction. (E) Panoramic view of Mahogany Mountain rhyolitic lava (Mlmm) at Badger Mountain overlying Mtab exposed as a result of north-trending normal faults. Elsewhere, Mlmm is onlapped by cogenetic Mtab.

We attribute the restricted areal extent of the tuff of Trough Mountain and its rapid thinning away from Trough Mountain to the densely welded component of the ignimbrite having filled a depression, perhaps a caldera fragment or possibly a paleobasin that also controlled the distribution of the Summit Lake Tuff and the Soldier Meadow Tuff (Fig. 4). Partially welded distal deposits presumably were removed by erosion where they were not protected by younger capping units.

Consistent with the observation that the tuff of Trough Mountain consists of the products of more than one eruption, we have obtained 2 resolvably different ages on the unit: an age of 16.25 ± 0.03 Ma (MC212) from sodic sanidine extracted from a densely welded exposure ~5 km north of Trough Mountain proper near the base of the section, and 16.15 ± 0.02 Ma (MC124) from a moderately welded exposure southeast of Summit Lake. All samples of the tuff of Trough Mountain define a trend on bivariate trace element plots (Figs. 11 and 12), suggesting that all the units included in the tuff were related to eruptions from a single magma reservoir over a period of ~100 k.y. Samples of the tuff of Trough Mountain and Hell Creek lavas span a range of compositions with Rb/Zr ratios higher than those for the tuff of Coyote Spring and associated pre–Hanging Rock caldera lavas. They plot on a trend that is similar to the zoning in the Idaho Canyon Tuff (Figs. 5, 11, and 12), suggesting that they have

affinities with a magma body related more closely to the Virgin Valley caldera than to the developing magma body beneath the Hanging Rock caldera.

See the Supplemental Text File for a discussion of distinguishing the petrographically similar tuff of Trough Mountain and tuff of Coyote Spring in the field.

Pre–Hanging Rock Caldera Alkali Rhyolite Lavas (Mlns, Mlmc, Mlwh) 16.2–16.1 Ma

We have mapped and chemically correlated three groups of crystal-poor alkali rhyolite lavas that occur south and southeast of the Badger Mountain caldera. New $^{40}Ar/^{39}Ar$ ages indicate that these lavas vented between 16.2 and 16.1 Ma, and several were truncated on collapse of the Hanging Rock caldera at 16.0 Ma (Figs. 4 and 5). These lavas include the 16.21 Ma low-silica alkali rhyolite lavas of Nellie Spring Mountain (Mlns), which are distinctive due to the presence of large sanidine (to 6 mm) and chevkinite (50–200 μm) and their lower silica content than most HRCC rhyolites, the 16.2 Ma aphyric alkali rhyolite lavas of Massacre Creek (Mlmc), and 16.1 Ma phenocryst-poor alkali rhyolite lavas of Wild Horse Pasture (Mlwh) (Table 1). See the Supplemental Text File for unit descriptions, a discussion of their $^{40}Ar/^{39}Ar$ ages, and how they are distinguished.

The lavas of Nellie Spring Mountain have compositions that plot between the Summit Lake Tuff and the tuff of Coyote Springs on bivariate plots, which, in turn, is very similar to the least-evolved composition erupted in the younger Soldier Meadow Tuff (e.g., Fig. 5). The Massacre Creek lavas and Wild Horse Pasture lavas have compositions similar to the tuff of Coyote Springs. We therefore interpret the pre–Hanging Rock caldera alkali rhyolite lavas and the tuff of Coyote Springs as erupting from a developing magma chamber that ultimately gave rise to the more voluminous Soldier Meadow Tuff and collapse of the Hanging Rock caldera.

Soldier Meadow Tuff (Mism) 16 Ma

The Soldier Meadow Tuff was named by Noble et al. (1970) and described by Korringa (1973) based on strongly welded exposures in the hills near Soldier Meadow (Figs. 3 and 4). It is distinctive in that it is phenocryst rich (40–50 vol%). It is typically strongly welded, with subequal amounts of adularescent sanidine and dark smoky-gray quartz phenocrysts. Extensive vapor-phase crystallization of sodic amphibole along flow foliations imparts a light bluish-green color to the rock. Incipiently welded ignimbrite is tan, light gray, or pale green on fresh surfaces, and typically contains >75% pumice lapilli and <5% lithic fragments composed of mafic lava. East of Soldier Meadow, nonwelded deposits grade upward over a distance of 1–2 m into strongly welded ignimbrite. At least 7 welding reversals can be identified in an ~200 m fault-bound exposure of strongly welded Soldier Meadow Tuff north of Fly Canyon. These features are consistent with the relatively low viscosities of peralkaline magmas, which lead to abrupt variations in welding intensity as a function of accumulation rate (Mahood, 1984). In strongly welded outcrops, pyroclastic textures can be completely obscured by intense welding, devitrification, and vapor-phase crystallization; thicker deposits exhibit prominent columnar jointing and, more rarely, rheomorphism (Korringa, 1973). We estimate the volume of the Soldier Meadow Tuff to be ~65 km^3, including inferred deposits buried beneath the younger Cottonwood Creek caldera, based on large lithics within the tuff of Yellow Rock Canyon (described in the following sections).

We obtained ages of 16.00 ± 0.02 Ma (MC121) and 16.01 ± 0.02 Ma (MC369) for samples of Soldier Meadow Tuff from strongly welded exposures south of Mud Meadow Reservoir and southwest of High Rock Lake, respectively. The average radiogenic yield (%$^{40}Ar^*$) for both samples is >97%, resulting in caluclated ages that are very precise (Fig. 7). Our ages overlap at the 2σ level the range of less precise ages for Soldier Meadow Tuff reported by Smith (2011). An age of 16 Ma for the Soldier Meadow Tuff is consistent with the observations that the tuff overlies the 16.34 Ma Summit Lake Tuff and the 16.25–16.15 Ma tuff of Trough Mountain south and southeast of the Hanging Rock caldera, and is, in turn, overlain by a petrologically similar 15.91 Ma Soldier Meadow lava north of Soldier Meadow and by the 15.70 Ma tuff of Yellow Rock Canyon in Little High Rock Canyon and north of Fly Canyon.

We attribute formation of the Hanging Rock caldera to eruption of the Soldier Meadow Tuff at 16 Ma. This age is consistent with 16.20 Ma Massacre Creek lavas and a 16.29 Ma Hell Creek lava at Hanging Rock Canyon being cut by the northern topographic wall of the caldera. We interpret a lava for which Smith (2011) reported an age of 15.93 ± 0.07 Ma to have erupted on the caldera floor and to have banked against the Hanging Rock caldera topographic wall north of Grassy Rock Canyon (Figs. 4 and 5).

Alkali Rhyolite Soldier Meadow Lavas (Mlsm) 16.0–15.9 Ma

Noble et al. (1970) and Korringa (1973) noted the petrographic similarity between the Soldier Meadow Tuff and phenocryst-rich (~40 vol%) lavas that erupted from a linear vent array north of Soldier Meadow (Figs. 3 and 4), and proposed that the lavas marked the vent for the Soldier Meadow Tuff. Although we believe that the distribution and welding relations of the Soldier Meadow Tuff are more consistent with it having vented from the southeastern segment of the ring fracture of the Hanging Rock caldera (Figs. 4 and 5), the close relationship between the ignimbrite and the lavas is supported by our $^{40}Ar/^{39}Ar$ age of 15.91 ± 0.02 Ma (MC315) for a lava sample from the linear vent array near Warm Spring Canyon, and 15.98 ± 0.02 Ma (MC213) for a chemically and petrographically similar lava dome northwest of Trough Mountain. Two additional lavas that erupted on the floor of the Hanging Rock caldera (Fig. 4) are included in this unit due to their chemical and petrographic similarity (Fig. 7) to the lavas erupted along the linear vent array. Smith (2011) reported a $^{40}Ar/^{39}Ar$ age of 15.93 ± 07 Ma for one of these lavas near Grassy Rock. We obtained an age of 16.14 ± 0.02 Ma (MC376) on a glassy, crystal-rich lava just north of Yellow Rock Canyon, and attribute its anomalous older age to inherited ^{40}Ar, most likely because the lava erupted into a caldera lake and was quenched quickly. We interpret the ages of the Soldier Meadow lavas and their

chemical and petrographic similarity to the Soldier Meadow Tuff (Fig. 9) to indicate that magma erupted as the lavas represented the further evolution of magma not tapped during eruption of the Soldier Meadow Tuff.

The Soldier Meadow lavas have well-developed meter-scale flow laminae, and contain sparse dark colored magmatic enclaves. Fresh devitrified surfaces are coarsely recrystallized and light gray, pale green, or light blue. Darker shades of blue and green characterize specimens from where the lavas were silicified as a result of erupting into a caldera lake. The lavas weather dark tan, brick red, or brown, except locally where they remain vitric due to having erupted into water.

Uplift and Renewed Magmatism in the Badger Mountain Caldera

Simultaneously with eruption of Soldier Meadow lavas, magmatism was occurring across the HRCC in two areas: to the southwest at what was to become the youngest caldera at Cottonwood Creek (described in the following sections), and to the northeast with renewed activity in the Badger Mountain caldera (Fig. 5). Intrusion of magma beneath the Badger Mountain caldera resulted in uplift and venting of alkali rhyolite lavas of Mahogany Mountain and the associated tuff of Alkali Flat and Badger Mountain (Fig. 4) along linear trapdoor faults and the reactivated southern ring fracture of the Virgin Valley caldera.

Tuff of Alkali Flat and Badger Mountain (Mtab) 15.8–15.7 Ma

Park (1983) suggested that nonwelded and partially welded ignimbrite exposed north of Trough Mountain and surrounding Badger Mountain (Figs. 3 and 4), previously identified by Noble et al. (1970) and Korringa (1973) as Soldier Meadow Tuff, consists of two petrographically similar but younger ignimbrites, based on evidence from paleomagnetic measurements and phenocryst proportions. Park (1983) named these units the tuff of Alkali Flat (normal paleomagnetic direction) and tuff of Badger Mountain (reversed). Although we mapped (scale 1:24,000) from Alkali Flat to Massacre Creek (Plate 2), we were not able to distinguish Park's (1983) tuff of Alkali Flat and tuff of Badger Mountain in the field. Therefore, we mapped exposures of nonwelded to partially welded ignimbrite and related fall deposits as a single unit, Mtab, for the tuff of Alkali Flat and Badger Mountain. We have, however, confirmed Park's (1983) paleomagnetic results (Fig. 17; Supplemental Table 4[9]) and his suggestion that these are younger ignimbrite deposits. We obtained three ages for samples of the tuff, all of which are analytically well resolved from the 16.00 ± 0.02 Ma age of the Soldier Meadow Tuff: 15.80 ± 0.03 Ma (MC217) on ignimbrite near Alkali Flat, and 15.71 ± 0.02 Ma (MC314) and 15.84 ± 0.02 Ma (MC429B) from exposures south of Badger Mountain (Fig. 4).

Exposures of the tuff of Alkali Flat and Badger Mountain are largely confined within the Badger Mountain caldera (Figs. 4, 5, and 22), although thin deposits are exposed north and east of Nut Mountain and north of Trough Mountain. The thickest exposure (>100 m) is located 4 km northeast of Alkali Flat, where it has been preserved by the overlying high-Al olivine tholeiite lava flow of Rock Springs Table (Figs. 3 and 4). Ignimbrite components of the tuff of Alkali Flat and Badger Mountain are typically nonwelded or incipiently welded, vapor-phase altered, light bluish gray, tan, or pink on fresh surfaces, and weather reddish-orange or brown. Nonwelded outcrops gradually grade into incipiently welded or partially welded ignimbrite where the deposits are thickest around the Mahogany Mountain lavas. Vapor-phase alteration is more common in exposures >25 m thick, where it produces a pervasive salmon color, causes pumice lapilli to weather in negative relief forming cavities 3–10 cm in diameter, and results in prominent columnar jointing. The tuff is usually strongly porphyritic (40 vol%), and is broadly similar to the petrography of the crystal-rich Mahogany Mountain lavas.

Our field observations of several flow units and welding reversals, along with the new $^{40}Ar/^{39}Ar$ ages (Table 1), indicate that a number of small-volume pyroclastic flows and falls totaling ~20 km^3 erupted over a period of ~100 k.y. between ca. 15.8 and 15.7 Ma in association with eruption of chemically and petrographically similar alkali rhyolite lavas of Mahogany Mountain surrounding Rodero Flat and Badger Flat (Figs. 3 and 4).

Alkali Rhyolite Lavas of Mahogany Mountain (Mlmm) 15.9–15.5 Ma

Named the rhyolite of Badger Mountain by Greene (1984), we have renamed the large number of lavas erupted within the Badger Mountain caldera the alkali rhyolite lavas of Mahogany Mountain (Mlmm) to avoid confusion with the Badger Mountain caldera, and because the lava that caps the southwest side of Badger Mountain is atypical in being very crystal poor, whereas the rest of the lavas are moderately to strongly porphyritic.

The Mahogany Mountain lavas erupted between 15.9 and 15.5 Ma along the reactivated southern ring-fracture zone of the Virgin Valley caldera and along northwest- and north-northeast–trending faults associated with intrusion of magma and trapdoor uplift within Badger Mountain caldera (Figs. 5 and 21). Most of the Mahogany Mountain lavas are crystal rich (Table 2) with subequal amounts of adularescent-blue sanidine and smoky quartz, but they span a wide range of phenocryst contents (2–55 vol%), with no clear correlation with age (Table 1; Supplemental Table 2). Most of the lavas are alkali rhyolites, but their trace element compositions show systematic variations with time (Fig. 5), becoming less alkalic in the younger lavas, some of which contain abundant dark colored magmatic enclaves, which can be locally abundant near vents.

We grouped Mahogany Mountain lavas as a single unit on our maps (Fig. 4; Plate 1), but distinguish three eruptive phases based on $^{40}Ar/^{39}Ar$ ages, stratigraphic relations, and trace element compositions (Table 3; Fig. 5; Supplemental Table 2). Mlmm-1 lavas have the highest Zr/Rb (2.9–3.0), and are stratigraphically the oldest. Mlmm-2 lavas have slightly lower Zr/Rb (2.0–2.5; Fig. 5). Mlmm-3 lavas are the youngest and least peralkaline, having lower Zr/Rb (1.0–1.4). See the Supplemental Text File for a discussion of

Supplemental Table 4. Paleomagnetic sample localities and a summary of results

Sample	Unit	lat.	long.	Polarity	Notes	n	D_g	I_g	D_s	I_s	k	α95
Rhyolite and Trachyte Lavas												
P01	Mlmm	41.6093	-119.4490	N		4	308.2	61.9	308.1	61.9	0.0	15.2
P02	Mlmm	41.5879	-119.4630	N		11	210.3	-74.0	210.3	-74.0	125.6	4.3
MC244	Mlbc	41.5265	-119.4935	R	silicified	9	160.2	-46.1	160.2	-46.1	244.7	3.3
MC343	Mlbc	41.5608	-119.4330	R		8	215.7	-68.3	228.4	-64.1	81.8	6.7
P05	Mlcm	41.8421	-119.2965	R-T		5	310.2	48.7	310.2	48.7	326.4	4.6
MC225	Mlmm	41.5970	-119.2148	R		6	197.6	-53.9	198.4	-51.0	0.0	11.3
MC280	Mla	41.7618	-119.2873	N	silicified	7	50.5	70.5	50.5	70.5	166.1	4.8
MC300A	Mt	41.4320	-119.4305	R	bottom flow	9	182.0	-38.3	182.0	-38.3	606.9	2.1
MC300B	Mt	41.4321	-119.4289	R	3rd flow from the bottom	6	183.8	-42.7	183.8	-42.7	731.2	2.5
Rhyolitic Ignimbrites												
P06	Mtcx	41.5346	-119.4948	R-T	strongly welded, silicified	4	195.0	-84.0	195.0	-84.0	301.1	5.6
MC124	Mtmn	41.4906	-119.0864	R		7	221.9	-63.7	221.9	-63.7	148.8	5.1
MC221	Mtic	41.9086	-119.3716	R	drilled 3 benches	10	185.3	-68.8	185.3	-68.8	368.6	2.5
P07	Mtab	41.5956	-119.1451	N	near Alkali Flat	11	353.7	51.9	353.7	51.9	241.2	3.0
MC429A	Mtab	41.5748	-119.3232	N	south of Badger Mtn.	5	343.9	61.6	343.9	61.6	141.6	6.6
P08	Mtab	41.5849	-119.3738	R	south of Badger Mtn.	11	239.0	-46.9	239.0	-46.9	196.6	3.4
P09	Mtab	41.5562	-119.3051	R	south of Badger Mtn.	9	220.1	-52.9	220.1	-52.9	1082.4	1.6
MC314	Mtab	41.5739	-119.3234	R	south of Badger Mtn.	7	235.0	-50.3	235.0	-50.3	175.5	5.3
MC429B	Mtab	41.5753	-119.3233	R	south of Badger Mtn.	7	213.4	-55.3	213.4	-55.3	152.1	5.0
MC85	Mtal	41.5676	-119.0211	R		9	194.8	-31.6	194.8	-31.6	399.2	2.6
MC286	Mtal	41.5449	-119.5396	R		8	184.5	-21.7	179.1	-24.4	294.4	3.4

R Reversed paleomagnetic polarity
N Normal paleomagnetic polarity
T Transitional paleomagnetic direction

[9]Supplemental Table 4. Paleomagnetic sample localities and a summary of results. Please visit http://dx.doi.org/10.1130/GES01162.S9 or the full-text article on www.gsapubs.org to view Supplemental Table 4.

$^{40}Ar/^{39}Ar$ ages for the three phases of Mahogany Mountain lavas.

Consistent with the range in $^{40}Ar/^{39}Ar$ ages for the Mahogany Mountain lavas (Table 1), the lavas both overlie and are onlapped by the crystal-rich tuff of Alkali Flat and Badger Mountain (Figs. 4 and 22). The tuffs are most similar in age and composition to Mlmm-2 (Fig. 17), so we infer that they were small-volume pyroclastic units associated with emplacement of these lavas. Eruption of the youngest crystal-poor lavas at Badger Mountain (Mlmm-3) was associated with a small-volume, nonwelded, phenocryst-poor, light pink ignimbrite that is exposed within Rodero Flat and along County Road 8A west of Badger Mountain.

Tuff of Yellow Rock Canyon and Alkali Rhyolite Lavas of Cottonwood Creek

Contemporaneously with the renewal of eruptions within Badger Mountain caldera, aerially extensive aphyric and weakly porphyritic alkali rhyolite lavas began erupting ca. 15.9 Ma at what was to become the youngest and southernmost major caldera in the HRCC, the Cottonwood Creek caldera (Fig. 5). We propose that it collapsed at 15.70 Ma on eruption of the newly recognized tuff of Yellow Rock Canyon.

Tuff of Yellow Rock Canyon (Miyc) 15.70 Ma

Most of the known exposures of the tuff of Yellow Rock Canyon occur north and northeast of the Cottonwood Creek caldera, where it flowed into the topographic depression of the Hanging Rock caldera (Figs. 20, 23, and 24) and was preserved by younger trachyte lavas that flowed over it (Fig. 4). The southern margin of the Cottonwood Creek caldera is composed of a large massif of phenocryst-poor precaldera lavas centered at Fox Mountain (Fig. 3), which may have prevented the tuff of Yellow Rock Canyon from being emplaced southward. The mapped extent of the ignimbrite is relatively limited, which we attribute to the poor preservation potential of the partially welded ignimbrite. The best outcrops of the tuff of Yellow Rock Canyon are in the footwalls of normal faults and in canyons incised through trachytic lavas that preserve the nonwelded deposits below. The most complete section is in High Rock Canyon (Figs. 3, 4, and 23), where ~80 m of ignimbrite is exposed below trachytic lavas. We estimate the total volume of ignimbrite to be ~50 km^3 (DRE).

The tuff of Yellow Rock Canyon is compositionally and mineralogically zoned from a base characterized by light tan pumice lapilli of crystal-poor (2%–5%) alkali rhyolite to an upper flow unit that contains gray-blue trachytic pumice lapilli with ~10 vol% phenocrysts. The upper trachyte-bearing flow unit is present only in thicker sections northeast of the Cottonwood Creek caldera. Exposures of nonwelded ignimbrite are 5–50 m thick and form white or light gray rounded mounds or hoodoos (Fig. 23). Nonwelded ignimbrite contains 30–60 vol% pumice lapilli, ranging in size from 5 to 30 cm, set in an ashy matrix. The degree of vapor-phase alteration, the size of pumice lapilli and lithics, and lithic abundance increase upward within the alkali rhyolite part of the ignimbrite. At the tops of thicker sections, 4–18 m of moderately welded ignimbrite can be present (Fig. 23). Basal exposures exhibit a 1–5-m-thick section of fall deposits and a minor surge deposit 3–5 cm thick.

The tuff of Yellow Rock Canyon contains silicified lithic fragments of Soldier Meadow Tuff that are typically <20 cm in diameter and locally concentrated in layers (Smith, 2011), but are as large as 1.5 m in diameter near Yellow Rock Canyon. We suggest that the pyroclastic flows entrained this coarse debris in canyons cut in Hanging Rock Canyon caldera fill. The upper trachytic part of the unit contains lithic fragments of crystal-poor rhyolitic and mafic lavas that are generally smaller (<20 cm) than lithics in the lower nonwelded parts (Fig. 23).

Previously, workers (Ach et al., 1991; Bussey, 1996; Smith, 2011) included the tuff of Yellow Rock Canyon exposed northwest of Fly Canyon (Figs. 3 and 4) with undifferentiated sedimentary deposits or bedded pyroclastic deposits. They may not have identified the unit as an ignimbrite due to its yellowish-orange alteration color and stratified character resulting from interaction with water on flowing into the caldera lake near what is now the eponymous Yellow Rock Canyon (Fig. 24).

We obtained an age of 15.69 ± 0.01 Ma from sanidine from a fall deposit at the base of the ignimbrite (MC256, Fig. 7B), 15.71 ± 0.03 Ma on sanidine from rhyolitic lapilli within the ignimbrite (MC428) north of the caldera, and 15.81 ± 0.03 Ma on trachytic lapilli (MC364, Fig. 7D) in the ignimbrite north of High Rock Lake. Our preferred age for the tuff of Yellow Rock Canyon is 15.70 Ma, based on these ages and the ages obtained on what we interpret to be precaldera and postcaldera lavas (described in the following sections). The two ages from the lower rhyolitic parts of the ignimbrite agree within 2σ uncertainties. We attribute the older age and more scattered results (cf. Figs. 7D, 7B) of the trachytic MC364 to extraneous radiogenic ^{40}Ar from incompletely degassed alkali feldspar. The anomalously old age for the trachytic part of the tuff is inconsistent with the stratigraphic relation that the tuff banks against an alkali lava of Cottonwood Creek with an age of 15.75 ± 0.02 Ma (Plate 1; MC254 in Table 1). In addition, there is no conspicuous eruptive break in sections of the tuff zoned from alkali rhyolite to trachyte. We therefore favor the interpretation that the tuff of Yellow Rock Canyon represents a single eruptive event, rather than a series of eruptions that took place over ~100 k.y., as we do for the tuff of Trough Mountain and for the tuff of Alkali Flat and Badger Mountain.

Alkali Rhyolite Lavas of Cottonwood Creek (Mlcc) 15.9–15.6 Ma

Based on the patterns of pressure ridges in what he interpreted as rheomorphic ignimbrites, Bussey (1996) mapped a circular pattern of vents ~20 km in diameter surrounding Cottonwood Creek. We interpret these as vents for aerially extensive alkali rhyolite lavas that erupted along ring fractures associated with the Cottonwood Creek caldera.

Lavas we have mapped as precaldera and postcaldera Cottonwood Creek lavas are megascopically similar in the field, being aphyric or weakly porphyritic (~5 vol%). They are similar in composition to the rhyolitic portion of the tuff of Yellow Rock Canyon (Table 3; Fig. 5). We report $^{40}Ar/^{39}Ar$ ages in the range 15.9–15.6 Ma for five lavas and a nonwelded ignimbrite associated with lava dome

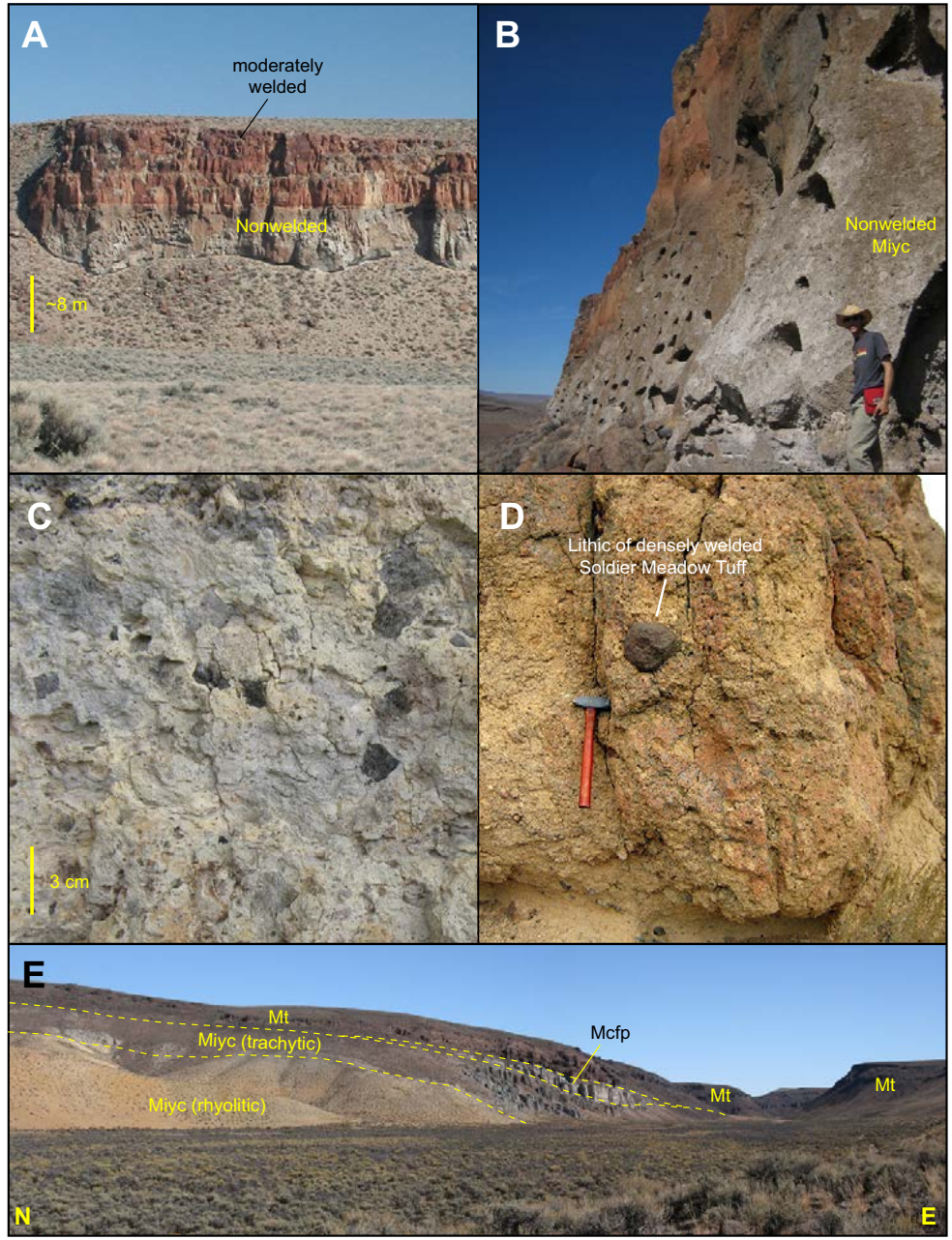

Figure 23. Photos of outcrops of the tuff of Yellow Rock Canyon. (A) Exposure of the rhyolitic lower member of the tuff of Yellow Rock Canyon (Miyc) where it grades from a nonwelded white ignimbrite near the base to a reddish moderately welded ignimbrite at the top. Photo taken along Bureau of Land Management (BLM) Road 37024, south of Yellow Rock Canyon. (B) Nonwelded base of the exposure of Miyc in A. White to light gray pumice lapilli are 5–30 cm in diameter. (C) Close-up of tuff of Yellow Rock Canyon (Miyc) shows black and light gray pumice lapilli in a tan ashy matrix, and a lack of sorting or reworking despite the crude stratification of the upper trachytic part of the tuff shown in E. (D) Lower rhyolitic part of tuff of Yellow Rock Canyon exposed north of High Rock Lake, where it flowed into Hanging Rock caldera and entrained large surface blocks of densely welded Soldier Meadow Tuff. (E) Yellow-altered rhyolitic part of the tuff of Yellow Rock Canyon grading abruptly into blue-gray trachytic upper part of the tuff in High Rock Canyon. The ignimbrite is overlain by ashy and pumice lapilli–rich caldera fill deposits (Mcfp) and trachytic lava (Mt).

emplacement (Table 1; Supplemental Table 2). The new $^{40}Ar/^{39}Ar$ results are consistent with precaldera lavas beginning to erupt ca. 15.9 Ma, the tuff of Yellow Rock Canyon erupting at 15.70 Ma, with postcaldera ring-fracture volcanism ceasing shortly afterward, perhaps within a few tens of thousands of years (Fig. 7).

The $^{40}Ar/^{39}Ar$ ages and mapped relations lead us to estimate that the total volume of precaldera Cottonwood Creek lavas, ~135 km^3, exceeds the volume of postcaldera lavas, ~85 km^3, and that, in contrast to the other calderas at the HRCC, the lavas greatly exceed the extracaldera volume of the caldera-forming tuff of Yellow Rock Canyon. Eruptions centered on the Cottonwood Creek caldera (Miyc and Mlcc) and contemporaneous magmatism within Badger Mountain caldera (Mlmm and Mtab) represent the highest overall volumetric eruptive rates in the HRCC (~2000–4000 km^3/m.y.; Fig. 25B). See the Supplemental Text File for a further discussion of $^{40}Ar/^{39}Ar$ ages and field attributes of the lavas.

Metaluminous Rhyolitic Lavas that Postdate Peralkaline Rhyolitic Volcanism

In the Virgin Valley and Badger Mountain calderas, small volumes of metaluminous rhyolite erupted through the caldera fill several hundred thousand years after alkali rhyolite volcanism

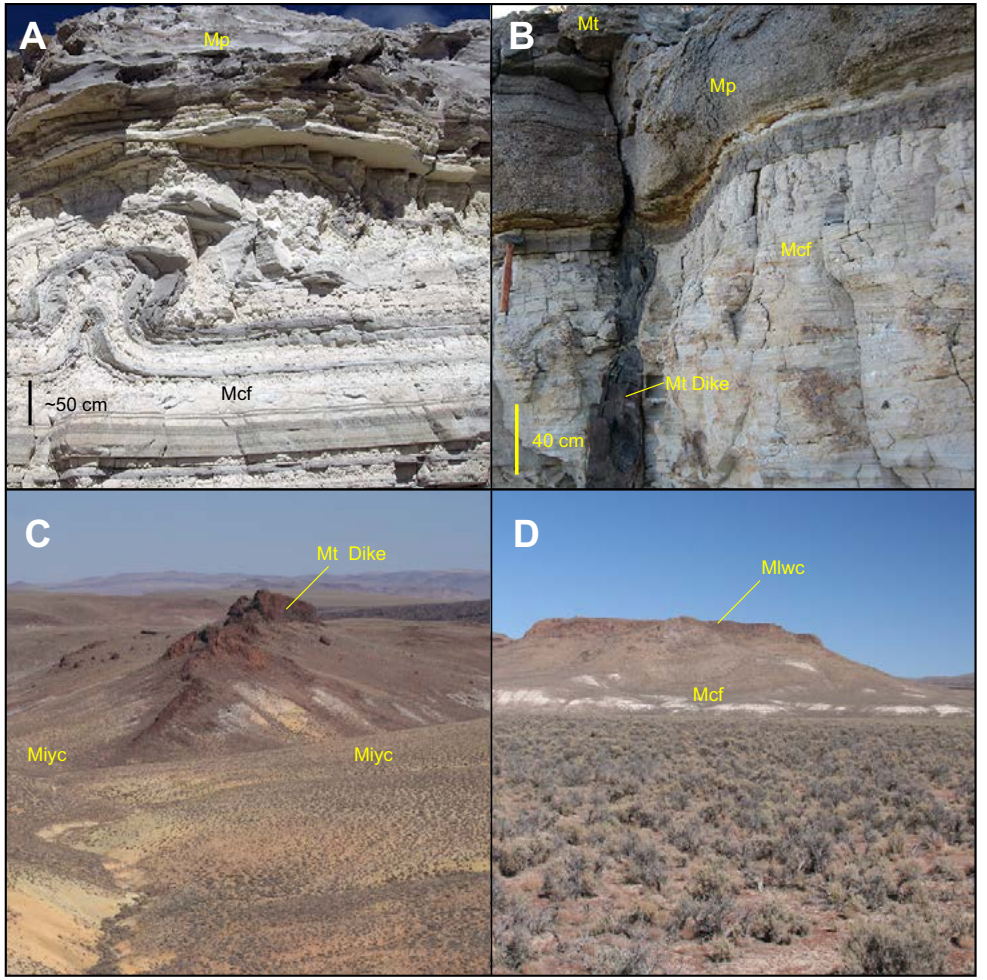

Figure 24. Photos of caldera fill and postcaldera mafic and intermediate lavas. (A) Soft-sediment deformation of caldera fill (Mcf) in Virgin Valley. White sedimentary layers are fine-grained, laminated, lacustrine deposits. Gray layers are reworked tuffaceous and pumiceous water-lain deposits. Mp—phreatomagmatic deposits. (B) Dike of postcaldera trachyte (Mt) intruding white, thinly bedded caldera fill of Hanging Rock caldera north of the Yellow Hills. The dike fragmented abruptly near the top of the caldera fill sediments, resulting in phreatomagmatic deposits (Mp) overlain by thin trachyte flows exposed at the top of the outcrop. (C) Dike of trachyte (Mt) 3.0–4.5 m wide intrudes tuff of Yellow Rock Canyon (Miyc) in Yellow Rock Canyon. (D) View looking north at 14.8 Ma crystal-poor trachyrhyolite lava of Wall Canyon (Mlwc). Erupting after alkali rhyolite volcanism was over, this metaluminous lava intruded and overlies ~150 m of white caldera fill sediments (Mcf) south of Wall Canyon.

ceased in that particular area. These lavas are chemically distinct from most of the HRCC rhyolites in being metaluminous, with much higher concentrations of Ca, Ba, and Sr. Compositionally they are more similar to the earliest rhyolitic lavas in the HRCC, those at Nut Mountain (Fig. 5).

A group of five 100–300-m-diameter trachyrhyolite lava domes forming an east-northeast–trending chain intruded caldera lake sediments on the east side of the Virgin Valley caldera 4 km west of McGee Mountain (Fig. 4). A sixth dome occurs south of the chain forming a cryptodomes, the jagged top of which is barely exposed amid enveloping sediments. Emplacement of all the domes was associated with phreatomagmatic explosions that are recorded in adjacent caldera fill as a series of surge and fall deposits. These rhyolite lavas of Rock Springs Canyon (Mlrs) have well-defined topographic forms, and are relatively fresh with well-preserved mafic phenocrysts set in a hydrated glassy matrix, in contrast to nearby strongly silicified, ring-fracture–related Antelope lavas. They contain ~12 vol% phenocrysts that reflect their metaluminous character: prominent biotite along with sanidine, amphibole, Fe-Ti oxides, and minor resorbed plagioclase and pyroxene. This chain of domes was mapped as rhyolite vitrophyre by Greene (1984) and Castor and Henry (2000), who reported a $^{40}Ar/^{39}Ar$ plateau age of 15.85 ± 0.11 Ma for one of the domes. This makes these lavas the youngest eruptive units in the Virgin Valley caldera, at least 250 k.y. younger than the ring-fracture Antelope lavas given the 2σ uncertainties on the ages.

Based on stratigraphy and $^{40}Ar/^{39}Ar$ dating, the youngest silicic lavas to erupt in the HRCC are the rhyolite lavas of Wall Canyon (Mlwc), which erupted through caldera fill at the intersection of caldera collapse- and uplift-related faults in the western part of Badger Mountain caldera (Figs. 4 and 21). These high-silica rhyolite lavas with <2 vol% alkali feldspar and trace quartz phenocrysts are commonly vesicular. We obtained an age of 14.68 ± 0.29 Ma (MC330) from devitrified whole-rock lava sampled from the largest outcrop, a dome that caps a thick section of caldera fill in Wall Canyon.

Postcaldera Alkalic Mafic and Intermediate Lavas (Mm and Mt) 15.5–14.2 Ma

Cessation of alkali rhyolite volcanism was followed by eruption of alkalic mafic and intermediate lavas (Fig. 26). In the Badger Mountain caldera,

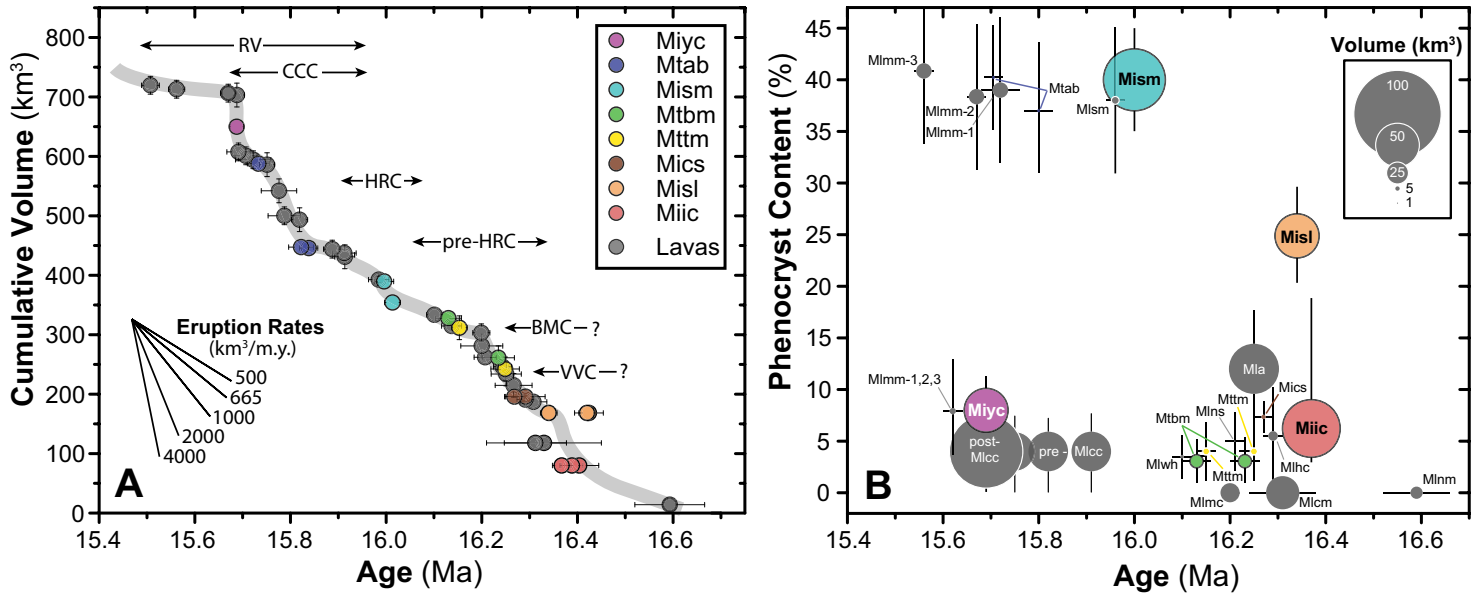

Figure 25. Eruptive rates, volumes, and crystal content of silicic units as a function of time. (A) Cumulative volume of rhyolitic magmas erupted during the interval 16.6–15.5 Ma. Individual points are the calculated $^{40}Ar/^{39}Ar$ model ages and errors from Table 1. Symbol colors for units are the same as in Figure 8. The approximate durations of magmatism at each of the calderas of the High Rock caldera complex (HRCC) are shown. VVC—Virgin Valley caldera, BMC—Badger Mountain caldera, HRC—Hanging Rock caldera, CCC—Cottonwood Creek caldera, RV—renewed volcanism in the Badger Mountain caldera surrounding Rodero Flat. The gray line is an approximate fit to the data showing changes in volumetric eruption rate during HRCC volcanism. (B) Crystal content as a function of age; size of data point is proportional to unit volume. Phenocryst-rich units erupted only in the last third of the life of the complex. Phenocryst abundances show a bimodal distribution. See text or Table 1 for unit abbreviations.

lavas ranging in composition from alkali basalt to trachyte erupted along preexisting faults associated with trapdoor uplift. Basaltic trachyandesite through trachyte lavas erupted in the Hanging Rock caldera, largely from vents along the southern ring-fracture zone, forming flows that protected underlying caldera fill from erosion. At the Cottonwood Creek caldera, alkali basalt erupted through the middle of the caldera lake. In all three calderas, venting through wet caldera lake sediments (Fig. 24) caused explosions that produced subaerial tuff rings and phreatomagmatic deposits of scoria and pumice that can be as much as 20 m thick beneath and adjacent to lava flows (mapped separately as Mp in Plate 2).

Postcaldera mafic lava flows are typically 3–6 m thick. Fresh surfaces are typically black, microcrystalline, and slightly vesicular with sparse (0–8 vol%) small phenocrysts of plagioclase, clinopyroxene, ± olivine. Flows weather dark reddish-brown or dark gray in color. Associated phreatomagmatic deposits typically weather yellowish-brown.

Individual trachyandesite to trachyte lava flows are typically 3–10 m thick. Fresh surfaces are typically aphanitic and black in color, giving them the appearance of basalt, despite their intermediate composition. Because the lavas are iron rich, they weather orange-brown. A thin brecciated basal zone is typical, which grades into a more massive, columnar jointed or platy zone, with a vesicular or rubbly top. Where flows are not massive, small rounded outcrops weather into thin, platy slabs typical of intermediate composition lavas. These lavas were mapped as andesite and dacite flows (Tad) by Ach (1988) and Ach et al. (1991) or basaltic andesite to dacite by Smith (2011).

Relatively precise ages can be determined for the postcaldera mafic and intermediate lavas because, with one exception, all the samples analyzed have relatively high K_2O contents (1.9–4.0 wt%), so the radiogenic yields for laser fusion analyses of individual microcrystalline groundmass fragments were relatively high (53–78 average % $^{40}Ar^*$, Fig. 8). These new ages show that all postcaldera alkalic basaltic to trachyte lavas identified in the HRCC are younger than ca. 15.5 Ma, and are among the youngest eruptive units.

At the Badger Mountain caldera we obtained an age of 15.55 ± 0.06 Ma (MC89, Fig. 8A) on a basalt west of Fish Creek Mountain, 15.08 ± 0.05 Ma (MC506) on a basaltic trachyandesite north of Badger Mountain, and 14.84 ± 0.03 Ma (MC237) on a trachybasalt southeast of Badger Mountain. Within the Hanging Rock caldera, we obtained ages of 14.5 ± 0.8 Ma (MC390) on a basaltic trachyandesite west of Soldier Meadow and 14.45 ± 0.07 Ma (MC249, Fig. 8D) from a trachyte lava flow

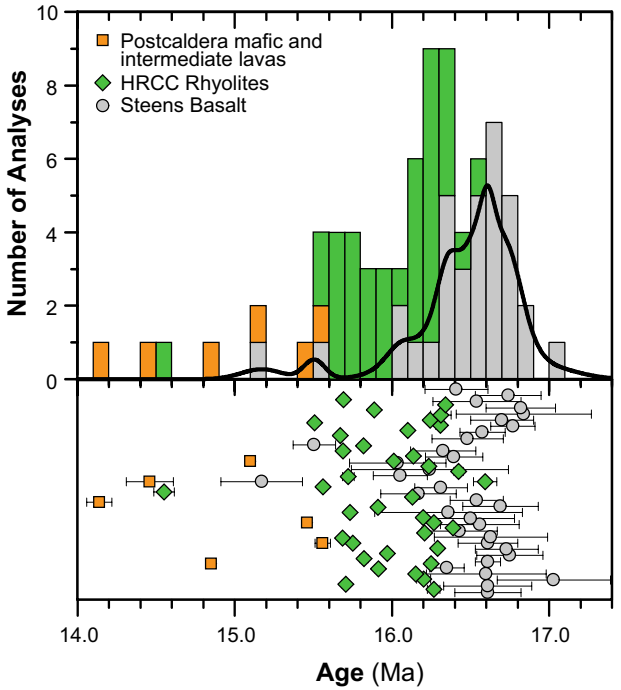

Figure 26. Ages of Steens Basalt compared to ages for High Rock caldera complex (HRCC) rhyolites and postcaldera mafic and intermediate lavas. The lower panel shows individual ages and reported errors (2σ) recalculated using $\lambda = 5.543e^{-10}$ yr^{-1} (Steiger and Jäger, 1977) and referenced to 28.02 Ma for the Fish Canyon Tuff (Renne et al., 1998). The upper panel shows a histogram with 100 k.y. bins and a probability density function for the Steens Basalt. All ages for HRCC are from this study, and duplicate dates on individual units have been removed to avoid sampling bias. Steens Basalt data are from Brueseke et al. (2007), Jarboe et al. (2008, 2010), and Camp et al. (2013).

overlying caldera lake sediments. The alkali basalt that erupted through the Cottonwood Creek caldera has the youngest age, 14.21 ± 0.04 Ma (MC266). Based on these ages, in any particular area within the HRCC, eruptions of mafic to intermediate lavas occurred at least 150 k.y. after the youngest alkali rhyolite volcanism, and marked the end of large-volume rhyolitic magmatism.

Late Miocene to Quaternary Basalts (NQm) 10–0.5 Ma

After an interval of nearly 5 m.y. without volcanic activity, eruptions of high-Al olivine tholeiitic basalt (HAOT) as thin (<10 m), dark colored, dikytaxitic, lava flows formed extensive, nearly flat-lying tables in the northern part of the HRCC (included within map unit Neogene to Quaternary undifferentiated volcanics, NQm in Figs. 3 and 4). These resistant lavas forming Rock Spring Table, Gooch Table, Big Spring Table, and Massacre Rim (Fig. 3) have preserved underlying caldera fill of the Virgin Valley and Badger Mountain calderas as well as older basinal sediments north of Nevada State Route 140 and at Massacre Rim.

We have found no evidence for vents for the HAOT flows within the calderas; these fluid lavas appear to have vented from low shield volcanoes north and northwest of the HRCC. Flows armoring tilted landslide blocks of caldera fill within the Virgin Valley caldera can give the superficial appearance of fin-like dikes, but on close inspection prove to be lavas, based on the presence of vesicle cylinders and the absence of horizontal columnar joints that would characterize dikes. The HAOT flows do not have associated phreatomagmatic deposits, pillowed bases, or peperite facies, suggesting that sizable bodies of water were no longer present in the HRCC during late Miocene time when they erupted.

We obtained $^{40}Ar/^{39}Ar$ ages of 10.1 ± 1.2 Ma (MC381) and 7.5 ± 0.9 Ma (MC358) for flat-lying HAOT flows of Rock Springs Table and Gooch Table. Farther west, 2 different flows at Massacre Rim yielded ages of 4.4 ± 0.7 Ma (AT13) and 4.7 ± 0.8 Ma (AT26) (Fig. 4). Carmichael et al. (2006) reported ages of 8–3 Ma for HAOT lavas in the Hays Canyon and Warner Ranges, west of the HRCC (Fig. 2). North of the HRCC, the HAOT flows are Pleistocene in age. The mesa referred to as the Oregon End Table (Fig. 3) is capped by a ca. 2 Ma HAOT (Legge, 1988), and the sinuous ~20-km-long ridge ending at Railroad Point (Fig. 3) is inverted topography where a ca. 1 Ma HAOT lava flow (McKee and Marvin, 1974) filled a paleochannel cut in basinal sediments that have since been eroded away. HAOT lavas in Hawks Valley are younger than 1 Ma (Wypych et al., 2011).

CALDERAS OF THE HRCC

One of the main focuses of this study has been delineating calderas and identifying the sources for ignimbrites based on mapping, geochronology, and chemical correlation of ignimbrites and lavas. Where possible we distinguish between the topographic walls of calderas and the structural margins defined by ring-fracture volcanism (Figs. 4 and 21). In the HRCC, where the relief was low and the caldera walls commonly consist of strong, thick, silicic lavas, the topographic rim and the structural margin may nearly coincide.

Caldera Fill Deposits

An important criterion for delineating the boundaries of calderas is the distribution of caldera fill deposits. We mapped caldera fill to include lacustrine sediments, alluvial deposits, and primary volcanic deposits formed in a range of depositional environments: caldera lakes that range from deep and persistent to ephemeral, shallow bodies of water, littoral zones and minor streams, and dominantly subaerial settings in which alluvium, lahars, primary pyroclastic deposits, and talus debris on caldera topographic walls and around lavas (e.g.,

Smith, 1991) are deposited and interfinger with littoral lacustrine sediments.

The hallmark sedimentary deposits of a rhyolitic caldera environment are white, laminated, diatomaceous, ashy sediments and light colored, stratified, tuffaceous siltstones characteristic of quiescent lacustrine conditions (e.g., Smith and Bailey, 1968; Mahood, 1980; Smith, 1991) (Mcf in Plate 2; Fig. 24A). Petrified logs and wood chips are a characteristic feature of these deposits, their abundance suggesting that wood fragments from trees felled and shattered by volcanic activity may have been incorporated in ashy sediments that promoted replacement of organic debris with silica or opal (Hilton et al., 2008). In the Virgin Valley caldera, fine-grained ashy horizons are the host for specimen-quality opal (e.g., Zielinski, 1982) that replaces branches of wood, conifer cones, and other organic debris. A pyroclastic flow near the head of Little High Rock Canyon in the Cottonwood Creek caldera, associated with emplacement of one of the postcaldera Cottonwood Creek lavas, contains petrified logs nearly a meter in diameter that have been toppled and oriented horizontally by the pyroclastic flow.

We emphasize that the term caldera fill is not synonymous with caldera lake sediments. A large part of the caldera fill in HRCC calderas consists of subaerial deposits. Phreatomagmatic eruptions were triggered by the intrusion of both silicic and mafic magmas, resulting in the construction of subaerial tuff rings. The emplacement of lava domes was accompanied by eruption of small ignimbrite and surge deposits, the construction of ramparts of vitric lithic debris, and the entrainment of unconsolidated lake sediments by autobrecciated lava. Three of the caldera lakes appear to have drained catastrophically, rapidly downcutting dramatic gorges through lavas making up the topographic walls of the calderas. The calderas remained depocenters of sediments in more restricted bodies of water, however, and continued to accumulate pyroclastic debris.

Rhyolitic pumiceous deposits make up a significant fraction of the caldera fill at the HRCC, enough to be differentiated as a separate unit (Mcfp) in Plate 2. These consist of multiple horizons (~10–50 cm thick) of well-stratified, centimeter-scale, normally graded beds that are variably reworked, with rounded pumice lapilli and subrounded lithics in an ashy matrix. The pumice-rich horizons are various shades of gray on fresh and weathered surfaces (gray layers in Fig 24A). They are typically located adjacent to postcaldera rhyolite lava flows and domes, and become finer grained upsequence and toward the interiors of the caldera lakes. They are interpreted as the products of subaerial and littoral reworking of pumice and ash fall and surge deposits associated with emplacement of silicic lavas into the caldera lakes. In the Virgin Valley caldera, these tuffaceous and pumice lapilli–rich sediments interfinger with Antelope lavas that erupted along ring fractures and with finer grained ashy sediments deposited in the interior of the Virgin Valley caldera that include distal ash fall deposits from other mid-Miocene centers (Perkins and Nash, 2002).

Where postcaldera trachytic and mafic lavas intruded caldera fill, dark gray, brown, or light yellow-brown phreatomagmatic deposits (Mp in Plate 2; Fig. 24B) up to 20 m thick consist of well-stratified, normally graded beds, which locally display meter-scale, low-angle, surge cross-bedding. They contain dark brown to black, scoriaceous lapilli and blocks 1–30 cm in diameter. Accretionary lapilli are common, typically concentrated within beds 3–10 cm thick. Locally the phreatomagmatic deposits grade into peperites or hyaloclastites, and at their distal edges they are interbedded with typical fine-grained, light colored caldera lake sediments.

At the HRCC, caldera fill is best exposed in the Virgin Valley (to ~450 m thick) and Hanging Rock calderas because the deposits have been preserved beneath younger lava flows, and incised by creeks (Fig. 24). Caldera fill is not well exposed in the Cottonwood Creek caldera due to low relief, and because most of it has been eroded away. Most caldera fill exposures in the Badger Mountain caldera consist of pumiceous sediments that incorporated debris from primary and reworked subaerial pyroclastic deposits formed in association with emplacement of the 15.9–15.5 Ma Mahogany Mountain lavas. Fine-grained sediments are found only locally.

Virgin Valley Caldera

The Virgin Valley caldera is the oldest and northernmost caldera in the chain of southwest-younging HRCC calderas (Figs. 2, 3, and 5) and is the source of the 16.38 Ma Idaho Canyon Tuff. The caldera is easily recognized by the distribution of fine-grained caldera lake sediments partially encircled by vents for postcaldera ring-fracture alkali rhyolite Antelope lavas surrounding Virgin Creek (Fig. 4).

Castor and Henry (2000) outlined the Virgin Valley caldera as a 22-km-diameter circular caldera. Based on our new mapping, $^{40}Ar/^{39}Ar$ geochronology, and chemical data for lavas and ignimbrites, we suggest that the caldera is somewhat larger, 34 × 24 km, with the eastern part of the caldera centered on Virgin Creek having collapsed more than the northwestern part. There is an abrupt break in the intracaldera topography ~6 km east of the western caldera rim, approximately where Castor and Henry (2000) drew the western margin of the caldera. Caldera fill west of this break in slope (i.e., north of Gooch Table and in western Hell Creek; Figs. 3 and 4) has a high proportion of reworked volcaniclastic sediments and subaerial pyroclastic deposits, consistent with small, shallow, and short-lived bodies of water. East of this break in slope, deposits are fine-grained, laminated, ashy, and diatomaceous, and thereby indicative of a persistent, quiescent lacustrine environment. These fully lacustrine deposits are centered at Virgin Creek (Figs. 3 and 4), where the thickest sequence of exposed caldera fill deposits (~450 m) defines the zone of greatest caldera collapse.

The distribution of welding facies and the two chemically and petrographically defined subunits of the Idaho Canyon Tuff , $Niic_a$ and $Niic_b$, along with variations in thickness (see Supplemental Fig. 2) can be used to elucidate the nature of collapse of the Virgin Valley caldera. The most chemically evolved and crystal-poor samples of the ignimbrite have been found northwest of the caldera, and the bulk of the volume of more-evolved $Miic_a$ Idaho Canyon Tuff was emplaced north and northwest of the caldera. In contrast, the less-evolved $Miic_b$ is exposed only in the fault scarp on the east side of the complex and locally as outflow southeast of

caldera (Fig. 16). We interpret that to mean that initial venting of the ignimbrite and caldera collapse occurred in the northwest, and that subsequent greater subsidence was associated with eruption of more mafic magma sourced deeper in the chamber venting from the southeast quadrant of the ring fracture. It is possible there was a small amount of additional collapse that occurred in the eastern part of the caldera as a result of the later eruption of the pyroclastic deposits making up the tuff of Big Mountain. See the Supplemental Text File for further discussion of this point.

The northeastern quadrant of the structural margin of the Virgin Valley caldera is well defined by the pattern of vents for the Antelope lavas, which erupted ~100–200 k.y. after caldera collapse. We speculatively locate the northwest quadrant of the structural margin along a major fault-controlled canyon through the vent area for the 16.31 ± 0.03 Ma Hell Creek lava in Echo Canyon (Fig. 4). We interpret the zones of pervasive hydrothermal alteration, silicification, and mineralization of the crystal-poor lavas in Hell Creek and all exposures of Antelope lavas as evidence for the location of buried caldera ring fractures.

The southern to southwestern margin of the caldera is obscured by the overlapping collapse of the younger Badger Mountain caldera and by products of younger volcanism. We believe that the structural margin is marked by the arcuate arrangement of vents for the Mahogany Mountain lavas. Although the Mahogany Mountain lavas erupted much later during a 15.9–15.5 Ma renewal of activity in the younger Badger Mountain caldera, we interpret the associated uplift as reactivating the southern ring fracture of the Virgin Valley caldera, leading to reversal of motion on the fault, and venting of alkali rhyolite magma as lava domes and flows along it (Figs. 4 and 21). We consider the chemical trends shown by the three groups of Mahogany Mountain lavas as supportive of this conclusion, as over time the lavas become chemically more like the Antelope lavas to the north (Fig. 5), suggesting shared magma sources and/or reservoirs.

The topographic margin of the Virgin Valley caldera is constrained by outcrops of caldera fill and the distribution of outflow Idaho Canyon Tuff exposed outside the caldera walls to the northwest and southeast. The northern topographic margin of the Virgin Valley caldera is partially covered by younger HAOT lavas of the Big Springs Table, but its position is apparent from the truncation of what we interpret to be Paleogene lavas at Big Springs Butte and by the outcrop pattern and pressure ridges of Antelope lavas east of Big Spring Reservoir along Nevada State Route 140 (Figs. 3 and 4). The topographic margin confines the westward extent of Antelope lavas and caldera fill south of Big Springs Reservoir, whereas basinal sediments are exposed just outboard of the caldera topographic margin. A thin veneer of moderately welded Idaho Canyon Tuff laps the sediments and an undated aphyric rhyolite lava we infer to be Paleogene near Big Springs Butte just outboard of what we interpret as the caldera margin. The outflow ignimbrite thickens abruptly to >80 m (base unexposed) and is densely welded throughout exposures in Catnip Creek and around the Sage Hen Hills (Figs. 3 and 4), where it apparently filled a broad paleovalley. At its northernmost extent, northwest of Hawks Mountain (Fig. 3), the Idaho Canyon Tuff thins, the intensity of welding decreases such that several welding reversals are apparent, and a nonwelded base is exposed locally. In addition to using welding relationships in the Idaho Canyon Tuff to locate the northwest quadrant of the topographic wall, we interpret a break in slope along the eastern side of the Catnip Mountain dome as marking where postcaldera Catnip Mountain lavas flowed over the caldera rim.

The outcrop pattern of postcaldera Antelope lavas defines the northeastern and eastern sectors of the topographic margin of the Virgin Valley caldera. On the north and east side of McGee Mountain and east side of Big Mountain, these lavas and the associated tuff of Big Mountain appear to have banked in against a caldera topographic wall that no longer exists, as they form a striking 300–500-m-high arcuate wall above the modern Bog Hot and Craine Creek Valleys (Figs. 3 and 4). We interpret this as a reversal of topography resulting from banking against a caldera topographic wall that was composed of weakly consolidated basinal sediments that have since been largely eroded away. Erosion along with what we interpret to be the reactivation of caldera collapse–related structures by northeast- and northwest-trending Basin and Range faulting has resulted in the continuation of this feature in a large, arcuate scarp south of McGee Mountain (Figs. 3 and 4).

We interpret the Idaho Canyon Tuff exposed south and southeast of the Virgin Valley caldera as outflow ignimbrite that flowed down a precursor basin to the modern Craine Creek Valley (Figs. 3 and 4). The absence of the Idaho Canyon Tuff northeast of the caldera is puzzling, particularly in light of the fact that a tilted section on the east side of the southern Pueblo Mountains contains the Oregon Canyon Tuff, the Trout Creek tuff, and the Long Ridge tuff, all from the MVF, that bracket the appropriate age interval (Coble and Mahood, 2012; Benson and Mahood, 2015). It may be that the presence of an active drainage east of the caldera prevented the preservation of the ignimbrite there, as well as its deposition on the west side of the southern Pueblo Mountains and northern Pine Forest Range. Farther south, thin deposits of $Miic_b$ are exposed in the westernmost Pine Forest Range, and thicken to the south toward the headwaters of Craine Creek (Figs. 3 and 4), suggesting that any drainage that prevented the spread of the Idaho Canyon Tuff must have been farther east, perhaps controlled by what are now prominent faults in the Pine Forest Range (Fig. 4).

Badger Mountain Caldera

We identify the newly defined Badger Mountain caldera as the source of the 16.34 Ma Summit Lake Tuff. It is the least confidently delineated of the calderas in the HRCC because it partly overlaps the older Virgin Valley caldera to the northwest, and is truncated by the younger Hanging Rock caldera and what we identify as scallop-shaped collapse features to the southwest. In addition, it was the site of uplift and renewed volcanism from ca. 15.9 to 15.5 Ma (Figs. 4, 5, and 21). Due to these complexities, it is difficult to distinguish between the topographic and structural margins of the caldera; instead we discuss the evidence used to delineate an outline of the caldera that we refer to more generically as the caldera margin. We believe it more

closely approximates the topographic margin, and given that the topographic rim retreats outward due to landslides and erosion, the original caldera was likely smaller than shown in Figures 2–4.

The southeast and southwest margins of the 40 × 30 km Badger Mountain caldera are delimited by locations of outflow Summit Lake Tuff (Fig. 4). Additional evidence used to place the southern and southeastern margin of the Badger Mountain caldera is the distribution of the younger tuff of Alkali Flat and Badger Mountain that we suggest was largely confined within the caldera (Fig. 4).

We interpret the prominent arcuate break in topography along the south side of Catnip Mountain as a result of truncation on collapse of the Badger Mountain caldera, although the two ages for Catnip Mountain lavas (Table 1) are insufficiently precise to determine whether the Catnip Mountain edifice predates or postdates eruption of the Summit Lake Tuff. The arcuate break continues to the west in more subdued topography that is buried by young high-Al olivine tholeiite lavas (Fig. 4). This break in slope also marks the northern limit of caldera fill. We have placed the caldera margin near two exposures of Catnip Mountain lavas located south of Alkali Flat and west of Trough Mountain. We have drawn this southern margin of the Badger Mountain caldera in such a way that inferred vents for the 16.1 Ma Wild Horse Pasture lavas, which also have chemical affinities with the Summit Lake Tuff (Fig. 5), could be postcaldera ring-fracture lavas of the Badger Mountain caldera.

The Badger Mountain caldera is reflected in regional gravity and magnetic maps (Fig. 18) by prominent negative anomalies. We have extrapolated the caldera margin in areas where stratigraphic evidence is not available by honoring the shapes of the geophysical anomalies, in particular the steep gradients in the magnetic map at the west margin of the caldera.

Post–Badger Mountain Caldera and Pre–Hanging Rock Caldera Volcanism

The eruption of two large ignimbrites on collapse of the Virgin Valley caldera and the overlapping Badger Mountain caldera within a relatively short time (<80 k.y., based on 2σ uncertainties of ages on the caldera-forming ignimbrites) means that eruptions following collapse of the younger Badger Mountain caldera reflect the rejuvenation of both magmatic systems. Because the two systems are slightly different chemically, we can utilize bivariate chemical plots (Figs. 5 and 12) to assign lavas and ignimbrites erupted in the interval between the eruption of the Summit Lake Tuff at 16.34 Ma and the Soldier Meadow Tuff and collapse of the Hanging Rock caldera at 16 Ma to one of two trends. A lower Rb/Zr trend associated with the Summit Lake Tuff consists of the 16.27 Ma tuff of Coyote Spring, which occurs west of the Badger Mountain caldera, the 16.2 Ma Nellie Springs Mountain lavas and Massacre Creek lavas west of what was to become the Hanging Rock caldera, the 16.1 Ma Wild Horse Pasture lavas near the southeastern ring fracture of the Badger Mountain caldera, and the caldera-forming 16 Ma Soldier Meadow Tuff. A higher Rb/Zr trend defined by the Idaho Canyon Tuff is shared by the 16.3–16.2 Ma Hell Creek lavas, and by the 16.25–16.15 Ma tuff of Trough Mountain, which vented south of the Badger Mountain caldera. At least locally these slightly different alkali rhyolite types commingled, as evidenced by a phenocryst-rich magmatic enclave in an aphyric high-Rb/Zr Hell Creek lava in Hell Creek that yielded an age of 16.2 Ma and a chemical composition similar to low-Rb/Zr Nellie Springs Mountain lavas (MC433 in Fig. 5), providing strong evidence that the higher and lower Rb/Zr magma types coexisted at 16.2 Ma.

More or less contemporaneous with eruption of both these magma types, rhyolitic magmas distinctly less alkalic (Fig. 5) were erupting as the Antelope lavas and the tuff of Big Mountain along the ring-fracture zone of the Virgin Valley caldera (Fig. 4); these eruptions were the last peralkaline rhyolitic eruptions in this northern part of the caldera. We interpret the high Rb/Zr ratios and the more metaluminous character of these magmas (Mla and Mtbm in Fig. 5) as reflecting the types of magmas formed in the waning stages of the caldera systems because they are compositionally similar to the last peralkaline lavas to erupt in the Badger Mountain caldera (Mlmm-3 in Fig. 5).

Possible Collapse Associated with Eruption of Tuffs of Coyote Spring and Trough Mountain

During the same interval that the Antelope lavas and tuff of Big Mountain were erupting in Virgin Valley, pre–Hanging Rock caldera eruptions were occurring south and west of the Badger Mountain caldera. We suggest that the topographically low area between the Badger Mountain and Hanging Rock calderas, from Wall Canyon (Fig. 21) to the west side of Trough Mountain, is an expression of collapse along structures synthetic to the older Badger Mountain and future Hanging Rock ring-fracture faults. Bounding this low area are two massifs, Nut Mountain and Trough Mountain, which contain spatially restricted exposures of the 16.27 Ma tuff of Coyote Springs and 16.25–16.15 Ma tuff of Trough Mountain, respectively. We interpret these ignimbrites as being associated with two poorly defined scallop-shaped collapse features west and southeast, respectively, of the Badger Mountain caldera, which were truncated on the southwest by the Hanging Rock caldera collapse at 16.0 Ma. The tuff of Trough Mountain is along the high Rb/Zr Idaho Canyon Tuff trend, and the tuff of Coyote Spring is along the low Rb/Zr Summit Lake Tuff trend (Fig. 5). Given the overlap in the ages of the tuffs, it seems possible that these magmas existed as laterally distinct bodies in the same magma chamber or as adjacent magma bodies.

The complicated fault zone that is well exposed on the west side of Wall Canyon (Plate 2) could have formed on collapse associated with eruption of the tuff of Coyote Springs. Blocks of silicified Nut Mountain lava, Summit Lake Tuff, and tuff of Coyote Spring occur as fault slivers within this zone (Fig. 21), indicating that the fault zone postdates collapse of the Badger Mountain caldera.

Based on our mapping and field observations, the distribution of the units, and the descriptions of Korringa (1973), we suggest that the ignimbrite component of the tuff of Trough Mountain vented from a northern portion of the lineament along which Soldier Meadows lavas later erupted. Collapse along this feature may have enlarged the Badger Mountain caldera to the south, accounting

for the topographic low and gravity low anomaly in the area between the Badger Mountain and Hanging Rock calderas (Fig. 18). We have interpreted the topographic margin of the collapse feature we relate to the tuff of Trough Mountain as having controlled the eastern extent of caldera fill and phreatomagmatic deposits (Mp) related to the younger Hanging Rock caldera.

Hanging Rock Caldera

We delineate the ~17-km-diameter Hanging Rock caldera by the distribution of ashy lake sediments inside the caldera and of outflow Soldier Meadow Tuff east and southeast of the caldera, and by the truncation of precaldera lavas and the position of vents for postcaldera lavas. We identify the Soldier Meadow Tuff as the caldera-forming unit based on its stratigraphic position above the tuff of Trough Mountain, which is cut by the caldera margin, and below the tuff of Yellow Rock Canyon, which flowed into the Hanging Rock caldera. In addition, the 16 Ma age of the Soldier Meadow Tuff is consistent with it being the caldera-forming unit, based on the fact that 16.2 Ma Massacre Creek lavas, similar in composition to the most-evolved Soldier Meadow Tuff, are truncated by collapse. Postcaldera lavas erupted within the caldera are petrographically and chemically similar to the Soldier Meadow Tuff, and have ages that are statistically indistinguishable.

We have not applied the name High Rock caldera used informally by Noble et al. (2009) and Smith (2011) to avoid confusion with our use, following that of Ach and Swisher (1990), of the place name for the regional-scale HRCC. In addition, Smith (2011) suggested that the 16.34 Ma Summit Lake Tuff erupted from the High Rock caldera or a location near it (cf. Noble et al., 1970). Our new mapping and geochronology demonstrate that the 16.2 Ma Massacre Creek lavas overlie the Summit Lake Tuff and are truncated by the northern margin of the caldera, requiring that at least this quadrant of the caldera is younger than 16.2 Ma and cannot be related to collapse on eruption of the Summit Lake Tuff.

The northwestern margin of the Hanging Rock caldera is well exposed because it has not been the site of subsequent eruptions. Both the topographic wall and structural margin here occupy a broad zone of normal faulting expressed in a series of arcuate structural benches along which precaldera lavas are step faulted down into the caldera (Figs. 3 and 4). South of Nut Mountain, northeast-trending parallel benches are continuous in the topography for more than 20 km (Fig. 21) and are prominent on aerial imagery. At their northern ends, these structures intersect and curve into north-northwest–oriented features that are parallel to the margin of the Badger Mountain caldera (Fig. 4; detailed quadrangle mapping in Plate 2). These fault-controlled benches wrap continuously around the Hanging Rock and Badger Mountain calderas, suggesting that some of the deformation is due to regional-scale downsagging toward the calderas that occurred on a longer time frame than individual collapse events.

Given the broad zone of deformation, it is somewhat arbitrary to assign the location of the structural margin; logically, the entire slope could be considered the topographic wall. We placed the northwest topographic wall at the break in slope, inboard of which precaldera lavas form striking cliffs, including at Hanging Rock Canyon. The western sector of the topographic margin is well marked by the truncation of an Oligocene dacite lava dome and the arcuate edge of a postcaldera Soldier Meadow lava that banks against it near Grassy Rock (Figs. 3 and 4). The western and southwestern sectors of the topographic wall are largely obscured by younger lavas derived from the Cottonwood Creek caldera, but we placed the topographic wall outboard of caldera fill and along breaks in slope in Cottonwood Creek lavas where we infer they cascaded over the caldera wall. The southern caldera wall is located based on the thickest accumulations of postcaldera trachyte lavas, which we interpret as erupting along the southern ring fracture to form low shields that ponded against the caldera wall, with a smaller number of flows spilling over the southern margin where they overlie outflow Soldier Meadow Tuff and the younger tuff of Yellow Rock Canyon. We place the southeastern and eastern topographic margin of the Hanging Rock caldera west (inboard) of exposures of Soldier Meadow Tuff and tuff of Trough Mountain (Fig. 4).

The northeastern and northern sectors of the topographic margin of the caldera are poorly defined because the margin overlaps the older Badger Mountain caldera and is buried by the younger tuff of Alkali Flat and Badger Mountain and caldera fill (Fig. 4). We believe that the topographic wall in this area was already low due to the cumulative effects of collapse of the Badger Mountain caldera and postulated scallop-shaped collapse associated with eruption of the tuff of Coyote Spring and the tuff of Trough Mountain. We envision that shortly following collapse of the Hanging Rock caldera there would have been a near-continuous lake basin that encompassed the Hanging Rock, Badger Mountain, and Virgin Valley calderas.

We infer that the structural margin of the Hanging Rock caldera is only slightly inboard of the topographic wall in the northwest sector of the caldera, mostly buried by caldera fill at the base of the resistant cliffs of precaldera rhyolitic lavas. In the western sector we locate the ring-fracture zone to pass through the locations of the vents for postcaldera Soldier Meadow and Cottonwood Creek lavas (Fig. 4). We locate the southern structural margin at the location of feeder dikes and the summits of low shields that were the sources for postcaldera trachytic lavas. The eastern and northern sectors of the structural margin are difficult to define. There are several rhyolitic lava flows in the age range of 16.0–15.7 Ma that could mark eruptions along ring fractures, but we think it is likely that due to overlap in this region of collapse structures of Summit Lake, Coyote Spring, Trough Mountain, and Soldier Meadow tuff ages, the cauldron block is sufficiently disrupted by faults that it is unlikely that lavas would mark a single ring fracture analogous to that in the Virgin Valley caldera.

Based on the outflow distribution of the Soldier Meadow Tuff and the thickness of caldera fill, the floor of the Hanging Rock caldera subsided more on the south than on the north. The section of caldera fill is thin on the north, and the caldera floor is exposed near the mouth of Hanging Rock Canyon, where Nut Mountain lavas occur on both sides of

the structural margin of the caldera. The thickness of sediment increases southward, and the thickest accumulation of the younger tuff of Yellow Rock Canyon ponded in the southern half of the caldera. Given that most of the Soldier Meadow Tuff is exposed southeast of the Hanging Rock caldera, it is possible that most of the ignimbrite vented from ring fractures along the southern margin, which resulted in greater collapse there.

Postcaldera Soldier Meadow Lavas and Uplift and Renewed Volcanism in the Badger Mountain Caldera

Shortly after collapse of the Hanging Rock caldera, lavas chemically and petrographically similar to the Soldier Meadow Tuff erupted in the western side of the caldera into a caldera lake, and erupted east of the caldera along a north-south chain of vents located north of Soldier Meadow (red dotted line in Fig. 4). The $^{40}Ar/^{39}Ar$ ages of the Soldier Meadow lavas and the petrographically similar Soldier Meadow Tuff overlap at 2σ uncertainty (Table 1), suggesting that no more than ~50 k.y. passed between eruption of the tuff and the postcaldera lavas. We interpret this short time span and the similar but more evolved compositions of the Soldier Meadow lavas (Fig. 5; Table 3) as indicating that the magma erupted as lavas represented either residual melts not tapped during the ignimbrite eruption or the further evolution following caldera collapse of magma remaining in the chamber.

Emplacement of Soldier Meadow lavas on the floor of the Hanging Rock caldera was not associated with significant uplift, as the lavas have patterns of pressure ridges indicating that they erupted onto a relatively flat surface and extensive glassy carapaces characteristic of erupting into a caldera lake. We interpret the vent array of Korringa (1973) east of the caldera as having formed when magma was intruded along faults that formed concentric to Hanging Rock caldera collapse or to collapse associated with eruption of the tuff of Trough Mountain.

The northernmost of the Soldier Meadow lavas along the vent array erupted within the poorly defined southern boundary of the Badger Mountain caldera, representing a rapid propagation of magmatism to the north. Intrusion of magma renewed volcanism in the caldera, and created a fault-bound trapdoor-style uplift ~18 × 12 km centered on Rodero Flat (Figs. 3 and 4). In Hell Creek, three northwest-trending benches are interpreted to represent a broad zone of faulting on the north side of the trapdoor uplift (Fig. 21), which reactivated the southwestern structural margin of the Virgin Valley caldera (Fig. 4). The alkali rhyolite lavas of Mahogany Mountain that erupted within the Badger Mountain caldera between 15.9 and 15.5 Ma, contemporaneous with and immediately following the Soldier Meadow lavas, vented along the northwest- and north-northeast–trending trapdoor faults and along the reactivated ring fracture of the Virgin Valley caldera (Fig. 4). The vents for the largest flows are located where trapdoor uplift was greatest, forming a linear north-northeast–trending chain of lava centers near Alkali Peak and Mahogany Mountain. In contrast, the hingeline for trapdoor uplift, located along County Road 8A, is characterized by a paucity of rhyolitic vents (Figs. 3 and 4).

Small-volume ignimbrites and pumice falls related to emplacement of these lava domes and flows were erupted at 15.8–15.7 Ma forming the crystal-rich alkali rhyolite tuff of Alkali Flat and Badger Mountain. Welding horizons in the ignimbrites now dip as much as 8° quaquaversally from Rodero Flat, indicating that a significant fraction of the magmatically driven uplift postdated these eruptions.

After peralkaline rhyolitic volcanism ceased, lavas of basalt, trachybasalt, and basaltic trachyandesite erupted along the trapdoor faults and hingeline between ca. 15.5 and 14.2 Ma. Phreatomagmatic deposits (Mp) associated with eruption of these mafic lavas into a caldera lake are exposed along County Road 8A (Fig. 4).

Cottonwood Creek Caldera

Postcaldera rhyolitic volcanism was short lived at the Hanging Rock caldera; activity rapidly migrated to the north to Badger Mountain caldera, and simultaneously occurred to the southwest at the Cottonwood Creek caldera, the youngest caldera in the HRCC. Ach and Swisher (1990) postulated the presence of a caldera in this area, and Bussey (1996) recognized a volcanic center in his study of the geology of the Hog Ranch gold mine, but no caldera-forming unit was identified in these previous studies. We suggest that eruption of the newly recognized 15.70 Ma tuff of Yellow Rock Canyon led to collapse of the 24 × 28 km Cottonwood Creek caldera (Figs. 3 and 4).

The Cottonwood Creek caldera is defined principally by the arcuate arrays of vents for precaldera and postcaldera phenocryst-poor and aphyric alkali rhyolite lavas of Cottonwood Creek that are inferred to have erupted along caldera ring faults (Fig. 4; Plate 1). Within the annular distribution of ring-fracture lavas is a low-relief basin containing poorly exposed caldera fill deposits that include fine-grained caldera lake sediments, small-scale pyroclastic deposits, and sediments representing reworking of volcanic debris. Near the center of the caldera lake these sediments were intruded by alkali olivine basalt, which gave rise to phreatomagmatic deposits and thin lava flows. The age of 14.21 ± 0.04 Ma (MC266) obtained from one of these flows is a maximum age for the cessation of caldera fill sedimentation.

There is also a pattern of arcuate normal faults within the alkali rhyolite lavas of Cottonwood Creek that are concentric around the caldera fill and athwart the younger northwest trends of Basin and Range faults (e.g., the topographic break north of Fox Mountain; Figs. 2–4). We interpret these arcuate faults as offsetting precaldera lavas in a manner sympathetic to the ring faults. In many places these faults are marked by the vents for postcaldera lavas.

Low sulfidation epithermal gold deposits are interpreted to be located within postcaldera ring-fracture lavas at the Hog Ranch Mine (Bussey, 1996) (Figs. 3 and 4). Economically significant mineral deposits have also been identified at other mid-Miocene calderas in northwest Nevada (Rytuba and Glanzman, 1979; Bussey 1996; Castor and Henry, 2000; Rytuba et al., 2003), presumably because silicic magma chambers fuel

shallow meteoric water–dominated hydrothermal systems concentrated along ring-fracture zones (Rytuba, 1994; Bussey, 1996; Saunders et al., 2008; this study).

The magnitude of collapse at the Cottonwood Creek caldera appears to be small relative to the other calderas at the HRCC. In all but the eastern sector of the caldera, Cottonwood Creek lavas that we interpret as precaldera are exposed within the caldera and are lapped by only a thin section of caldera fill, indicating that the top of the cauldron block was not entirely covered by intracaldera ignimbrite and subsided only hundreds of meters. The amount of caldera collapse is greatest in the northeastern quadrant of the Cottonwood Creek caldera, which coincides with inferred vent locations for the tuff of Yellow Rock Canyon.

Most of the known exposures of the tuff of Yellow Rock Canyon are north of the caldera, where the ignimbrite flowed into the topographic depression of the Hanging Rock caldera. Small exposures of ignimbrite located north of Hog Ranch Mine and south of Hart Mountain that are preserved beneath postcaldera Cottonwood Creek lavas are interpreted as being between the structural margin and the topographic wall of the caldera (Fig. 4).

DISCUSSION

Redefinition of the Beginning of the Snake River Plain–Yellowstone Trend

Many researchers attribute eruption of mid-Miocene flood basalts to mantle melting caused by upwelling of a mantle plume head beneath the base of the North American lithosphere ca. 17 Ma, and the northeast-younging silicic centers of the Snake River Plain–Yellowstone trend to subsequent passage of the North American plate over a stationary plume tail (e.g., Pierce and Morgan, 1992; Nash et al., 2006; Hooper et al., 2007; Shervais and Hanan, 2008). The beginning of the Snake River Plain–Yellowstone trend has been depicted frequently in the literature as beginning at the McDermitt caldera in northern Oregon, with the implication that this was also the location of the initial impingement of the plume head on North American lithosphere.

Numerous studies, however, have suggested that mid-Miocene silicic volcanism is widespread (e.g., Pierce and Morgan, 1992; Brueseke and Hart, 2008; Shervais and Hanan, 2008; Castor and Henry, 2000; Cummings et al., 2000; John et al., 2000; Camp et al., 2013; Streck et al., 2015). Nash and Perkins (2012) concluded that there was widespread, abundant silicic volcanism between 16 and 15 Ma in southeastern Oregon and northern Nevada, based on the abundance and distribution of ash fall tuffs of this age in sedimentary basins. Independently, we reached a similar conclusion based on a compilation of the existing evidence for the locations of calderas and lava fields of this age (Coble and Mahood, 2012). In addition, we suggested that the plume head was focused beneath Steens Mountain, and that broadly distributed silicic volcanism at the HRCC, MVF, Lake Owyhee volcanic field, and numerous smaller, lava-dominated centers (see other 16.6–15.0 Ma centers in Fig. 1), and the eruption of voluminous flood basalts of the Columbia River Basalt Group were associated with spreading of a plume head.

These regional studies combined with our work delineating the HRCC, which is the source of ignimbrites similar in age (ca. 16.5–15.7 Ma), volume, and composition to ignimbrites erupted from the MVF, require a modification of the common depiction of the McDermitt caldera sensu stricto as the inception point of the Snake River Plain–Yellowstone trend. We suggest that the HRCC and MVF together with the nearby, smaller lava-dominated Hawks Valley–Lone Mountain, and Santa Rosa–Calico volcanic centers (Fig. 1) should be taken as the origin of the trend. In this model, the transition to the more focused Snake River Plain–Yellowstone track coincided with the passage ca. 15.2 Ma (Nash et al., 2006) of the edge of the North American craton over the mantle thermal anomaly interpreted as a plume tail. This transition was also accompanied by a change from the peralkaline compositions among the rhyolites that erupted at in the Nevada-Oregon-Idaho border region to the metaluminous compositions of the Snake River Plain and at Yellowstone (Nash et al., 2006). The large volumes of the younger rhyolites, despite being associated with lesser volumes of basalt associated with a plume tail, as well as their metaluminous composition, can be explained by the thicker and more felsic composition of the crust east of the craton boundary.

HRCC as an Analog for the Geometry of Calderas Buried Beneath the Snake River Plain

The well-preserved and well-exposed calderas of the HRCC may provide a template for thinking about the nature of the sources of voluminous ignimbrites buried beneath younger basaltic lavas of the Snake River Plain. Based on map patterns for calderas in the HRCC and Yellowstone calderas (Christiansen, 2001), we suggest that the representation of broad eruptive centers postulated beneath basalts and sediments along the Snake River Plain (Fig. 1; Bonnichsen, 1982) should not be taken to represent individual calderas. To do so would greatly exaggerate their sizes and eruptive volumes. Branney et al. (2008) also made this argument based on a similar inference from the geometry of the Yellowstone calderas and the distributions of Pliocene ignimbrites erupted from centers buried beneath the Snake River Plain basalts. The pattern of physical and temporal overlap of calderas at Yellowstone and the HRCC suggests that at each buried Snake River Plain center there would be a clustering of calderas, with nesting of smaller calderas and overlap of larger ones, and there would not be a continuous trail of calderas that young unidirectionally toward the northeast. This clustering may reflect a feedback mechanism in which a locally greater flux of basaltic dikes initiates local crustal melting, which causes stagnation of basaltic dikes, and in turn leads to even more partial melting and hybridization (e.g., Hildreth, 1981; Annen and Sparks, 2002; de Silva and Gregg, 2014). Mechanical focusing of rising dikes by a silicic magma chamber in the middle or upper crust (Karlstrom et al., 2009) could lead to clustering of clustering of calderas. This process may account for the appearance of discrete centers with 1–2 m.y. lifespans along the Snake River Plain–Yellowstone trend (Fig. 1).

Relationship Between Mid-Miocene Basalts and Silicic Volcanism

Contemporaneity of Eruption of Columbia River Basalt Group and Rhyolite Volcanism

Mid-Miocene eruption of more than 210,000 km^3 of magma as flood basalts of the Columbia River Basalt Group covered much of the area that is now Oregon, Washington, western Idaho, and northern Nevada (Fig. 1) (Reidel et al., 2013). The main phase of flood lavas erupted between 16.9 and 15.0 Ma, accounting for ~97% of the volume of the Columbia River Basalt Group based on the volume estimates of Barry et al. (2013). In Coble and Mahood (2012) we highlighted that widespread and voluminous silicic volcanism was contemporaneous with eruption of this main phase of the Steens and Columbia River flood basalt lavas. Between 16.6 and 15.0 Ma, a minimum of 3900 km^3 of silicic magma erupted across a wide area (Figs. 1 and 2), most of it from 3 main caldera complexes located along a north-northeast–trending band in northwest Nevada and southeast Oregon: the MVF, HRCC, and Lake Owyhee volcanic field (Fig. 1; Rytuba and McKee, 1984; Cummings et al., 2000; Coble and Mahood, 2012). In addition to the three main caldera complexes, there are several lava fields where caldera-forming volcanism appears to be subordinate or lacking, including the Santa Rosa–Calico volcanic field (Brueseke et al., 2007), Hawks Valley–Lone Mountain region (Wypych et al., 2011), and the particularly voluminous Jarbidge Rhyolite (Coats, 1964; Brueseke et al., 2014) (Fig. 1), as well as volumetrically less significant silicic lava domes and flows dispersed throughout eastern Oregon, western Idaho, and northern Nevada with ages between 16.6 and 15.0 Ma (yellow and orange dots in Fig. 1).

The earliest mid-Miocene rhyolitic eruptions overlap the 16.9–16.4 Ma age of the earliest flood basalts, the Steens Basalt (Barry et al., 2013 Camp et al., 2013; cf. Baksi, 2013) (Fig. 26). The beginning of caldera-forming silicic volcanism at the HRCC and MVF at 16.4 and 16.5 Ma, respectively, coincided with a decline in Steens Basalt eruptions ca. 16.6 Ma (Fig. 26) and a shift of the locus of mafic volcanism northward from Steens Mountain to the Chief Joseph and Monument dike swarms that gave rise to Columbia River Basalt lavas between 16.7 and 15.0 Ma (e.g., Camp et al., 2003; Barry et al., 2010, 2013; Reidel et al., 2013). The northward shift of mafic volcanism was accompanied by initiation of more northern major silicic volcanism in the Lake Owyhee volcanic field (Rytuba and Vander Muelen, 1991; Rytuba, 1994; Cummings et al., 2000). A major rhyolitic ignimbrite that is interbedded within a section of Columbia River Basalt, the Dinner Creek Tuff (Rytuba and Vander Muelen, 1991; Streck et al., 2015), erupted from the northern part of the field at 16.0 ± 0.1 Ma (Nash and Perkins, 2012). The Mascall tuff, a younger widespread ash fall tuff (Nash and Perkins, 2012) that yielded a $^{40}Ar/^{39}Ar$ age of ca. 15.9 Ma at the type locality near Picture Gorge, Oregon (Swisher, 1992), is from a nearby source (Streck et al., 2015). At the southern end of the Lake Owyhee volcanic field, the weakly peralkaline, high-silica alkali rhyolite Leslie Gulch tuff erupted at 15.8 Ma, forming an ~20 × 25 km caldera (Benson et al., 2013) (Fig. 1).

Role of Columbia River Basalt Group Flood Basalts in the Petrogenesis of Alkali Rhyolites at the HRCC

The location of the three major caldera complexes (i.e., the MVF, HRCC, and Lake Owyhee volcanic field) at the periphery of the most intense flood basalt volcanism along a north-northeast–trending band that closely coincides with location of the $^{87}Sr/^{86}Sr_i = 0.704$ isopleth for basement granitoids (Fig. 1), suggests that although a large basaltic flux through the crust favors the formation of silicic magmas (e.g., Annen and Sparks, 2002; Hughes and Mahood, 2011; de Silva and Gregg, 2014), it is a necessary but not sufficient condition. The composition and thickness of the crust are the main factors controlling where large volumes of silicic magma are produced in association with flood basalts (Coble and Mahood, 2012). The 0.704 isopleth is interpreted as the western margin of transitional crust, i.e., accreted mafic terrains thrust over a craton edge attenuated by rifting and overlain by miogeoclinal sediments. It appears that all 3 caldera fields were formed on transitional crust as they all erupted rhyolites with ε_{Nd} values of ~–0.5 to +6.7 (Table 5; Tegtmeyer and Farmer, 1990; Nash et al., 2006; Coble, 2012).

We interpret the $\delta^{18}O$ and Nd isotopic compositions of the HRCC rhyolites (Table 5) as requiring that they contain partial melts of this transitional continental crust and/or Mesozoic granitoids that formed within it. The analyzed samples of HRCC rhyolite yielded $\delta^{18}O$ values for quartz phenocrysts in the narrow range +7.3 to +8.4‰, with the exception of the most peralkaline ignimbrite, the Soldier Meadow Tuff, which has a slightly lower value of +6.7‰ (Table 5). These data require the involvement of partial melts of crust because values >6‰ cannot be attained by fractional crystallization of mantle-derived basalt. In addition, the ε_{Nd} values of the 6 analyzed rhyolites at the HRCC, –0.5 to +3.7, range to values lower than those reported for the Steens Basalt (Carlson and Hart, 1987; Wolff et al., 2008), stratigraphically the most logical parental magma and the only mid-Miocene basaltic unit voluminous enough to give rise by fractionation-assimilation processes to the large amount of mid-Miocene rhyolite erupted at the HRCC. However, given the ε_{Nd} values, the origin of the HRCC rhyolites cannot have involved large amounts of felsic Paleozoic or older metamorphic or granitic basement rock.

We suggest that intrusion of the Steens Basalt provided the thermal energy to promote crustal anatexis and sustain the silicic magma chambers at the HRCC for ~1 m.y. (Figs. 26 and 27), and given the similarities in eruptive volumes and compositions of coeval magmatism at the MVF, it is likely that the same processes operated at both caldera complexes. Modeling of isotopic compositions at both centers (Starkel, 2014; Mallis, 2014) demonstrates that fractionation of the upper Steens Basalt must have been accompanied by assimilation of transitional crust, probably in the form of Mesozoic granitoids, to produce trachytes, but little or no involvement of crust is required in fractionating trachytes to form alkali rhyolites. Similar conclusions were reached in Novak and Mahood (1986) for the mid-Miocene Kane Springs Wash caldera in southern Nevada, and by Brueseke and Hart (2009)

TABLE 5. Nd AND O ISOTOPIC ANALYSES OF ROCKS AT THE HIGH ROCK CALDERA COMPLEX

Sample	Lat (°N)	Long (°W)	Unit	$^{143}Nd/^{144}Nd$	error (±2σ)	ε_{Nd}	error (±2σ)	$\delta^{18}O_{Qtz}$ (‰)	error (±2σ)
MC358	41.7744	119.3502	LKOT	0.512835*	0.000013	3.8	0.3	–	–
MC381	41.7366	119.1030	LKOT	0.512826*	0.000013	3.7	0.3	–	–
MC266	41.1655	119.5236	Mm	0.512802*	0.000013	3.2	0.3	–	–
MC342	41.5650	119.4431	Mm	0.512843*	0.000013	4.0	0.3	–	–
MC300	41.4321	119.4289	Mt	0.512722*	0.000013	1.6	0.3	–	–
MC87b	41.7567	119.3548	Mlmm	0.512717	0.000008	1.5	0.2	–	–
MC421	41.6505	119.1604	Mlmm	–	–	–	–	8.02	0.07
MC138	41.2553	119.4249	Miyc	0.512671	0.000008	0.6	0.2	–	–
MC375	41.3810	119.4150	Miyc	0.512700*	0.000013	1.2	0.3	–	–
MC391	41.3682	119.3704	Miyc	–	–	–	–	8.34	0.04
								8.35	0.04
MC105	41.3884	119.1778	Mism	0.512612	0.000014	–0.5	0.3	6.71	0.02
								6.78	0.04
MC124	41.4902	119.0852	Mttm	0.512828*	0.000013	3.7	0.3	7.57	0.08
MC212	41.5349	119.1804	Mttm	–	–	–	–	7.32	0.02
MC85	41.5689	119.0213	Misl	0.512629	0.000012	–0.2	0.2	–	–
MC352	41.5818	119.5780	Misl	–	–	–	–	8.15†	0.04
MC82a	41.5879	118.9143	Miic	0.512711	0.000005	1.4	0.1	7.59	0.03
MC409	41.6934	118.8469	Local Steens Basalt	0.512899*	0.000013	5.1	0.3	7.41	0.04

Note: Dash indicates not analyzed. Qtz—quartz.
*Sample numbers had Nd measured by multicollector–inductively coupled plasma–mass spectrometry; all others measured by thermal ionization mass spectrometry.
†Sample number was an analysis made on alkali feldspar; value reported is that for quartz in equilibrium with alkali feldspar with measured δ18O = 7.31‰, based on equilibrium conditions at a temperature of 850 °C using $\delta_{Qtz-K\text{-}feldspar} = 1000 \ln \alpha = 0.84$ (Kheng, 1993).

with regard to intermediate-composition lavas at the mid-Miocene Santa Rosa–Calico volcanic field in northern Nevada.

We suggest that voluminous mid-Miocene silicic volcanism is located where a large flux of basalt coincided with relatively fertile crustal lithologies (see also Camp et al., 2013; Streck et al., 2015). Although the greatest volume of basalt erupted at Steens Mountain, where ~950 m of lavas created a broad shield, the intrusion of flood basalt caused significant partial melting of the crust only where dikes intruded the more fertile transitional crust at the western edge of the North American craton (i.e., between the $^{87}Sr/^{86}Sr_i$ = 0.704 and 0.706 isopleths). Voluminous, coeval, silicic magma chambers formed at a distance of ~75–200 km from Steens Mountain. Existing mapping indicates that there are fewer mid-Miocene calderas associated with the Columbia River Basalt than with the Steens Basalt, despite the greater volume of the former. We think that this is the case because, along most of their length, the Chief Joseph and Monument dike swarms that fed Columbia River Basalt lavas strike north or north-northwest into an area west of the 0.704 isopleth, traversing mafic accreted terrains rather than transitional crust (e.g., Camp, 1995; Camp et al., 2003, 2013). Similarly, although the greatest flux of Steens Basalt occurred at Steens Mountain, as indicated by the thickest accumulation of basaltic lavas and the highest density of mafic dikes, the silicic centers did not occur there. Instead, the voluminous rhyolitic centers of the HRCC and MVF occur where Steens Basalt intruded transitional crust.

Moreover, we suggest that where mafic intrusion rates are as high as those documented for flood basalt provinces and the crust is not fertile, sizable bodies of silicic magma do not accumulate in the upper crust to form calderas. For example, near intense zones of diking at Steens Mountain that produced extraordinarily high eruption rates of 0.3–0.6 km³/yr (Jarboe et al., 2010; Barry et al., 2013), the small amounts of silicic melts produced from partially melting mafic crust may have been insufficient to coalesce into separate magma bodies and were incorporated into the basaltic magmas instead. Partial melting of the crust in the absence of accumulation of silicic magma bodies of significant size may explain at least part of the difference in composition between the lower and upper Steens Basalt (e.g., Hart et al., 1989; Johnson et al., 1998; Camp et al., 2003, 2013). The more evolved and alkalic character of the upper Steens may reflect the temporal evolution of the thermal state of the middle and upper crust, with the upper Steens compositions reflecting significant contamination by crust (e.g., Hart et al., 1989; Wolff et al., 2008; Ramos et al., 2013), whether by direct incorporation of crustal partial melts or by cannibalization of hybridized gabbroic bodies by subsequent intrusions.

Dikes and shallow sills within the section of Steens Basalt in the Pueblo Mountains (Hart et al., 1989) and the Pine Forest Range (Colgan et al., 2010) are proof that basalt was being injected into the crust near the HRCC and Hawks Valley–Lone Mountain center, and that the flood basalt in these sections does not simply consist of far-traveled lava flows that erupted from the focus at Steens Mountain farther north. We suggest that the abrupt southward thinning of the flood basalt section across what is now the Oregon-Nevada border, from nearly 1 km in the northern Pueblo Mountains to its near-absence south of 41.55°N, is due to a feedback mechanism, wherein once a critical mass of silicic magma is generated in the crust by advection of heat by basaltic intrusions, eruptions of flood basalt largely cease in that area as subsequent intrusions of basaltic magma are intercepted by a low-density silicic melt zone (e.g., Annen and Sparks, 2002; de Silva and Gregg, 2014). While flood basalt eruptions continue elsewhere (Figs. 26 and 28), the stagnation of rising basaltic intrusions

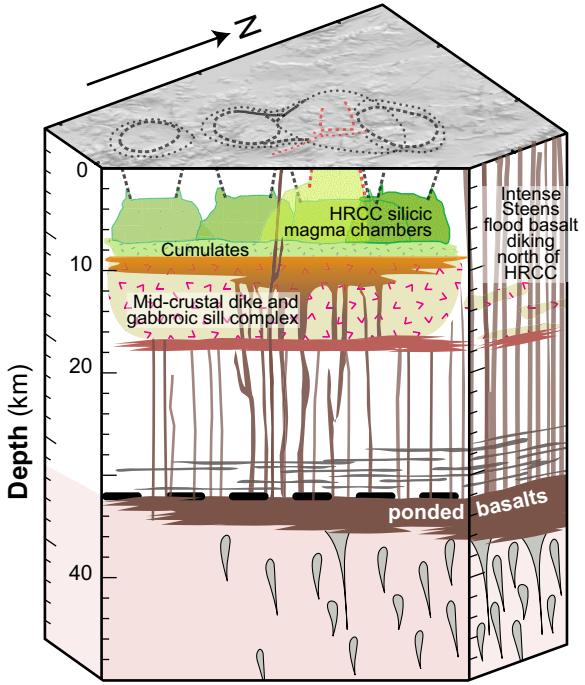

Figure 27. Schematic cross section of the continental crust and upper mantle beneath the High Rock caldera complex (HRCC) in northwest Nevada, illustrating how mid-Miocene caldera volcanism was fueled by injection of Steens flood basalt, and how resulting gabbros and cumulates strengthened the crust. The upper crust is dominated by mid-Miocene granitoid bodies (green) and related cumulates and hybridized rocks (yellow) that are the solidified remnants of HRCC magma chambers. These are underlain by a mid-crustal complex of gabbroic sills and dikes formed from ponded Steens Basalt, which we suggest strengthened the crust beneath HRCC.

thermally sustains the silicic magma chambers and contributes to their growth (Fig. 27).

A consequence of this model is that one would not expect to see the causative Steens Basalt erupting at the surface above the locus of partial melting; there is a near absence of basaltic eruptions for ~1 m.y. in the HRCC. We have analyzed two alkali basalts from localities within the HRCC proper that have chemical similarities to upper Steens Basalt (MC342 and MC434 in Figs. 4, 6, 13–15). MC342 has an ε_{Nd} value of +4 (Table 5), within the range for the Steens Basalt (Wolff et al., 2008). Both are strongly porphyritic, with plagioclase phenocrysts exceeding olivine. MC342 is a small outcrop near the ring fault of the Hanging Rock caldera. Although the field relations are not entirely clear due to extensive faulting along the caldera margin, the lava appears to overlie the 16.34 Ma Summit Lake Tuff and underlie 16.3 Ma Hell Creek lavas, an age consistent with it being upper Steens Basalt. MC434 is from a phreatomagmatic deposit within the caldera fill sequence at the overlap of the Badger Mountain and Hanging Rock calderas. Its stratigraphic position suggests an age between ca. 16.0 and 15.5 Ma, which would make it younger than nearly all dated examples of Steens Basalt lavas (Fig. 26).

An important observation concerning mafic volcanism at the HRCC is that we have found almost no stratigraphic or geochronologic evidence for eruption of basaltic magmas during the interval silicic volcanism was active within the HRCC. The possible exceptions are the aforementioned small volumes of Steens composition basalt that erupted along the intersections of the ring-fracture zones of the Badger Mountain and Hanging Rock calderas. The fact that almost no basalt erupted for ~1 m.y. along the entire 110 km length of the HRCC suggests that there was a continuous zone of partial melting and/or silicic magma bodies that largely prevented penetration of basalt into the upper crust (Fig. 27).

A large flux of flood basalt into the roots of the HRCC magma chambers would allow eruption of large volumes of crystal-poor rhyolite. We observe that crystal-poor rhyolites (<15 vol% phenocrysts) erupted throughout most of the history of the HRCC but appear to be lacking for the interval 16.1–15.9 Ma (Fig. 25B). This is also an interval of much lower than average volumetric eruptive rate (Fig. 25A). We speculate that this interval may represent a relative lull in the flux of Steens Basalt beneath the HRCC, which allowed magma within the Hanging Rock caldera magma chamber to differentiate to the highly evolved yet phenocryst-rich compositions found in the Soldier Meadow Tuff and Soldier Meadow lavas, and allowed magma beneath Badger Mountain caldera to crystallize to a high degree. At 15.9 Ma, rhyolitic eruptions began at the site of the southernmost caldera, Cottonwood Creek, and, simultaneously, eruptive activity renewed within Badger Mountain caldera. This suggests that intrusion of Steens basalt dikes beneath the HRCC reached their southernmost extent at this time, initiating activity in the south with crystal-poor alkali rhyolites, while, beneath the older Badger Mountain caldera, mobilizing crystal mushes to erupt as the Mahogany Mountain lavas (to 55% phenocrysts) (Table 2; Fig. 25B).

The compositions of alkali rhyolite lavas of Mahogany Mountain lavas became less alkalic over the ~0.5 m.y. they erupted. MImm-1 lavas are similar to the Soldier Meadow Tuff (Fig. 5), suggesting some physical continuity between magma beneath the Hanging Rock caldera and the magma that initiated uplift and renewed activity in the Badger Mountain caldera. MImm-3 lavas are the least peralkaline, and overlap the compositional range of the tuff of Big Mountain and Antelope lavas (Fig. 5), which erupted along the Virgin Valley caldera ring fracture ~600 k.y. earlier, suggesting that this may represent a baseline composition to which HRCC magmas return after highly fractionated magmas are removed by eruption, similar to other large silicic magma systems (e.g., Smith, 1979; Hildreth et al., 1991).

Based on our new $^{40}Ar/^{39}Ar$ ages, it appears that the volumetric eruptive rate of alkali rhyolites at the HRCC declined precipitously by ca. 15.6 Ma (Fig.

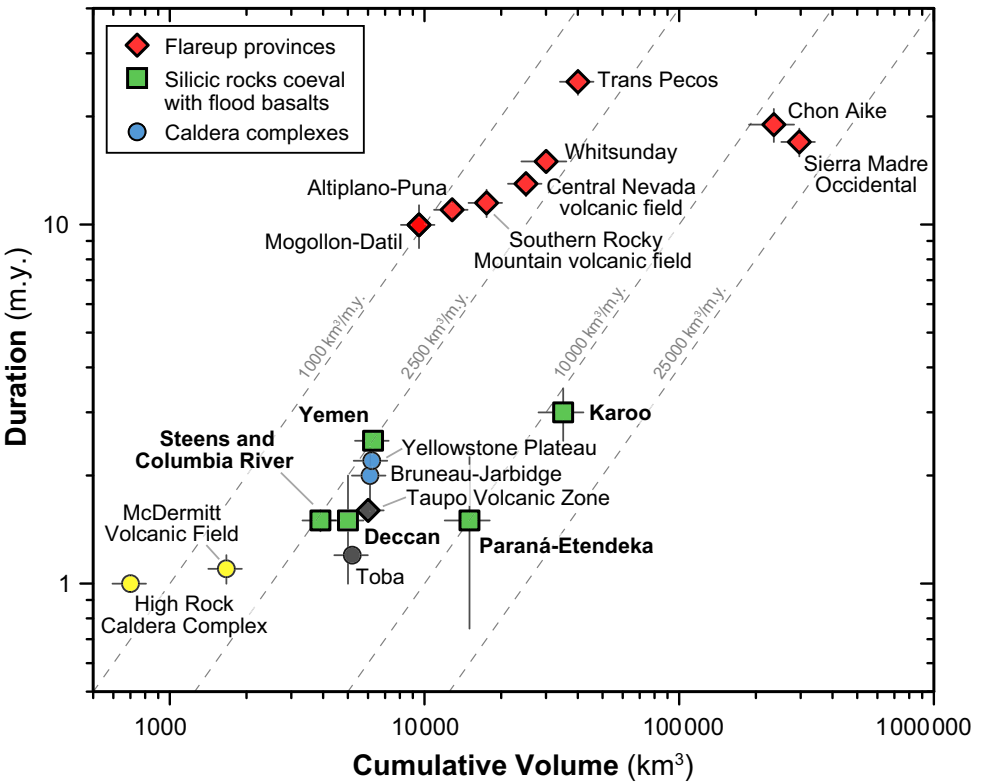

Figure 28. Comparison of eruptive duration versus cumulative volume for silicic caldera complexes, silicic volcanism related to flood basalts, and ignimbrite flare-up provinces. Dashed gray lines show volumetric eruption rates. Yellow circles depict individual silicic caldera complexes associated with Steens and/or Columbia River flood basalts and thought to be associated with initial impingement and spreading of the Yellowstone mantle plume head beneath North American lithosphere, and blue circles are caldera complexes linked with passage of North America over the plume tail. Silicic rocks associated with Steens and Columbia River flood basalt include ca. 16.7–15.0 Ma caldera complexes and regional lava fields. Toba (gray circle) is included as Earth's largest Pleistocene subduction-related caldera complex. Taupo Volcanic Zone (gray diamond) may be an ignimbrite flare-up province that is still ongoing. All volumes are plotted as equivalent magma volumes (i.e., dense rock equivalent, DRE). Data sources as follows: High Rock caldera complex (HRCC)—this study; McDermitt volcanic field (MVF)—Coble and Mahood (2012), Rytuba and McKee (1984); Yellowstone Plateau volcanic field—Christiansen (1984); Bruneau-Jarbidge volcanic center—Leeman et al. (2008); Toba—Chesner and Rose (1991); ignimbrite flare-up provinces—Bryan et al. (1997), Bryan and Ferrari (2013), Wilson et al. (1995), Houghton et al. (1995), Pankhurst et al. (1998, 2000), White et al. (2006), Salisbury et al. (2011), McDowell and McIntosh (2012), Best et al. (2013), Henry and John (2013), Lipman and Bachmann (2015); flood basalt–related silicic provinces—Duncan and Pyle (1988), Milner et al. (1995), Garland et al. (1995), Pankhurst et al. (2011), Ukstins Peate et al. (2005), Coble and Mahood (2012, this study). See Supplemental Table 5 for a compilation of data shown in this figure.

25A). Given that magma chambers associated with peralkaline rhyolites are neither deep nor large (Mahood, 1984), they would cool quickly in the absence of continued heat inputs from below. Therefore, we postulate that flood basalt dikes ceased propagating beneath the HRCC at about that time.

Interaction of Postcaldera Alkali Basalt and Intermediate Lavas with the HRCC Silicic Magma Reservoir

After peralkaline volcanism ceased at the HRCC, mafic to intermediate lavas (Mm, Mt) erupted (Fig. 26) from vents within HRCC calderas along buried ring-fracture zones and trapdoor-uplift faults in all but the Virgin Valley caldera (Fig. 4). In each case these lavas erupted ~400 k.y. after the youngest peralkaline rhyolite in that particular caldera. We interpret this as representing the time required for the underlying silicic magma bodies to cool and crystallize to a rigid crystal mush, allowing brittle fracture and intrusion of younger mafic dikes.

Feldspar-rich cumulate mush beneath the HRCC must have been partially rejuvenated and remelted during intrusion of postcaldera mafic magma, as some of the nearly aphyric 15.4–14.5 Ma trachytic lavas erupted in the Hanging Rock caldera have positive Eu anomalies (Fig. 15) and Ba concentrations exceeding 9600 ppm (Table 4), suggesting a contribution from an anorthoclase-rich cumulate. However, we have not found evidence of basalts making it to the surface in the Hanging Rock caldera.

We link the small-volume, metaluminous lavas that postdate all the peralkaline volcanism to the postcaldera alkalic basalts and intermediate lavas. Stratigraphically, the rhyolite lavas of Wall Canyon (Mlwc) and Rock Springs Canyon (Mlrs) overlap in age with immediately postcaldera alkalic mafic and intermediate lavas. They are small in volume and erupted at the intersection of structural features that were also utilized by the postcaldera mafic and intermediate lavas. Rhyolite lavas of Wall Canyon contain abundant dark colored, trachytic(?) magmatic enclaves near vents. These observations, along with their metaluminous compositions, lead us to suggest that they represent local melting of hot wall rocks by intrusion of small volumes of postcaldera mafic magmas, rather than significant renewal of an underlying silicic magma reservoir; they are only indirectly related petrogenetically to the large volume of peralkaline rhyolites that dominated most of the eruptive history of the HRCC.

We suggest that the metaluminous rhyolite lavas that characterize the earliest (Mlnm) and latest stages (Mlwc and Mlrs) of silicic volcanism at the HRCC may represent small-scale partial melting involving a greater proportion of crust during the waxing and waning stages, respectively, of basaltic magmatism. During the waxing stages, this low-melting-temperature component was transitional crust. During the waning stages of silicic volcanism, the crust was extensively transformed by the preceding HRCC magmatism (Fig. 27), and the most easily melted material would be heated wall rocks around former HRCC magma reservoirs and alkali granites or syenitic cumulates that remain within them.

Comparison of Eruptive Rates at the HRCC with Large Silicic Provinces Globally

The intensity of the silicic volcanism contemporaneous with flood basalt magmatism can be demonstrated for the HRCC due to the level of mapping and the number of new ages determined in this study. Four calderas 24–40 km in diameter formed in a span of only ~0.7 m.y. During the interval 16.6–15.5 Ma, an estimated minimum volume of 700 km³ (DRE) of rhyolitic magma erupted at the HRCC, which accounts for nearly 20% of the total volume of silicic magma erupted regionally between 16.5 and 15.0 Ma. Estimated volumetric eruptive rates average ~700 km³/m.y., but rates were as low as ~200 km³/m.y. prior to eruption of the most peralkaline of the units, the Soldier Meadow Tuff, and, shortly thereafter, briefly as high as 2000–4000 km³/m.y. during eruption of lavas associated with uplift and renewed volcanism in the Badger Mountain caldera (Fig. 25). During the interval of lowest eruptive rates, there was time for differentiation in the subjacent magma reservoirs to produce the most evolved alkali rhyolites erupted in HRCC history. When eruptive rates were highest, evolved magmas were tapped out, resulting in a progressive decline in the peralkalinity of Mahogany Mountain lavas with time.

Our estimates of volumes and eruptive rates are minimum values. They are based on a conservative reconstruction of the distribution of extracaldera ignimbrite (Fig. 5; see Supplemental Fig. 2 for isopach maps), which could be underestimated by as much as 25% because the bases of measured sections are rarely exposed. More significantly, unexposed intracaldera ignimbrite may equal or exceed the volume of outflow sheets. Adopting a conservative estimate of 1:1 for the ratio of extracaldera to intracaldera ignimbrite would make the total eruptive volume at the HRCC ~1400 km³. We note that the resulting volumetric eruptive rates using these larger estimates are still only ~1% of those for the Columbia River Basalt Group flood lavas.

The eruptive volumes for the HRCC and MVF (assuming extracaldera:intracaldera = 1:1), the oldest caldera complexes along the Snake River Plain–Yellowstone trend, are less than half those of the younger Bruneau-Jarbidge and Yellowstone Plateau complexes, and the volcanism lasted about half as long (Fig. 28). This is the case despite the spatial and temporal association of the HRCC and MVF with the voluminous flux of Steens and Columbia River flood basalts, whereas the younger complexes are interpreted as being related to the smaller volumes of mantle melt associated with the Yellowstone plume tail. This highlights the importance of the nature of the crust in controlling the volume of silicic magma produced. The caldera complexes along the Snake River Plain–Yellowstone are east of the Sr_i = 0.706 isopleth, and formed in thicker, more fertile cratonic crust, which promotes growth and storage of larger, longer lived silicic magma reservoirs than those in mafic crust (e.g., Hildreth, 1981; Annen et al., 2006; White et al., 2006; Hughes and Mahood, 2011; Lipman and Bachmann, 2015).

In aggregate, the pulse of silicic magmatism between ca. 16.7 and 15.0 Ma contemporaneous with Steens Basalt and Columbia River Basalt has a total volume and duration similar to other silicic provinces coeval with flood basalt eruptions globally (Fig. 28). Although the number of published studies with volume estimates and accurate geochronology is limited (e.g., Garland et al., 1995; Ukstins Peate et al., 2005; Pankhurst et al., 2011), the available data for the Steens, Columbia River, Deccan Traps, Karoo, Yemen-Ethiopia, and Paraná-Etendeka flood basalt provinces indicate that they have volumetric eruptive rates of silicic magmas between ~2500 and 12,000 km³/m.y. (Fig. 28; see Supplemental Table 5[10] for data shown in this figure).

The relatively short pulse of moderate-volume silicic magmatism from 16.7 to 15.0 Ma in northern Nevada, southern Oregon, and western Idaho associated with the Steens and Columbia River flood basalts is in contrast to the regional magmatic events during the Eocene to Oligocene ignimbrite flare-ups in the Great Basin and Rocky Mountains (e.g., Best and Christiansen, 1991; Christiansen and McCurry, 2008) that culminated in the some of the largest supereruptions on Earth (Bryan et al., 2010; Best et al., 2013; Henry and John, 2013; Lipman and Bachmann, 2015). Globally, the total volumes of silicic magma erupted in ignimbrite flare-up provinces is 2–10 times greater than the volumes erupted in flood basalt provinces (Fig. 28). These enormous volumes are not, however, a result of more intense silicic volcanism. Most ignimbrite flare-up provinces have volumetric eruptive rates smaller than flood basalt provinces, ~1000–2000 km³/m.y., and only the Sierra Madre Occidental (Bryan and Ferrari, 2013; McDowell and McIntosh, 2012) and Chon Aike (Pankhurst et al., 1998, 2000) flare-up provinces have rates that equal the upper end of those calculated for the flood basalt provinces, 12,000 km³/m.y. Ignimbrite flare-up provinces have huge volumes because eruptions continue for 10–20 m.y., ~10 times longer than silicic volcanism associated with flood basalts (Fig. 28). We suggest that these contrasts in total volume and duration are due primarily to the different time scales over which heat is advected into the crust by mantle melts in these two types of provinces, and secondarily to the nature of the crust in which they occur.

In continental flood basalt provinces, >100,000 km³ of basaltic magma (Bryan and Ernst, 2008) erupts over a period of 1–2 m.y., with most of the volume being supplied over intervals as short as hundreds of thousands of years (e.g., Courtillot and Fluteau, 2014). This huge throughput is consistent with the model that the basalts are produced rapidly by decompression partial melting of a mantle

Supplemental Table 5. Cumulative volume and eruptive duration for silicic volcanism related to flood basalts and ignimbrite flare-up provinces shown in Figure 28

Key	Center/Province	Volume (Km³)	error	Duration (Ma)	error	Approx.Age (Ma)	References
Center	High Rock CC	700	105	1	0.05	16	This study
Center	Yellowstone Plateau VF	6,240	936	2.2	0.1	2	Christiansen (1984)
Center	Tobe Caldera Complex	5,200	780	1.2	0.05	1	Chesner and Rose (1991); Chesner (2012)
Center	Bruneau-Jarbidge VC	6,100	915	2	0.4	11	Cozzens et al. (2006)
Center	McDermitt VF	1,665	250	1.1	0.1	16	Rytuba and McKee (2012); Rytuba and McKee (1984); Castor and Henry (2000); This study
Flare	Sierra Madre Occidental	296,000	44,400	17	1.5	~ 46	Bryan et al. (2013); McDowell et al. (2012)
Flare	Altiplano-Puna	12,820	1,923	11	0.5	12	Salisbury et al. (2011)
Flare	Chon Aike	225,000	47,000	19	2	175	Pankhurst et al. (1998); (2000); (2011)
Flare	Whitsunday	30,000	6,000	15	1	130	Bryan et al. (1997)
Flare	Southern Rocky Mtn VF	17,500	2,625	11.5	1	~ 36	Lipman (2013)
Flare	Mogollon-Datil	9,500	1,425	10	1.5	~ 36	McIntosh et al. (1992)
Flare	Central Nevada VF	25,000	3,750	13	1	~ 36	Best et al. (2013); Henry and John (2013)
Flare	Trans Pecos	40,000	6,000	25	2	43 - 16	Barker, (1977)
Flare	Taupo VF	6,000	900	1.6	0.1	~2	Houghton et al. (1995); Wilson (1995)
Plume	Deccan	5,000	750	1.5	0.5	60	Pankhurst et al. (2011); Duncan and Pyle (1988)
Plume	Karoo	25,000	7,000	3	0.5	180	Pankhurst et al. (2011)
Plume	Yemen	5,375	840	2.5	0.15	30	Ukstins Peate et al. (2005)
Plume	Paraná	15,000	3,000	1.5	0.75	130	Milner et al. (1995); Garland et al. (1995)
Plume	Steens & Columbia River	3,960	585	1.5	0.1	16	Coble and Mahood (2012)

Volume error is conservatively estimated to be 15% for Cenozoic provinces, and 20% for Mesozoic and older provinces.
Duration error is conservative based on a survey of the range and quality of published ages
CC = Caldera Complex
VF = Volcanic Field

[10]Supplemental Table 5. Cumulative volume and eruptive duration for silicic volcanism related to flood basalts and ignimbrite flare-up provinces shown in Figure 28. Please visit http://dx.doi.org/10.1130/GES01162.S10 or the full-text article on www.gsapubs.org to view Supplemental Table 5.

plume head upwelling beneath the base of the lithosphere (e.g., Campbell and Griffiths, 1990; Anders and Sleep, 1992; Pierce and Morgan, 1992; Pierce et al., 2002; Hooper et al., 2007). Once the plume head has undergone shallow melting, the basaltic flux would drastically decrease to produce the small-degree partial melts that might be induced in the subcontinental mantle lithosphere or the asthenosphere by conductive heating by the plume (e.g., at the HRCC, the chemically distinct, relatively small volume, postcaldera alkali basalts and similar basalts erupted in the Smoke Creek Mountains and Northern Nevada Rift; Fig. 13).

In comparison to this short-lived event, the prolonged duration of volcanism in ignimbrite flare-ups (Fig. 28), which can wax and wane through time (Salisbury et al., 2011; McDowell and McIntosh, 2012), suggests a geodynamic process that causes much longer term production of mantle melting. Ignimbrite flare-up provinces typically occur or are interpreted to have formed in subduction settings behind the volcanic front, in some cases in crust overthickened by a previous flat-slab subduction event (e.g., Best et al., 2009; Lipman and Bachmann, 2015). They are thought to be associated with backarc extension, rollback of a subducting slab, delamination of the base of overthickened lithosphere (Kay et al., 1994; Dufek and Bergantz, 2005; de Silva et al., 2006; Farmer at al., 2008), or, in the particular case of the Eocene to Oligocene of western North America, the falling away of the Farallon slab, which brought hot mantle into contact with subcontinental lithosphere previously hydrated by subduction processes (e.g., Best and Christiansen, 1991; Humphreys, 1995, 2009; Henry and John, 2013). All of these processes involve the upward flow of depleted, upper mantle asthenosphere to shallower depths in compensation, which would undergo decompression melting and also heat the overlying mantle lithosphere (e.g., Farmer et al., 2008). We speculate that although mantle melting may not be as productive as when undepleted plume-related mantle undergoes partial melting, the magmatism in this tectonic setting is sustained over a longer period of time.

The differences in composition and phenocryst mineralogy of the rhyolites erupted in ignimbrite flare-ups and in flood basalt–related provinces indicate a contrast in the type and proportion of crustal melts involved in their genesis. Silicic magmas in ignimbrite flare-ups tend to be cooler, richer in water, and more oxidized than those in flood basalt provinces, and peralkaline rhyolites are lacking (Christiansen and McCurry, 2008). This is consistent with the observation that ignimbrite flare-up provinces occur where the continental crust is relatively thick and fertile. Although basalts are greatly subordinate to intermediate and silicic rocks at the surface in ignimbrite flare-up provinces, the huge volumes of rhyolite produced that contain significant proportions of mantle-derived material (e.g., ~50% for the southern Rocky Mountain and Mogollon-Datil volcanic fields; Farmer et al., 2008; ~30% for Altiplano-Puna; de Silva et al., 2006) require a sizable supply of basalt into the lower and middle crust that drives crustal anatexis (de Silva and Gregg, 2014). A sustained basaltic flux into thick, fertile crust creates the conditions for development of a large zone of partial melting in the crust, and the assembly and thermal maintenance of large, long-lived silicic magma chambers (e.g., Annen et al., 2006; Bachmann et al., 2005; Lipman, 2007; de Silva and Gregg, 2014).

Expression of Mid-Miocene Caldera Magmatism in Modern Basin and Range Topography

The modern topography in northwestern Nevada and southern Oregon is largely the result of post-HRCC Basin and Range extension concentrated along large-magnitude, north-northeast–trending, range-bounding normal faults (Colgan et al., 2006; Colgan and Henry, 2009). The HRCC is on the eastern edge of the Modoc Plateau, which has undergone less extension than the rest of northwest Nevada (5%–10% versus 15%–25% since the mid-Miocene; Wells and Heller, 1988; Colgan et al., 2006). Even so, the calderas of the HRCC are remarkably little affected by Basin and Range faulting. The largest faults within the complex are all associated with caldera collapse, and many of the smaller faults are associated with magmatic uplift or with regional postcollapse downsagging around the calderas (Figs. 2–4). Normal faults with the regional north-northwest to north-northeast extension-related trends have maximum offsets of a few tens of meters within the calderas, whereas immediately east of the calderas in the Black Rock Range outflow ignimbrites are offset hundreds of meters along regional normal faults, and farther north in the southern Pueblo Mountains and northern Pine Forest Range, the section of Steens Basalt and overlying outflow ignimbrites from the MVF are tilted westward as much as 45° (Burnam, 1970; Colgan et al., 2010).

The same pattern can be seen at the MVF, where large-offset normal faults (shown with thick black lines in Fig. 2) do not offset the McDermitt or Whitehorse calderas, but sections consisting of stacked outflow ignimbrites are faulted and tilted. We interpret the fault along the west side of the Montana Mountains to have reactivated a McDermitt caldera ring-fracture zone, just as the normal fault on the east side of McGee Mountain at the HRCC reactivated the Virgin Valley caldera ring fracture (Figs. 3 and 4).

Based on apatite fission-track data from the Pine Forest Range, it was suggested (Colgan et al., 2006) that in northwestern Nevada the onset of significant extension occurred at 12–7 Ma. This age range coincides with the onset of eruption of HAOT lavas across southern Oregon, northern Nevada, and northeastern California (Hart et al., 1984; Hart, 1985; Carlson and Hart, 1987; Bailey and Conrey, 1992; Jordan et al., 2004; Carmichael et al., 2006; this study), suggesting that a post–16 Ma episode of extension allowed these partial melts of depleted, asthenospheric, upper mantle (Hart et al., 1984) to erupt at the surface. HAOT lavas are present only in the northern part of the HRCC, where they are 10–8 Ma, and the thin (<10 m) flows form prominent mesas or tables that are flat-lying or tilted <5°. In contrast, 8–3 Ma HAOT lavas west of the HRCC are cut by prominent normal faults and are tilted as much as 15° in the Hays Canyon Range (Carmichael et al., 2006) and at Massacre Rim (Trugman, 2011). Moreover, we have not identified vents for HAOT flows within the HRCC; the lavas in the northern half of the complex flowed south from vents north and northwest of the com-

plex (e.g., Bitner Butte in Fig. 3), suggesting that the complex was not affected by the minor extension that allowed eruption of HAOT lavas.

Additional evidence that the HRCC complex has not undergone significant extension since its formation is that we have not identified basinal sediments between the HAOT lavas and underlying caldera fill (cf. Greene, 1984; Castor and Henry, 2000). The Rock Spring Table HAOT flow directly overlies the tuff of Big Mountain and fine-grained lacustrine sediments in the Virgin Valley caldera, and, where it flowed into the Badger Mountain caldera, it directly overlies the tuff of Alkali Flat and Badger Mountain east of Alkali Flat (Figs. 3 and 4). These observations are consistent with the results of Nash and Perkins (2012) that show, through chemical correlation of ashes in the Virgin Valley caldera with regionally extensive units, that the upper part of the caldera fill is ca. 14.3 Ma. The absence of late Miocene sediment is evidence that the HRCC remained an elevated plateau, and was not significantly affected by the regional extensional event that began ca. 16 Ma (Colgan and Henry, 2009), or by local extension that began ca. 12 Ma (Colgan et al., 2006). As a result of the only minor offset on extension-related faults (as opposed to caldera collapse– or trapdoor uplift–related faults), the HRCC today is a volcanic plateau that is physiographically similar to conditions in the mid-Miocene (Merriam, 1910; Mulch et al., 2008; Hilton et al., 2008).

Role of Mid-Miocene Magmatism in Strengthening the Crust

We interpret the observation that major Basin and Range normal faults do not transect the High Rock and McDermitt caldera complexes, and that major range-bounding faults appear to be deflected around them, as evidence that mid-Miocene magmatism at the HRCC and MVF transformed the lithosphere beneath the caldera complexes to make it stronger than surrounding areas. We suggest that intense, focused rhyolitic and basaltic magmatism locally modified the entire crustal column and created strong localized structural blocks that have not been cut by Basin and Range normal faults. As a result, the caldera complexes remain as elevated plateaus, and the structural and topographic margins of the calderas are unusually well preserved.

Low seismic velocities in the middle to upper crust beneath the HRCC have been interpreted as reflecting the presence of Jurassic and Cretaceous granitic rocks (Lerch et al., 2007; Van Buer et al., 2009). Although this is possible, we note that the nearest granitic rocks are exposed well east of the HRCC in the Pine Forest Range and Pueblo Mountains. Granitic lithics are absent in the many ignimbrites erupted from the HRCC, indicating that granitic rocks (and, for that matter, other basement lithologies) are absent from the upper crust beneath the calderas. We think it is equally or more plausible to interpret the low seismic velocities in the middle to upper crust beneath the HRCC (Lerch et al., 2007) as silicic to intermediate plutons associated with mid-Miocene silicic volcanism.

However, we do not believe that the crustal blocks beneath the HRCC and MVF are strong solely because they have been stitched together by overlapping upper crustal plutons into small batholiths the sizes of the caldera complexes. Quartz-rich rocks are not strong at mid-crustal depths, especially under conditions of high heat flow characteristic of the Basin and Range Province (Kusznir and Park, 1987; Bürgmann and Dresen, 2008). Rather, we believe that the strength of these blocks is due mostly to the presence of a significant volume of dry gabbros in the middle crust, largely the crystallized remains of flood basalt magmas that were intercepted by bodies of low-density silicic melt and the cumulates that resulted from their fractionation and the extraction of trachytic and rhyolitic melts (Fig. 27). We suggest that the resulting network of mafic sills and dikes in the middle crust began to cool ca. 15.6 Ma, at the end of peralkaline volcanism at the HRCC, which we interpret as the time when the focus of intrusion of flood basalt magmas shifted northward and the flux of Steens Basalt declined (Fig. 26). Final cooling of mid-crustal gabbroic bodies would have occurred at the cessation of postcaldera mafic and trachytic magmatism in the HRCC by ca. 14 Ma. These solidified gabbroic bodies locally strengthened the crust beneath the HRCC and MVF. Later, when major regional normal faulting began ca. 12–7 Ma as a result of the northward progression of the Basin and Range extension into the HRCC area (Colgan et al., 2004, 2006), large-magnitude, north-northeast–trending normal faults were concentrated along the Santa Rosa, Pine Forest, Black Rock, and Warner Ranges, and avoided the HRCC and MVF (Fig. 2).

The Pueblo Mountains and Steens Mountain expose thick sections of Steens flood basalt lavas along major range-bounding normal faults, indicating that the crust beneath these areas was not as strong as at the HRCC and MVF. In our model, despite the intense intrusion of mafic magma at Steens Mountain, only minor volumes of silicic partial melts were formed there due to the less fertile nature of the crust (i.e., west of the 0.704 Sr_i isopleth). We suggest that in the absence of significant bodies of silicic magma in the middle and upper crust, basaltic dikes were not impeded in their rise through the crust, and large mid-crustal gabbroic bodies did not form. Therefore, despite the large volume of basalt erupted at Steens Mountain, the middle crust beneath Steens Mountain was not rendered as strong as at the HRCC or at MVF, where upper crustal silicic bodies caused large volumes of mafic magma to pond and hybridize in mid-crustal reservoirs (Fig. 27).

Additional evidence for the importance of mid-crustal gabbroic bodies for strengthening the crust is the observation that Paleogene calderas of the ignimbrite flare-up in the central Great Basin have been strongly extended and tilted such that cross sections of the calderas and the underlying plutonic underpinnings are exposed (e.g., Caetano caldera, Colgan et al., 2008; Stillwater caldera complex, John, 1995). These calderas differ from the mid-Miocene plume-related rhyolites in that they formed in fertile, cratonic crust that was close to its solidus due to thermal relaxation following a Laramide shortening event and exposure to strong thermal gradients due to delamination of the lower crust and/or the falling away of a shallowly dipping slab (e.g., Humphreys, 1995; Christiansen and McCurry, 2008; Best et al., 2009). As a result, a smaller flux of basalt was required to melt the crust, and there was extensive hybridization between basalts and crustal melts (e.g., the isotopic data for the Mogollon Datil and San Juan Mountains fields requiring that the rhyolites consist of a 50:50 mixture

of crust and mantle-derived basalt; Farmer et al., 2008). Because of the extensive crustal anatexis and hybridization of the basalts, large volumes of mid-crustal gabbroic bodies did not form and the crust was not significantly strengthened beneath Paleogene caldera complexes. We argue that the crust beneath the HRCC and MVF has been uniquely modified by voluminous and intense intrusion of flood basalt magmas that fueled moderate amounts of melting of transitional continental crust, enough to cause ponding of basalt in the middle crust, but not enough for extensive hybridization between basalt and crustal melts. We suggest that, as a result, mid-crustal mafic intrusions are below a seismically imaged low-density HRCC granitoid in the upper crust (Fig. 27).

CONCLUSIONS

The volcanic and volcaniclastic rocks of the HRCC represent one of the best-preserved and best-exposed examples of the original geometry and geomorphology of silicic volcanism related to flood basalt eruptions anywhere on Earth. The HRCC consists of overlapping mid-Miocene rhyolitic calderas and their products that cover an area of ~8300 km^2 in northwestern Nevada and southern Oregon near the southern extent of the Steens Basalt flood lavas (Figs. 1, 4, and 5). A minimum estimated volume of ~700 km^3 of peralkaline rhyolitic magma (DRE), ~60% of the total as lavas, erupted during an ~1 m.y. interval between 16.4 and 15.5 Ma. Four major calderas 24–40 km in diameter formed at 16.38, 16.34, 16, and 15.70 Ma on eruption of moderate-sized ignimbrites that ranged in composition from high-silica alkali rhyolite to trachyte (Figs. 5 and 6).

Thick sequences of caldera fill accumulated in caldera lakes, including fine-grained, diatomaceous, ashy sediments that contain abundant petrified wood and opal. Ring-fracture lavas that erupted into the caldera lakes at the Virgin Valley and Cottonwood Creek calderas were strongly altered and host minor Au and U mineralization. In contrast, volcanism associated with uplift and late-stage renewal of magmatism in the Badger Mountain caldera is associated with little alteration, only fault-localized silicification.

After peralkaline rhyolitic volcanism ceased, trachyte to trachyandesite lavas erupted along the ring fracture of the Hanging Rock caldera. The positive Eu anomalies and high Ba concentrations in these phenocryst-poor lavas suggest that they represent melting of feldspar-rich cumulate material formed earlier in the history of the HRCC. Alkali basalts through trachytes erupted at the Badger Mountain caldera, and alkali basalt erupted at the Cottonwood Creek caldera. Eruption of these mafic to intermediate lavas between 15.5 and 14.2 Ma indicates that the underlying silicic magma reservoirs had cooled to the point that they could sustain brittle fracture and diking.

Voluminous mid-Miocene silicic magmatism at the HRCC, MVF, and Lake Owyhee volcanic field is located where flood basalt dikes encountered fertile crustal lithologies at the western margin of the North American craton. Beginning ca. 16.9 Ma, flood basalt magma focused at Steens Mountain began to intrude southward as dikes along zones of preexisting crustal weakness, causing significant partial melting of the crust where dikes intruded transitional crust at the craton margin (i.e., between the $^{87}Sr/^{86}Sr_i$ = 0.704 and 0.706 isopleths). The stagnation of these basaltic dikes within zones of partial melting in the crust and beneath low-density upper crustal magma chambers provided heat that sustained voluminous rhyolitic magmatism at both the HRCC and MVF for ~1 m.y. Upon cooling, hybridized gabbroic equivalents of intruded Steens Basalt locally strengthened the crust beneath calderas at the MVF and HRCC, so they are little affected by normal faulting compared to surrounding areas of the Basin and Range Province and remain elevated plateaus.

The eruptive products of the HRCC and MVF are among the >3900 km^3 of rhyolite that erupted across a large area in the Nevada-Oregon-Idaho border region between 16.6 and 15.0 Ma. This widespread occurrence over a short period of time that followed initiation of Steens Basalt volcanism by ~0.2 m.y. and coincided with main stage Steens and Columbia River flood basalt volcanism (Fig. 26) is consistent with the rhyolitic centers of the Nevada-Oregon-Idaho border region marking the spread of a mantle plume head at the base of the North American lithosphere beginning ca. 17 Ma. The overall volumetric eruptive rates of widespread mid-Miocene silicic volcanism associated with Steens Basalt and Columbia River Basalt are in the range of other flood basalt–related silicic provinces globally, 2500–12,000 km^3/m.y. These rates exceed those at most ignimbrite flare-up provinces, which attain their large volumes by having durations an order of magnitude longer than the short lived but more intense volcanism that is interpreted as being related to arrival of a mantle plume beneath continental lithosphere.

We suggest that the initiation point of the focused trend of eastward-younging silicic calderas along the Snake River Plain encompasses the caldera complexes of the HRCC and MVF along with nearby lava-dominated centers at Hawks Valley–Lone Mountain and Santa Rosa–Calico volcanic centers. The smaller volume and presence of peralkaline compositions among the rhyolites that erupted at 16.6–15.0 Ma in the Nevada-Oregon-Idaho border region compared to the younger, metaluminous, and voluminous rhyolitic eruptions in the Snake River Plain and at Yellowstone can be explained by the thinner and more mafic composition of the crust west of the craton boundary.

ACKNOWLEDGMENTS

This paper is based on Coble's Ph.D. thesis. Coble thanks Joseph Colgan, Derek Lerch, and Chris Henry for discussing their work in the area at the initiation of this project, Jim Rytuba for his continued support and guidance, and Jonathan Glen for instructing him on collecting paleomagnetic data. This project would not have been possible without the work of Marty Grove to revitalize the argon geochronology laboratory at Stanford, and the help of Andy Calvert in calibrating the Nu instrument. We thank Tom Benson for performing additional X-ray fluorescence analyses that allowed further correlation of ignimbrites, and Jonathan Glen for providing the regional aeromagnetic and gravity maps. We appreciate the efforts of Benson, A. Strickland, H. Mix, S. Pitter, E. Pope, V. Mitchell, K. Maier, G. Hughes, and A. Trugman as field assistants. Discussions with Benson, Grove, and Elizabeth Miller were helpful in writing early drafts of the manuscript. We appreciate the efforts of reviewers Matt Brueseke and Martin Streck, and editors Ben Ellis and Shan de Silva. Financial support was provided by the U.S. Geological Survey, National Cooperative Geologic Mapping Program, under Award No. 185 08HQAG0037 awarded to Mahood, and a Stanford–U.S. Geological Survey Fellowship and a Stanford School of Earth Sciences McGee Fund grant to Coble.

REFERENCES CITED

Ach, A.J., 1988, Geologic map of the Yellow Hills East quadrangle, Washoe and Humboldt Counties, Nevada: U.S. Geological Survey Miscellaneous Field Studies Map MF-2029, scale 1:24,000.

Ach, A.J., and Swisher, C.C., 1990, The High Rock caldera complex: Nested "failed" calderas in northwestern Nevada: Eos (Transactions, American Geophysical Union), v. 71, p. 1614.

Ach, A.J., Bateson, J.T., Turrin, B.D., Keith, W.J., Noble, D.C., and Swisher, C.C., 1991, Geologic map of the High Rock Lake quadrangle, Washoe and Humboldt Counties, Nevada: U.S. Geological Survey Miscellaneous Field Studies Map MF-2157.

Anders, M.H., and Sleep, N.H., 1992, Magmatism and extension: The thermal and mechanical effects of the Yellowstone hotspot: Journal of Geothermal Research, v. 97, p. 15,279–15,393.

Annen, C., and Sparks, R.S.J., 2002, Effects of repetitive emplacement of basaltic intrusions on thermal evolution and melt generation in the crust: Earth and Planetary Science Letters, v. 203, p. 937–955, doi:10.1016/S0012-821X(02)00929-9.

Annen, C., Blundy, J.D., and Sparks, R.S.J., 2006, The genesis of intermediate and silicic magmas in deep crustal hot zones: Journal of Petrology, v. 47, p. 505–539, doi:10.1093/petrology/egi084.

Armstrong, R.L., Taubeneck, W.H., and Hales, P.O., 1977, Rb-Sr and K-Ar geochronometry of Mesozoic granitic rocks and their Sr isotopic composition, Oregon, Washington, and Idaho: Geological Society of America Bulletin, v. 88, p. 397–411, doi:10.1130/0016-7606(1977)88<397:RAKGOM>2.0.CO;2.

Bachmann, O., Dungan, M.A., and Bussy, F., 2005, Insight into shallow magmatic processes in large silicic magma bodies: the trace element record in the Fish Canyon magma body, Colorado: Contributions to Mineralogy and Petrology, v. 149, p. 338–349, doi:10.1007/s00410-005-0653-z.

Bailey, R.A., and Conrey, R.M., 1992, Common parent magma for Miocene to Holocene mafic volcanism in the northwestern United States: Geology, v. 20, p. 1131–1134, doi:10.1130/0091-7613(1992)020<1131:CPMFMT>2.3.CO;2.

Baksi, A.J., 2013, Timing and duration of volcanism in the Columbia River Basalt Group: A review of existing radiometric data and new constraints on the age of the Steens through Wanapum Basalt extrusion, *in* Reidel, S.P., et al., eds., The Columbia River flood basalt province: Geological Society of America Special Paper 497, p. 67–85, doi:10.1130/2013.2497(03).

Barry, T.L., Self, S., Kelley, S.P., Reidel, S., Hooper, P., and Widdowson, M., 2010, New $^{40}Ar/^{39}Ar$ dating of the Grande Ronde Lavas, Columbia River basalts, USA: Implications for duration of flood basalt eruption episodes: Lithos, v. 118, p. 213–222, doi:10.1016/j.lithos.2010.03.014.

Barry, T.L., Kelley, S.P., Reidel, S.P., Camp, V.E., Self, S., Jarboe, N.A., Duncan, R.A., and Renne, P.R., 2013, Eruption chronology of the Columbia River Basalt Group, *in* Reidel, S.P., et al., eds., The Columbia River flood basalt province: Geological Society of America Special Paper 497, p. 45–66, doi:10.1130/2013.2497(02).

Benson, T.R., and Mahood, G.A., 2015, The oldest known caldera associated with the Yellowstone hotspot: New geologic mapping, geochemistry, and $^{40}Ar/^{39}Ar$ geochronology for the northern McDermitt Volcanic Field, northern Nevada and southeastern Oregon: American Geophysical Union Fall Meeting Abstracts, v. 5, abs. 85816.

Benson, T.R., Mahood, G.A., and Grove, M., 2013, New geologic and geochronologic data on the Lake Owyhee Volcanic Field, Oregon: A silicic center contemporaneous with flood basalt volcanism: Geological Society of America Abstracts with Programs, v. 45, no. 6, p. 14.

Best, M.G., and Christiansen, E.H., 1991, Limited extension during peak Tertiary volcanism, Great Basin, Nevada and Utah: Journal of Geophysical Research, v. 96, p. 13,509–13,528, doi:10.1029/91JB00244.

Best, M.G., Barr, D.L., Christiansen, E.H., Gromme, S., Deino, A.L., and Tingey, D.G., 2009, The Great Basin Altiplano during the middle Cenozoic ignimbrite flareup: Insights from volcanic rocks: International Geology Review, v. 51, p. 589–633, doi:10.1080/00206810902867690.

Best, M.G., Gromme, S., Deino, A.L., Christiansen, E.H., Hart, G.L., and Tingey, D.G., 2013, The 36–18 Ma central Nevada ignimbrite field and calderas, Great Basin, USA: Multicyclic super-eruptions: Geosphere, v. 9, p. 1562–1636, doi:10.1130/GES00945.1.

Binger, G.B., 1997, The volcanic stratigraphy of the Juntura region, eastern Oregon [M.S. thesis]: Pullman, Washington State University, 206 p.

Bonham, H.F., and Papke, K.G., 1969, Geology and mineral deposits of Washoe and Storey Counties, Nevada: Nevada Bureau of Mines and Geology Bulletin 70, 140 p.

Bonnichsen, B., 1982, Rhyolite lava flows in the Bruneau-Jarbidge eruptive center, southwestern Idaho, *in* Bonnichsen, B., and Breckenridge, R.M., eds., Cenozoic geology of Idaho: Idaho Bureau of Mines and Geology Bulletin 26, p. 283–320.

Branney, M.J., Bonnichsen, B., Andrews, G.D.M., Ellis, B., Barry, T.L., and McCurry, M., 2008, 'Snake River (SR)-type' volcanism at the Yellowstone hotspot track: Distinctive products from unusual high-temperature silicic super-eruptions: Bulletin of Volcanology, v. 70, p. 293–314, doi:10.1007/s00445-007-0140-7.

Bryan, S.E., and Ernst, R.E., 2008, Revised definition of large igneous provinces (LIPs): Earth-Science Reviews, v. 86, p. 175–202, doi:10.1016/j.earscirev.2007.08.008.

Bryan, S.E., and Ferrari, L., 2013, Large igneous provinces and silicic large igneous provinces: Progress in our understanding over the last 25 years: Geological Society of America Bulletin, v. 125, p. 1053–1078, doi:10.1130/B30820.1.

Bryan, S.E., Constantine, A.E., Stephens, C.J., Ewart, A., Schön, R.W., and Parianos, J., 1997, Early Cretaceous volcano-sedimentary successions along the eastern Australian continental margin: Implications for the break-up of eastern Gondwana: Earth and Planetary Science Letters, v. 153, p. 85–102, doi:10.1016/S0012-821X(97)00124-6.

Bryan, S.E., Riley, T.R., Jerram, D.A., Stephens, C.J., and Leat, P.T., 2002, Silicic volcanism: An undervalued component of large igneous provinces and volcanic rifted margins, *in* Menzies, M.A., et al., eds., Volcanic rifted margins: Geological Society of America Special Paper 362, p. 97–118, doi:10.1130/0-8137-2362-0.97.

Bryan, S.E., Peate, I.U., Peate, D.W., Self, S., Jerram, D.A., Mawby, M.R., Marsh, J.S., and Miller, J.A., 2010, The largest volcanic eruptions on Earth: Earth-Science Reviews, v. 102, p. 207–229, doi:10.1016/j.earscirev.2010.07.001.

Brueseke, M.E., and Hart, W.K., 2008, Geology and petrology of the Mid-Miocene Santa Rosa–Calico volcanic field, northern Nevada: Nevada Bureau of Mines and Geology Bulletin 113, 99 p.

Brueseke, M.E., and Hart, W.K., 2009, Intermediate composition magma production in an intracontinental setting: Unusual andesites and dacites of the mid-Miocene Santa Rosa–Calico volcanic field, northern Nevada: Journal of Volcanology and Geothermal Research, v. 188, p. 197–213, doi:10.1016/j.jvolgeores.2008.12.015.

Brueseke, M.E., Heizler, M.T., Hart, W.K., and Mertzman, S.A., 2007, Distribution and geochronology of Oregon Plateau (U.S.A.) flood basalt volcanism: The Steens Basalt revisited: Journal of Volcanology and Geothermal Research, v. 161, p. 187–214, doi:10.1016/j.jvolgeores.2006.12.004.

Brueseke, M.E., Callicoat, J.S., Hames, W., and Larson, P.B., 2014, Mid-Miocene rhyolite volcanism in northeast Nevada: The Jarbidge Rhyolite and its relationship to the Cenozoic evolution of the northern Great Basin (USA): Geological Society of America Bulletin, v. 126, p. 1047–1067, doi:10.1130/B30736.1, doi:10.1130/B30736.1.

Bürgmann, R., and Dresen, G., 2008, Rheology of the lower crust and upper mantle: Evidence from rock mechanics, geodesy, and field observations: Annual Review of Earth and Planetary Sciences, v. 36, p. 531–567, doi:10.1146/annurev.earth.36.031207.124326.

Burnam, R., 1970, The geology of the southern part of the Pueblo Mountains, Humboldt County, Nevada [M.S. thesis]: Corvallis, Oregon State University, 170 p.

Bussey, S.D., 1996, Gold mineralization and associated rhyolitic volcanism at the Hog Ranch District, northwest Nevada, *in* Coyner, A.R., and Fahey, P.L., eds., Geology and ore deposits of the American Cordillera: Reno, Geological Society of Nevada Symposium Proceedings, p. 181–207.

Camp, V.E., 1995, Mid-Miocene propagation of the Yellowstone mantle plume head beneath the Columbia River basalt source region: Geology, v. 23, p. 435–438, doi:10.1130/0091-7613(1995)023<0435:MMPOTY>2.3.CO;2.

Camp, V.E., Ross, E.M., and Hanson, W.E., 2003, Genesis of flood basalts and Basin and Range volcanic rocks from Steens Mountain to the Malheur River Gorge, Oregon: Geological Society of America Bulletin, v. 115, p. 105–128, doi:10.1130/0016-7606(2003)115<0105:GOFBAB>2.0.CO;2.

Camp, V.E., Ross, M.E., Duncan, R.A., Jarboe, N.A., Coe, R.S., Hanan, B.B., and Johnson, J.A., 2013, The Steens Basalt: Earliest lavas of the Columbia River Basalt Group, *in* Reidel, S.P., et al., eds., The Columbia River flood basalt province: Geological Society of America Special Paper 497, p. 87–116, doi:10.1130/2013.2497(04).

Campbell, I.H., and Griffiths, R.W., 1990, Implications of mantle plume structure for the evolution of flood basalts: Earth and Planetary Science Letters, v. 99, p. 79–93, doi:10.1016/0012-821X(90)90072-6.

Carlson, R.W., and Hart, W.K., 1987, Crustal genesis on the Oregon Plateau: Journal of Geophysical Research, v. 92, p. 6191–6206, doi:10.1029/JB092iB07p06191.

Carmichael, I.S.E., Lange, R., Hall, C.M., and Renne, P.R., 2006, Faulted and tilted Pliocene olivine-tholeiite lavas near Alturas, NE California, and their bearing on uplift of the Warner Range: Geological Society of America Bulletin, v. 118, p. 1196–1211, doi:10.1130/B25918.1.

Castor, S.B., and Henry, C.D., 2000, Geology, geochemistry, and origin of volcanic rock-hosted uranium deposits in northwest Nevada and southeastern Oregon, USA: Ore Geology Reviews, v. 16, p. 1–40, doi:10.1016/S0169-1368(99)00021-9.

Chesner, C.A., 2012, The Toba caldera complex: Quaternary International, v. 258, p. 5–18, doi:10.1016/j.quaint.2011.09.025.
Chesner, C.A., and Rose, W.I., 1991, Stratigraphy of the Toba Tuffs and the evolution of the Toba caldera complex, Sumatra, Indonesia: Bulletin of Volcanology, v. 53, p. 343–356, doi:10.1007/BF00280226.
Christiansen, R.L., 1984, Yellowstone magmatic evolution: Its bearing on understanding large-volume explosive volcanism, *in* Geophysics Study Committee, eds., Explosive volcanism, its inception, evolution and hazards: Studies in Geophysics Series II: Washington, D.C., National Academies Press, p. 84–95.
Christiansen, R.L., 2001, The Quaternary and Pliocene Yellowstone Plateau Volcanic Field of Wyoming Idaho, and Montana: U.S. Geological Survey Professional Paper 729-G, 102 p.
Christiansen, E.H., and McCurry, M., 2008, Contrasting origins of Cenozoic silicic volcanic rocks from the western Cordillera in the United States: Bulletin of Volcanology, v. 70, p. 251–267, doi:10.1007/s00445-007-0138-1.
Christiansen, R.L., and Yeats, R.L., 1992, Post-Laramide geology of the U.S. Cordilleran region, *in* Burchfiel, B.C., et al., eds., The Cordilleran orogen: Conterminous U.S.: Boulder, Colorado, Geological Society of America, Geology of North America, v. G-3, p. 261–406.
Christiansen, R.L., Foulger, G.R., and Evans, J.R., 2002, Upper-mantle origin of the Yellowstone hotspot: Geological Society of America Bulletin, v. 114, p. 1245–1256, doi:10.1130/0016-7606(2002)114<1245:UMOOTY>2.0.CO;2.
Coats, R.R., 1964, Geology of the Jarbidge quadrangle, Nevada-Idaho: U.S. Geological Survey Bulletin 1141-M, p. M1–M24.
Coble, M.A., 2012, Geology and 40-argon/39-argon geochronology of the mid-Miocene High Rock Caldera Complex, northwest Nevada [Ph.D. thesis]: Stanford, California, Stanford University, 564 p.
Coble, M.A., and Mahood, G.A., 2012, Initial impingement of the Yellowstone plume located by widespread silicic volcanism contemporaneous with Columbia River flood basalts: Geology, v. 40, p. 655–658, doi:10.1130/G32692.1.
Coble, M.A., Grove, M., and Calvert, A.T., 2011, Calibration of Nu-Instruments Noblesse multicollector mass spectrometers for argon isotopic measurements using a newly developed reference gas: Chemical Geology, v. 290, p. 75–87, doi:10.1016/j.chemgeo.2011.09.003.
Colgan, J.P., and Henry, C.D., 2009, Rapid middle Miocene collapse of the Mesozoic orogenic plateau in north-central Nevada: International Geology Review, v. 51, p. 920–961, doi:10.1080/00206810903056731.
Colgan, J.P., Dumitru, T.A., and Miller, E.L., 2004, Diachroneity of Basin and Range extension and Yellowstone hotspot volcanism in northwestern Nevada: Geology, v. 32, p. 121–124, doi:10.1130/G20037.1.
Colgan, J.P., Dumitru, T.A., Miller, E.L., and McWilliams, M.O., 2006, Timing of Cenozoic volcanism and Basin and Range extension in northwestern Nevada: New constraints from the northern Pine Forest Range: Geological Society of America Bulletin, v. 118, p. 126–139, doi:10.1130/B25681.1.
Colgan, J.P., John, D.A., Henry, C.D., and Fleck, R.J., 2008, Large-magnitude Miocene extension of the Eocene Caetano caldera, Shoshone and Toiyabe Range, Nevada: Geosphere, v. 4, p. 107–130, doi:10.1130/GES00115.1.
Colgan, J.P., Wyld, S.J., and Wright, J.E., 2010, Geologic map of the Vicksburg Canyon quadrangle, Humboldt County, Nevada: Nevada Bureau of Mines and Geology Map 169, scale 1:24,000.
Colgan, J.P., Egger, A.E., John, D.A., Cousens, B., Fleck, R.J., and Henry, C.D., 2011, Oligocene and Miocene arc volcanism in northeastern California: Evidence for post-Eocene segmentation of the subducting Farallon plate: Geosphere, v. 7, p. 733–755, doi:10.1130/GES00650.1.
Conrad, W.K., 1984, The mineralogy and petrology of compositionally zoned ash flow tuffs, and related silicic volcanic rocks, from the McDermitt caldera complex, Nevada-Oregon: Journal of Geophysical Research, v. 89, p. 8639–8664, doi:10.1029/JB089iB10p08639.
Courtillot, V., and Fluteau, F., 2014, A review of the embedded time scales of flood basalt volcanism with special emphasis on dramatically short magmatic pulses, *in* Keller, G., and Kerr, A., eds., Volcanism, impacts, and mass extinctions: Causes and effects: Geological Society of America Special Paper 505, p. 301–317, doi:10.1130/2014.2505(15).
Cummings, M.L., Evans, J.G., Ferns, M.L., and Lees, K.R., 2000, Stratigraphic and structural evolution of the middle Miocene synvolcanic Oregon-Idaho graben: Geological Society of America Bulletin, v. 112, p. 668–682, doi:10.1130/0016-7606(2000)112<668:SASEOT>2.0.CO;2.
Courtillot, V.E., and Renne, P.R., 2003, On the ages of flood basalt events: Geodynamics, v. 335, p. 113–140, doi:10.1016/S1631-0713(03)00006-3.
de Silva, S.L., and Gregg, P.M., 2014, Thermomechanical feedbacks in magmatic systems: Implications for growth, longevity, and evolution of large caldera-forming magma reservoirs and their supereruptions: Journal of Volcanology and Geothermal Research, v. 282, p. 77–91, doi:10.1016/j.jvolgeores.2014.06.001.
de Silva, S.L., Zandt, G., Trumbull, R., Viramonte, J.G., Salas, G., and Jiménez, N., 2006, Large ignimbrite eruptions and volcano-tectonic depressions in the Central Andes: A thermomechanical perspective, *in* Troise, C., et al., eds., Mechanisms of activity and unrest at large calderas: Geological Society, London, Special Publication 269, p. 47–63, doi:10.1144/GSL.SP.2006.269.01.04.
Dufek, J., and Bergantz, G., 2005, Lower crustal magma genesis and preservation: A stochastic framework for the evaluation of basalt–crust interaction: Journal of Petrology, v. 46, p. 2167–2195, doi:10.1093/petrology/egi049.
Duffield, W.A., and McKee, E.H., 1986, Geochronology, structure, and basin-range tectonism of the Warner Range, northeastern California: Geological Society of America Bulletin, v. 97, p. 142–146, doi:10.1130/0016-7606(1986)97<142:GSABTO>2.0.CO;2.
Duncan, R.A., and Pyle, D.G., 1988, Rapid eruption of the Deccan flood basalts at the Cretaceous/Tertiary boundary: Nature, v. 333, p. 841–843, doi:10.1038/333841a0.
Egger, A.E., and Miller, E.L., 2011, Evolution of the northwest margin of the Basin and Range: The geology and extensional history of the Warner Range and environs, northeastern California: Geosphere, v. 7, p. 756–773, doi:10.1130/GES00620.1.
Farmer, G.L., Bailley, T., and Elkins-Tanton, L.T., 2008, Mantle source volumes and the origin of the mid-Tertiary ignimbrite flare-up in the southern Rocky Mountains: Lithos, v. 102, p. 279–294, doi:10.1016/j.lithos.2007.08.014.
Ford, M.T., Grunder, A.L., and Duncan, R.A., 2013, Bimodal volcanism of the High Lava Plains and northwestern Basin and Range of Oregon: Distribution and tectonic implications of age-progressive rhyolites: Geochemistry, Geophysics, Geosystems, v. 14, p. 2836–2857, doi:10.1002/ggge.20175.
Garland, F., Hawksworth, C.J., and Mantovani, M.S.M., 1995, Description and petrogenesis of the Paraná Rhyolites, southern Brazil: Journal of Petrology, v. 36, p. 1193–1227, doi:10.1093/petrology/36.5.1193.
Gibson, S.A., Thompson, R.N., and Day, J.A., 2006, Time scales and mechanisms of plume-lithosphere interactions: $^{40}Ar/^{39}Ar$ geochronology and geochemistry of alkaline igneous rocks from the Paraná-Etendeka large igneous province: Earth and Planetary Science Letters, v. 251, p. 1–17, doi:10.1016/j.epsl.2006.08.004.
Greene, R.C., 1984, Geologic appraisal of the Charles Sheldon Wilderness study area, Nevada and Oregon, *in* Mineral resources of the Charles Sheldon Wilderness Study Area, Humboldt and Washoe Counties, Nevada, and Lake and Harney Counties, Oregon: U.S. Geological Survey Bulletin 1538-A, p. 17–34.
Greene, R.C., and Plouff, D., 1981, Location of a caldera source for the Soldier Meadow Tuff, northwestern Nevada, indicated by gravity and aeromagnetic data: Geological Society of America Bulletin, v. 92, part II, p. 39–56, doi:10.1130/GSAB-P2-92-39.
Hart, W.K., 1985, Chemical and isotopic evidence for mixing between depleted and enriched mantle, northwestern U.S.A: Geochimica et Cosmochimica Acta, v. 49, p. 131–144, doi:10.1016/0016-7037(85)90197-8.
Hart, W.K., Aronson, J.L., and Mertzman, S.A., 1984, Areal distribution and age of low-K, high-alumina olivine tholeiite magmatism in the northwestern Great Basin: Geological Society of America Bulletin, v. 95, p. 186–195, doi:10.1130/0016-7606(1984)95<186:ADAAOL>2.0.CO;2.
Hart, W.K., Carlson, R.W., and Mosher, S.A., 1989, Petrogenesis of the Pueblo Mountains basalts, southeastern Oregon and northern Nevada, *in* Reidel, S., and Hooper, P., eds., Volcanism and tectonism in the Columbia River flood-basalt province: Geological Society of America Special Paper 239, p. 367–378, doi:10.1130/SPE239-p367.
Harvey, S.D., Noble, D.C., and McKee, E.H., 1986, Hog Ranch gold property, northwest Nevada: Age and genetic relation of hydrothermal mineralization to coeval peralkaline silicic associated basaltic magmatism: Isochron-West, v. 47, p. 9–11.
Hawthorne, F.C., and Oberti, R., 2007, Classification of amphiboles: Reviews in Mineralogy and Geochemistry, v. 67, p. 55–88, doi:10.2138/rmg.2007.67.2.
Henry, C.D., and John, D.A., 2013, Magmatism, ash-flow tuffs, and calderas of the ignimbrite flareup in the western Nevada volcanic field, Great Basin, USA: Geosphere, v. 9, p. 951–1008, doi:10.1130/GES00867.1.
Hildreth, W., 1981, Gradients in silicic magma chambers: Implication for lithospheric magmatism, Journal of Geophysical Research, v. 86, p. 10,153–10,192, doi:10.1029/JB086iB11p10153.
Hildreth, W., Halliday, A.N., and Christiansen, R.L., 1991, Isotopic and chemical evidence concerning the genesis and contamination of basaltic and rhyolitic magma beneath the Yellowstone Plateau Volcanic Field: Journal of Petrology, v. 32, p. 63–138, doi:10.1093/petrology/32.1.63.
Hilton, R.P., Hausback, B.P., Bromm, G.E., and Schorn, H.E., 2008, Disruption of a mid-Miocene ecosystem associated with incipient "Yellowstone Hotspot" volcanism in north-

west Nevada: Geological Society of America Abstracts with Programs, v. 40, no. 1, p. 39.

Hooper, P.R., Camp, V.E., Reidel, S.P., and Ross, M.E., 2007, The origin of the Columbia River flood basalt province: Plume versus nonplume models *in* Foulger, G.R., and Jurdy, D.M., eds., Plates, Plumes, and Planetary Processes: Geological Society of America Special Paper 430, p. 635–668, doi:10.1130/2007.2430(30).

Houghton, B.F., Wilson, C.J.N., McWilliams, M.O., Lanphere, M.A., Weaver, S.D., Briggs, R.M., and Pringle, M.S., 1995, Chronology and dynamics of a large silicic magmatic system: Central Taupo Volcanic Zone, New Zealand: Geology, v. 23, p. 13–16, doi:10.1130/0091-7613(1995)023<0013:CADOAL>2.3.CO;2.

Hughes, G.R., and Mahood, G.A., 2011, Silicic caldera in arc settings: Characteristics, distribution, and tectonic controls: Geological Society of America Bulletin, v. 123, p. 1577–1595, doi:10.1130/B30232.1.

Humphreys, E.D., 1995, Post-Laramide removal of the Farallon slab, western United States: Geology, v. 23, p. 987–990, doi:10.1130/0091-7613(1995)023<0987:PLROTF>2.3.CO;2.

Humphreys, E.D., 2009, Relation of flat subduction to magmatism and deformation in the western United States, *in* Kay, S., et al., eds., Backbone of the Americas: Shallow subduction, plateau uplift, and ridge and terrane collision: Geological Society of America, v. 204, p. 85–98, doi:10.1130/2009.1204(04).

Jarboe, N.A., Coe, R.S., Renne, P.R., Glen, J.M.G., and Mankinen, E.A., 2008, Quickly erupted volcanic sections of the Steens Basalt, Columbia River Basalt Group: Secular variation, tectonic rotation, and the Steens Mountain reversal: Geochemistry, Geophysics, Geosystems, v. 9, Q11010, doi:10.1029/2008GC002067.

Jarboe, N.A., Coe, R.S., Renne, P.R., and Glen, J.M.G., 2010, The age of the Steens reversal and the Columbia River Basalt Group: Chemical Geology, v. 274, p. 158–168, doi:10.1016/j.chemgeo.2010.04.001.

John, D.A., 1995, Tilted middle Tertiary ash-flow calderas and subjacent granitic plutons, southern Stillwater Range, Nevada: Cross sections of an Oligocene igneous center: Geological Society of America Bulletin, v. 107, p. 180–200, doi:10.1130/0016-7606(1995)107<0180:TMTAFC>2.3.CO;2.

John, D.A., Wallace, A.R., Ponce, D.A., Fleck, R.B., and Conrad, J.E., 2000, New perspectives on the geology and origin of the Northern Nevada Rift: Geological Society of Nevada Symposium Proceedings, v. 7, p. 127–154.

Johnson, J.A., Hawksworth, C.J., Hooper, P.R., and Binger, G.B., 1998, Major- and trace-element analyses of Steens Basalts, southeastern Oregon: U.S. Geological Survey Open-File Report 98-482, 30 p.

Jordan, B.T., Grunder, A.L., Duncan, R.A., and Deino, A.L., 2004, Geochronology of age progressive volcanism of the Oregon High Lava Plains: Implications for the plume interpretation of Yellowstone: Journal of Geophysical Research, v. 109, B10202, doi:10.1029/2003JB002776.

Karlstrom, L., Dufek, J., and Manga, J., 2009, Organization of volcanic plumbing through magmatic lensing by magma chambers and volcanic loads: Journal of Geophysical Research, v. 114, B10204, doi:10.1029/2009JB006339.

Kay, S.M., Coira, B., and Viramonte, J., 1994, Young mafic back-arc volcanic rocks as indicators of continental lithospheric delamination beneath the Argentine Puna plateau, Central Andes: Journal of Geophysical Research, v. 99, p. 24,323–24,339, doi:10.1029/94JB00896.

Kheng, Y.-F., 1993, Calculation of oxygen isotope fractionation in anhydrous silicate minerals: Geochimica et Cosmochimica Acta, v. 57, p. 1079–1091, doi:10.1016/0016-7037(93)90042-U.

Kistler, R.W., and Peterman, Z.E., 1973, Variation in Sr, Rb, K, Na, and initial Sr^{87}/Sr^{86} in Mesozoic granitic rocks and intruded wall rocks in central California: Geological Society of America Bulletin, v. 84, p. 3489–3512, doi:10.1130/0016-7606(1973)84<3489:VISRKN>2.0.CO;2.

Korringa, M.K., 1973, Linear vent area of the Soldier Meadow Tuff, an ash-flow sheet in northwestern Nevada: Geological Society of America Bulletin, v. 84, p. 3849–3866, doi:10.1130/0016-7606(1973)84<3849:LVAOTS>2.0.CO;2.

Kusznir, N.J., and Park, R.G., 1987, The extensional strength of the continental lithosphere: Its dependence on geothermal gradient, and crustal composition and thickness, *in* Coward, M.P., et al., eds., Continental extensional tectonics: Geological Society, London, Special Publication 28, p. 35–52, doi:10.1144/GSL.SP.1987.028.01.04.

Le Bas, M.J., Le Maitre, R.W., Streckeisen, A., and Zanenin, B., 1986, A chemical classification of volcanic rocks based on the total alkali-silica diagram: Journal of Petrology, v. 27, p. 745–750, doi:10.1093/petrology/27.3.745.

Leeman, W.P., Annen, C., and Dufek, J., 2008, 2008, Snake River Plain—Yellowstone silicic volcanism: Implications for magma genesis and magma fluxes, *in* Annen, C., and Zellmer, G.F., eds., Dynamics of crustal magma transfer, storage and differentiation: Geological Society, London, Special Publication 304, p. 235–259, doi:10.1144/SP304.12.

Legge, P.W., 1988, The bimodal basalt-rhyolite association west of and adjacent to the Pueblo Mountains, southeastern Oregon [M.S. thesis]: Corvallis, Oregon State University, 131 p.

Lerch, D.W., Klemperer, S.L., Glen, J.M.G., Ponce, D.A., Miller, E.L., and Colgan, J.P., 2007, Crustal structure of the northwestern Basin and Range Province and its transition to unextended volcanic plateaus: Geochemistry, Geophysics, Geosystems, v. 8, Q02011, doi:10.1029/2006GC001429.

Lerch, D.W., Miller, E.L., McWilliams, M., and Colgan, J.P., 2008, Tectonic and magmatic evolution of the northwestern Basin and Range and its transition to unextended volcanic Plateaus: Black Rock Range, NV: Geological Society of America Bulletin, v. 120, p. 300–311, doi:10.1130/B26151.1.

Lipman, P.W., 2007, Incremental assembly and prolonged consolidation of Cordilleran magma chambers: Evidence from the Southern Rocky Mountain volcanic field: Geosphere, v. 3, p. 42–70, doi:10.1130/GES00061.1.

Lipman, P.W., and Bachmann, O., 2015, Ignimbrites to batholiths: Integrating perspectives from geological, geophysical, and geochronological data: Geosphere, v. 11, p. 705–743, doi:10.1130/GES01091.1.

Macdonald, K.C., 1986, The crest of the Mid-Atlantic Ridge: Models for crustal generation processes and tectonics, *in* Vogt, P.R., and Tucholke, B.E., eds., The western Atlantic region: Boulder, Colorado, Geological Society of America, Geology of North America, v. M, p. 51–68.

Mahon, K.I., 1996, The New "York" regression: Application of an improved statistical method to geochemistry: International Geology Review, v. 38, p. 293–303, doi:10.1080/00206819709465336.

Mahood, G.A., 1980, Geological evolution of a Pleistocene rhyolitic center—Sierra La Primavera, Jalisco, Mexico: Journal of Volcanology and Geothermal Research, v. 8, p. 199–230, doi:10.1016/0377-0273(80)90105-5.

Mahood, G.A., 1984, Pyroclastic rocks and calderas associated with strongly peralkaline magmatism: Journal of Geophysical Research, v. 89, p. 8540–8552, doi:10.1029/JB089iB10p08540.

Mallis, J.D., 2014, $\delta^{18}O$ of rhyolites at High Rock Caldera Complex, NW Nevada: Implications for silicic magma genesis associated with Mid-Miocene flood basalts [M.S. thesis]: Stanford, California, Stanford University, 121 p.

McDonough, W.F., 1991, Partial melting of subducted oceanic crust and isolation of its residual eclogitic lithology: Royal Society of London Philosophical Transactions, ser. A, v. 335, p. 407–418, doi:10.1098/rsta.1991.0055.

McDowell, F.W., and McIntosh, W.C., 2012, Timing of intense magmatic episodes in the northern and central Sierra Madre Occidental, western Mexico: Geosphere, v. 8, p. 1505–1526, doi:10.1130/GES00792.1.

McKee, E.H., and Marvin, R.F., 1974, Summary of radiometric ages of Tertiary volcanic rocks in Nevada, Part IV—Northwestern Nevada: Isochron-West, no. 10, p. 1–6.

Merriam, J.C., 1910, Tertiary mammal beds of Virgin Valley and Thousand Creek in northwest Nevada: Part 1, Geologic history: University of California Department of Geology Bulletin, v. 6, p. 21–53.

Milner, S.C., Duncan, A.R., Whittingham, A.M., and Ewart, A., 1995, Trans-Atlantic correlation of eruptive sequences and individual silicic volcanic units within the Paraná-Etendeka igneous province: Journal of Volcanology and Geothermal Research, v. 69, p. 137–157, doi:10.1016/0377-0273(95)00040-2.

Mulch, A., Sarna-Wojcicki, A.M., Perkins, M.E., and Chamberlain, C.P., 2008, A Miocene to Pleistocene climate and elevation record of the Sierra Nevada (California): National Academy of Sciences Proceedings, v. 105, p. 6819–6824, doi:10.1073/pnas.0708811105.

Nash, B.P., and Perkins, M.E., 2012, Neogene fallout tuffs from the Yellowstone hotspot in the Columbia Plateau region, Oregon, Washington and Idaho, USA: PLoS ONE, v. 7, p. e44205, doi:10.1371/journal.pone.0044205.

Nash, B.P., Perkins, M.E., Christiansen, J.N., Lee, D.-C., and Halliday, A.N., 2006, The Yellowstone hotspot in space and time: Nd and Hf isotopes in silicic magmas: Earth and Planetary Science Letters, v. 247, p. 143–156, doi:10.1016/j.epsl.2006.04.030.

Noble, D.C., McKee, E.H., Smith, J.G., and Korringa, M.K., 1970, Stratigraphy and geochronology of Miocene rocks in northwestern Nevada: U.S. Geological Survey Professional Paper 700-D, p. D23–D32.

Noble, D.C., Henry, C.D., Park, S.L., Smith, J.A., Hausback, B.P., and Hilton, R.P., 2009, Geological framework and evolution of the High Rock Canyon Volcanic Center, northwest Nevada: An early caldera-focused system of the Yellowstone hotspot track: Geological Society of America Abstracts with Programs, v. 41, no. 7, p. 57.

Novak, S.W., and Mahood, G.A., 1986, Rise and fall of a basalt-trachyte-rhyolite magma system at the Kane Springs Wash Caldera, Nevada: Contributions to Mineralogy and Petrology, v. 94, p. 352–373, doi:10.1007/BF00371444.

Pankhurst, R.J., Leat, P.T., Sruoga, P., Rapela, C.W., Márquez, M., Storey, B.C., and Riley, T.R., 1998, The Chon Aike province of Patagonia and related rocks in West Antarctica: A silicic large igneous province: Journal of Volcanology and Geothermal Research, v. 81, p. 113–136, doi:10.1016/S0377-0273(97)00070-X.

Pankhurst, R.J., Riley, T.R., Fanning, C.M., and Kelley, S.P., 2000, Episodic silicic volcanism in Patagonia and the Antarctic Peninsula: Chronology of magmatism associated

with the break-up of Gondwana: Journal of Petrology, v. 41, p. 605–625, doi:10.1093/petrology/41.5.605.
Pankhurst, M.J., Schaefer, B.F., and Betts, P.G., 2011, Geodynamics of rapid voluminous felsic magmatism through time: Lithos, v. 123, p. 92–101, doi:10.1016/j.lithos.2010.11.014.
Park, S.L., 1983, Paleomagnetic stratigraphy, geochemistry and source areas of Miocene ash-flow tuffs and lavas of the Badger Mountain area, northwestern Nevada [M.S. thesis]: Reno, University of Nevada, 112 p.
Parsons, T., Thompson, G.A., and Sleep, N.H., 1994, Mantle plume influence on the Neogene uplift and extension of the U.S. western Cordillera?: Geology, v. 22, p. 83–86, doi:10.1130/0091-7613(1994)022<0083:MPIOTN>2.3.CO;2.
Perkins, M.E., and Nash, B.P., 2002, Explosive silicic volcanism of the Yellowstone hotspot: The ash fall tuff record: Geological Society of America Bulletin, v. 114, p. 367–381, doi:10.1130/0016-7606(2002)114<0367:ESVOTY>2.0.CO;2.
Pierce, K.L., and Morgan, L.A., 1992, The track of the Yellowstone hot spot: Volcanism, faulting, and uplift, *in* Link, P.K., et al., eds., Regional geology of eastern Idaho and western Wyoming: Geological Society of America Memoir 179, p. 1–53, doi:10.1130/MEM179-p1.
Pierce, K.L., Morgan, L.A., and Saltus, R.W., 2002, Yellowstone plume head: Postulated tectonic relations to the Vancouver slab, continental boundaries, and climate, *in* Bonnichsen, B., et al., eds., Tectonic and magmatic evolution of the Snake River Plain Volcanic Province: Idaho Geological Survey Bulletin, v. 30, p. 5–33.
Ramos, F.C., Wolff, J.A., Starkel, W., Eckberg, A., Tollstrup, D.L., and Scott, S., 2013, The changing nature of sources associated with Columbia River flood basalts: Evidence from strontium isotope ratio variations in plagioclase phenocrysts, *in* Reidel, S.P., et al., eds., The Columbia River flood basalt province: Geological Society of America Special Paper 497, p. 231–257, doi:10.1130/2013.2497(09).
Reidel, S.P., Camp, V.E., Tolan, T.L., and Martin, B.S., 2013, The Columbia River flood basalt province: Stratigraphy, areal extent, volume, and physical volcanology, *in* Reidel, S.P., et al., eds., The Columbia River flood basalt province: Geological Society of America Special Paper 497, p. 1–43, doi:10.1130/2013.2497(01).
Renne, P.R., Swisher, C.C., Deino, A.L., Karner, D.B., Owens, T.L., and DePaolo, D.J., 1998, Intercalibration of standards, absolute ages and uncertainties in $^{40}Ar/^{39}Ar$ dating: Chemical Geology, v. 145, p. 117–152, doi:10.1016/S0009-2541(97)00159-9.
Rytuba, J.J., 1994, Evolution of volcanic and tectonic features in caldera settings and their importance in the localization of ore deposits: Economic Geology and the Bulletin of the Society of Economic Geologists, v. 89, p. 1687–1696, doi:10.2113/gsecongeo.89.8.1687.
Rytuba, J.J., and Glanzman, R.K., 1979, Relation of mercury, uranium, and lithium deposits to the McDermitt Caldera complex, Nevada-Oregon, *in* Papers on mineral deposits of western North America: Nevada Bureau of Mines and Geology Report 33, p. 109–117.
Rytuba, J.J., and McKee, E.H., 1984, Peralkaline ash flow tuffs and calderas of the McDermitt Volcanic Field, southwest Oregon and north central Nevada: Journal of Geophysical Research, v. 89, p. 8616–8628, doi:10.1029/JB089iB10p08616.
Rytuba, J.J., and Vander Muelen, D.B., 1991. Hot-spring precious-metal systems in the Lake Owyhee Volcanic Field, Oregon-Idaho, *in* Raines, G.L., et al., eds., Geology and ore deposits of the Great Basin: Reno, Geological Society of Nevada, p. 1085–1096.
Rytuba, J.J., John, D.A., Foster, A., Luddington, S.D., and Kotlyar, B., 2003, Hydrothermal enrichment of gallium in zones of advanced argillic alteration—Examples from the Paradise Peak and McDermitt ore deposits, Nevada: U.S. Geological Survey Bulletin 2209C, 16 p.
Rytuba, J.J., Coble, M.A., Luddington, S., and Goldstein, D., 2010, Mineral deposits and prospects in the Sheldon National Antelope Refuge, Nevada and Oregon: U.S. Geological Survey Administrative Report 2010, 53 p.
Salisbury, M.J., Jicha, B.R., de Silva, S.L., Singer, B.S., Jiménez, N.C., and Ort, M.H., 2011, $^{40}Ar/^{39}Ar$ chronostratigraphy of Altiplano-Puna volcanic complex ignimbrites reveals the development of a major magmatic province: Geological Society of America Bulletin, v. 123, p. 821–840, doi:10.1130/B30280.1.
Saunders, J.A., Unger, D.L., Kamenov, G.D., Fayek, M., Hames, W.E., and Utterback, W.C., 2008, Genesis of middle Miocene Yellowstone hotspot-related bonanza epithermal Au-Ag deposits, northern Great Basin, USA: Mineralium Deposita, v. 43, p. 715–734, doi:10.1007/s00126-008-0201-7.
Shervais, J.W., and Hanan, B.B., 2008, Lithospheric topography, tilted plumes, and the track of the Snake River–Yellowstone hot spot: Tectonics, v. 27, TC5004, doi:10.1029/2007TC002181.
Smith, J.A., 2011, Characterizing and identifying the eruptive source of the Soldier Meadow Tuff in northwest Nevada [M.S. thesis]: Sacramento, California State University, 105 p.
Smith, J.A., Hausback, B.P., Henry, C.D., and Noble, D.C., 2010, The Soldier Meadow Tuff: Eruptive and depositional processes and relationship to the High Rock Caldera, NW Nevada: American Geophysical Union Fall Meeting, abs. V13A-2338, p. 2338.
Smith, R.C.M., 1991, Post-eruption sedimentation on the margin of a caldera lake, Taupo Volcanic Centre, New Zealand: Sedimentary Geology, v. 74, p. 89–138, doi:10.1016/0037-0738(91)90036-D.
Smith, R.L., 1979, Ash-flow magmatism, *in* Chapin, C.E., and Elston, W.E., eds., Ash-flow tuffs: Geological Society of America Special Paper 180, p. 5–28, doi:10.1130/SPE180-p5.
Smith, R.L., and Bailey, R.A., 1968, Resurgent cauldrons, *in* Coats, R.R., et al., eds., Studies in volcanology: Geological Society of America Memoir 116, p. 613–662, doi:10.1130/MEM116-p613.
Starkel, W.A., 2014, Mapping, geologic evolution and petrogenesis of the McDermitt Caldera Center, northern Nevada and southern Oregon [Ph.D. thesis]: Pullman, Washington State University, 393 p.
Steiger, R.H., and Jäger, E., 1977, Subcommission on geochronology: Convention on the use of decay constants in geo- and cosmochronology: Earth and Planetary Science Letters, v. 36, p. 359–362, doi:10.1016/0012-821X(77)90060-7.
Streck, M.J., Ferns, M.L., and McIntosh, W., 2015, Large, persistent rhyolite magma reservoirs above Columbia River Basalt storage sites: The Dinner Creek Tuff eruptive center, eastern Oregon: Geosphere, v. 11, p. 226–235, doi:10.1130/GES01086.1.
Swisher, C.C.I., 1992, $^{40}Ar/^{39}Ar$ dating and its application to the calibration of the North American land mammal ages [Ph.D. thesis]: Berkeley, University of California at Berkeley, 239 p.
Tegtmeyer, K.J., and Farmer, G.L., 1990, Nd isotopic gradients in upper crustal magma chambers: Evidence for in situ magma–wall-rock interaction: Geology, v. 18, p. 5–9, doi:10.1130/0091-7613(1990)018<0005:NIGIUC>2.3.CO;2.
Trugman, A.T., 2011, Volcanic stratigraphy of Massacre Rim, northwest Nevada: Mantle source magma in the mid- to late-Tertiary [thesis]: Stanford, California, Stanford University, 53 p.
Ukstins Peate, I., Baker, J.A., Al-Kadasi, M., Al-Subbary, A., Knight, K.B., Riisager, P., Thirlwall, M.F., Peate, D.W., Renne, P.R., and Menzies, M.A., 2005, Volcanic stratigraphy of large-volume silicic pyroclastic eruptions during Oligocene Afro-Arabian flood volcanism in Yemen: Bulletin of Volcanology, v. 68, p. 135–156, doi:10.1007/s00445-005-0428-4.
Van Buer, N.J., Miller, E.L., and Dumitru, T.A., 2009, Early Tertiary paleogeologic map of the northern Sierra Nevada batholiths and the northern Basin and Range: Geology, v. 37, p. 371–374, doi:10.1130/G25448A.1.
Watson, E.B., and Harrison, T.M., 1983, Zircon saturation revisited: Temperature and composition effects in a variety of crustal magma types: Earth and Planetary Science Letters, v. 64, p. 295–304, doi:10.1016/0012-821X(83)90211-X.
Wells, R.E., and Heller, P.L., 1988, The relative contribution of accretion, shear, and extension to Cenozoic tectonic rotation in the Pacific Northwest: Geological Society of America Bulletin, v. 100, p. 325–338, doi:10.1130/0016-7606(1988)100<0325:TRCOAS>2.3.CO;2.
White, S.M., Crisp, J.A., and Spera, F.J., 2006, Long-term volumetric eruption rates and magma budgets: Geochemistry, Geophysics, Geosystems, v. 7, Q03010, doi:10.1029/2005GC001002.
Wilson, C.J.N., Houghton, B.F., McWilliams, M.O., Lanphere, M.A., Weaver, S.D., and Briggs, R.M., 1995, Volcanic and structural evolution of Taupo Volcanic Zone, New Zealand: A review: Journal of Volcanology and Geothermal Research, v. 68, p. 1–28.
Wolfe, J.A., Schorn, H.E., Forst, C.E., and Molnar, P., 1997, Paleobotanical evidence for high altitudes in Nevada during the Miocene: Science, v. 276, p. 1672–1675, doi:10.1126/science.276.5319.1672.
Wolff, J.A., Ramos, F.C., Hart, G.L., Patterson, J.D., and Brandon, A.D., 2008, Columbia River flood basalts from a centralized crustal magmatic system: Nature Geoscience, v. 1, p. 177–180, doi:10.1038/ngeo124.
Wypych, A., Hart, W., Scarberry, K., McHugh, K., Pasquale, S.A., and Legge, P.W., 2011, Geologic map of the Hawks Valley–Lone Mountain region, Harney County, Oregon: Oregon Department of Geology and Mineral Industries Open-File Report 0-11-12, 28 p., scale: 1:36,000.
York, D., 1968, Least-squares fitting of a straight line with correlated errors: Earth and Planetary Science Letters, v. 5, p. 320–324, doi:10.1016/S0012-821X(68)80059-7.
Zielinski, R.A., 1982, Uraniferous opal, Virgin Valley, Nevada: Conditions of formation and implications for uranium exploration: Journal of Geochemical Exploration, v. 16, p. 197–216, doi:10.1016/0375-6742(82)90010-3.